AD NUMBER

ADB023874

NEW LIMITATION CHANGE

TO

Approved for public release, distribution unlimited

FROM

Distribution authorized to U.S. Gov't. agencies only; Test and Evaluation; 15 August 1977. Other requests shall be referred to Naval Weapons Center, China Lake, CA.

AUTHORITY

USNWC notice, 23 Jan 1979

NWC TP 5951

Additive Drag of Two-Dimensional Inlets

by
Robert B. Hall
Ordnance Systems Department

NOVEMBER 1977

Naval Weapons Center
CHINA LAKE, CALIFORNIA 93555

Naval Weapons Center

AN ACTIVITY OF THE NAVAL MATERIAL COMMAND

FOREWORD

This report was originally written as a dissertation for the degree of Doctor of Philosophy in Mechanical Engineering from the University of Arizona, Tucson, AZ. The research was performed under the direction of Professor Russell E. Petersen of the Aerospace and Mechanical Engineering Department of the University.

The author attended the University of Arizona under sponsorship of WEPCOSE and NWC Fellowships from September 1969 to June 1972. The work described herein covers the period from September 1971 to April 1977. The effort was supported by the Naval Air Systems Command under AirTask A03W-3300/008B/6F31330300, Paired Submerged Inlets.

Mr. John J. Mahoney has reviewed this report for technical accuracy.

Approved by
B. W. HAYS, *Head*
Ordnance Systems Department
31 October 1977

Under authority of
W. L. HARRIS, JR.
RAdm., U.S. Navy
Commander

Released for publication by
R. M. HILLYER
Technical Director (Acting)

NWC Technical Publication 5951

Published by . . . . . Technical Information Department
Collation . . . . . Cover, 68 leaves
First printing . . . . . 210 unnumbered copies

UNCLASSIFIED

SECURITY CLASSIFICATION OF THIS PAGE (When Data Entered)

REPORT DOCUMENTATION PAGE	READ INSTRUCTIONS BEFORE COMPLETING FORM
1. REPORT NUMBER: NWC-TP-5951 (14)	2. GOVT ACCESSION NO. / 3. RECIPIENT'S CATALOG NUMBER
4. TITLE (and Subtitle): (6) ADDITIVE DRAG OF TWO-DIMENSIONAL INLETS,	5. TYPE OF REPORT & PERIOD COVERED: (9) Final report, Sep 1969-June 1977,
	6. PERFORMING ORG. REPORT NUMBER
7. AUTHOR(s): (10) Robert B. Hall	8. CONTRACT OR GRANT NUMBER(s): AirTask A03W-3300/00[illegible] F3133[illegible] (15)
9. PERFORMING ORGANIZATION NAME AND ADDRESS: Naval Weapons Center, China Lake, California 93555	10. PROGRAM ELEMENT, PROJECT, TASK AREA & WORK UNIT NUMBERS
11. CONTROLLING OFFICE NAME AND ADDRESS: Naval Weapons Center, China Lake, California 93555 (11)	12. REPORT DATE: Nov[illegible] 1977
	13. NUMBER OF PAGES: 194 (12) 135 p.
14. MONITORING AGENCY NAME & ADDRESS (if different from Controlling Office)	15. SECURITY CLASS. (of this report): UNCLASSIFIED
	15a. DECLASSIFICATION/DOWNGRADING SCHEDULE

16. DISTRIBUTION STATEMENT (of this Report)

Distribution limited to U.S. Government agencies only; test and evaluation; 15 August 1977. Other requests for this document must be referred to the Naval Weapons Center.

17. DISTRIBUTION STATEMENT (of the abstract entered in Block 20, if different from Report)

DDC RECEIVED JAN 3 1978 B

18. SUPPLEMENTARY NOTES

19. KEY WORDS (Continue on reverse side if necessary and identify by block number)

Additive Drag	Two-Dimensional Inlets
Inlet Drag	Inlet Flowfield
Inlet Spillage	Conical Flow

20. ABSTRACT (Continue on reverse side if necessary and identify by block number)

See reverse side of this form.

DD FORM 1 JAN 73 1473 EDITION OF 1 NOV 65 IS OBSOLETE S/N 0102-014-6601

UNCLASSIFIED

SECURITY CLASSIFICATION OF THIS PAGE (When Data Entered)

403019

(U) *Additive Drag of Two-Dimensional Inlets*, by Robert B. Hall. China Lake, Calif., Naval Weapons Center, November 1977, 134 pp. (NWC TP 5951, publication UNCLASSIFIED.)

(U) A theoretical analysis of additive drag of two-dimensional inlets has been performed. A preliminary review of supersonic inlets provides a description of the various types of inlets, an introduction to inlet terminology and performance criteria, and the definition of additive drag. The application of geometrical streamline tracing is introduced for simple geometries as a method of determining inlet capture area ratio.

(U) The spillage from the sides of a two-dimensional inlet is treated by the method of homogeneous conical flows. This method is described and extended to determine the three-dimensional perturbation velocities within the conical flowfield.

(U) A computer program has been written to determine the shape of the streamtube captured by the inlet. In addition to tracing the streamlines, the program also numerically integrates the pressures over the streamtube to calculate the additive drag with sidespillage.

(U) The computer program has been applied to several inlet designs. Comparisons of spillage are made with experimental data. The effects of various inlet variables are considered. These variables include ramp angle, Mach number, presence of sidewalls, and leading edge sweepback.

CONTENTS

Introduction 3

Review of Supersonic Inlets 3

Previous Investigations 21
Investigation of Carriere and Leynaert 21
Homogeneous Conical Flow 28

Streamtube Calculations 50
Description of Computer Program 53
Pawlikowski's Analysis 58

Applications of Computer Program 75
Comparison with Experimental Data 76
Effect of Inlet Design Variables 76

Summary and Discussion of Applicability 94

References 98

Appendices
A. Derivation of Compatibility Relationships 99
B. Derivation of Simplifying Relationships for the Busemann Transformation 107
C. Listing and Sample Prinout of Computer Program 111
D. Derivations of Two-Dimensional Perturbation Velocities 125

Nomenclature 131

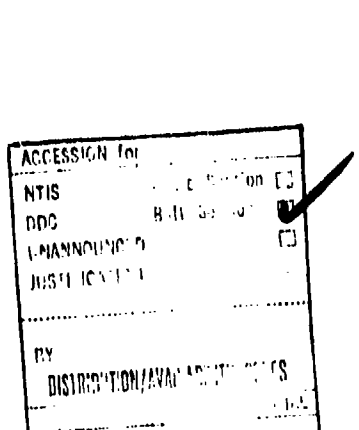

Chapter 1. INTRODUCTION

In recent years, there has been an increasing emphasis in supersonic airbreathing propulsion. Military aircraft are being designed for sustained supersonic flight. There is renewed interest in ramjet propulsion for missile applications at supersonic conditions. The inlet is a major component of these airbreathing propulsion systems. For some applications, two-dimensional inlets are supplanting the standard axisymmetric inlet. To determine the overall performance of any propulsion system, all of the various drag components must be properly accounted. One of the drag components attributed to the inlet is additive drag. Determination of additive drag is relatively simple for an axisymmetric inlet or for a simplified model of a two-dimensional inlet. However, when sidespillage of a two-dimensional inlet is included, the determination of inlet mass flow and additive drag becomes complicated. This problem is considered herein.

Chapter 2 contains a review of supersonic inlets. The operation and terminology of inlets are discussed, and additive drag is defined. The method of streamline tracing to determine inlet mass flow and additive drag is introduced. Chapter 3 reviews previous investigations of spillage of two-dimensional inlets. The method of homogeneous conical flow is introduced and extended to determine the perturbation velocity components. In Chapter 4, this extended theory is employed in a numerical technique for streamline tracing. A computer program is described. Applications of this computer program are presented in Chapter 5. Mass flow determined by this method is compared to measured data. The program is applied to demonstrate the effects of various inlet design variables. Most of the conclusions concerning the design of inlets is included in this chapter. Chapter 6 summarizes the previous work and discusses the range of applicability of the computer program.

Chapter 2. REVIEW OF SUPERSONIC INLETS

Before proceeding to a discussion of spillage in two-dimensional inlets, it would be useful to review the operation and terminology of inlets for airbreathing propulsion systems. More complete discussions are presented by Faro (Ref. 1) and the staff of Johns Hopkins Applied Physics Laboratory (Ref. 2). The inlets are probably the most prominent feature distinguishing an airbreathing propulsion system (such as a ramjet, turbojet, or air-augmented rocket) from a rocket propulsion system. Obviously, the primary function of an inlet is to capture and induct air as a working fluid to a desired location for combustion and subsequent expulsion through an exhaust nozzle. In addition, the inlet is usually required to decelerate the flow. For a turbojet, the velocity must be reduced to a value compatible with the compressor blades, a Mach number of about 0.5. For a ramjet, the velocity of the air must be reduced to the order of magnitude of the flame speed or to the order of a hundred feet per second. In a supersonic inlet this is achieved by a series of shock waves.

Inlets typically are of two types, axisymmetric or two-dimensional, although special circumstances may dictate a more complex three-dimensional inlet. Axisymmetric inlets have demonstrated utility and applicability in some of the earlier ramjet programs such as BOMARC and TALOS. Axisymmetric inlets are relatively inexpensive to build. Structurally, the circular duct offers the best shape for the pressure loads. This permits lighter weight construction. The boundary layer bleed requirements for an axisymmetric inlet are minimal. However, the performance of an axisymmetric inlet decreases with angle-of-attack. A two-dimensional inlet may be oriented to achieve improved angle-of-attack performance. The Modern Ramjet Engine (MRE) and some aircraft, such as the F14 and F15, have employed two-dimensional inlets for this reason. Two-dimensional inlets also provide packaging flexibility in that any combination of width to height may be chosen to achieve a given inlet area. The two-dimensional inlet also offers versatility in the choice of direction of compression. The inlets may be mounted so that the compression turns the flow inward toward the vehicle or outward away from the vehicle, or may be side-mounted with downward-turning inlets. The compression direction may be selected to enhance angle-of-attack performance or drag characteristics. For variable geometry inlets, the ramp construction permits the greatest range of configurations providing near-optimum performance over a wide flight envelope. The two-dimensional inlet is heavier and more expensive to fabricate than the axisymmetric inlet. In addition, the corner flow creates a thicker boundary layer requiring more bleed.

The simplest type of supersonic inlet is a normal shock inlet in which a normal shock stands at the front of the inlet, as shown in Figure 1a. With subsonic flow behind the shock, the flow may be further decelerated by a diverging duct, as in a subsonic inlet. This inlet is typically the most stable and least sensitive to upstream conditions. Satisfactory performance can be obtained from a normal shock inlet at low supersonic speeds.

The diffuser duct may be converging-diverging to form a reverse de Laval nozzle as is shown in Figure 1b. When the inlet is started, the supersonic flow decelerates in the converging entrance section, passes through a normal shock just downstream of the throat, and further decelerates subsonically in the divergent section. This type of inlet has a starting problem. In the unstarted mode, the normal shock will stand in front of the inlet. The throat area must be increased or the inlet must be oversped (if possible) in order to "swallow" the shock.

The total pressure loss of a supersonic inlet may be reduced by means of an oblique shock. This type of inlet, shown in Figure 1c, may be either a conical inlet or a two-dimensional ramp inlet; many of the conclusions are applicable to both kinds. As indicated in the figure, an initial compression surface causes an oblique shock which decelerates the flow. At the entrance to the inlet duct, a normal shock occurs at a Mach number lower than freestream. The product of the total pressure recovery of the oblique and normal shocks is greater than that of a single normal shock at freestream conditions. Figure 2 indicates the total pressure recovery of conical inlets for several Mach numbers. As can be seen, there is an optimum cone angle for each

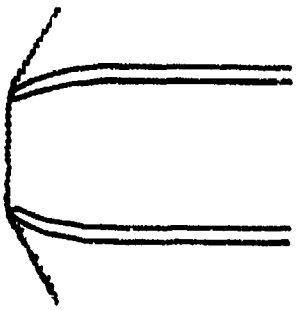

(a) NORMAL SHOCK INLET.

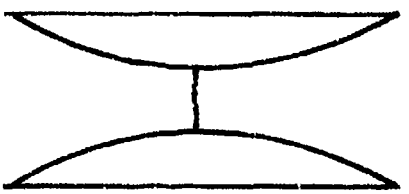

(b) CONVERGING-DIVERGING INLET (REVERSE DE LAVAL).

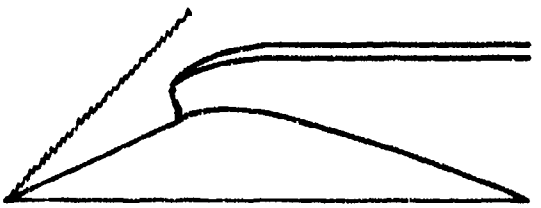

(c) SINGLE RAMP/CONE INLET.

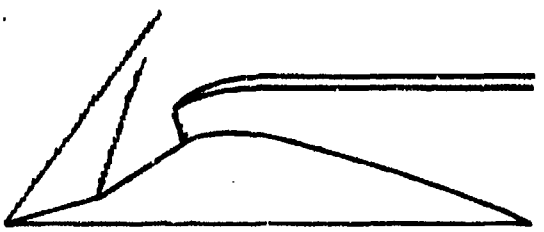

(d) DOUBLE RAMP/CONE INLET.

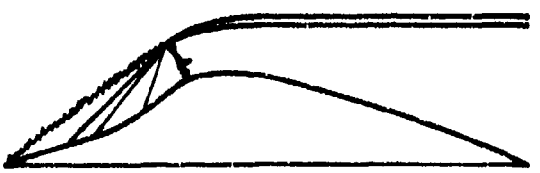

(e) ISENTROPIC INLET.

FIGURE 1. Types of Supersonic Inlets.

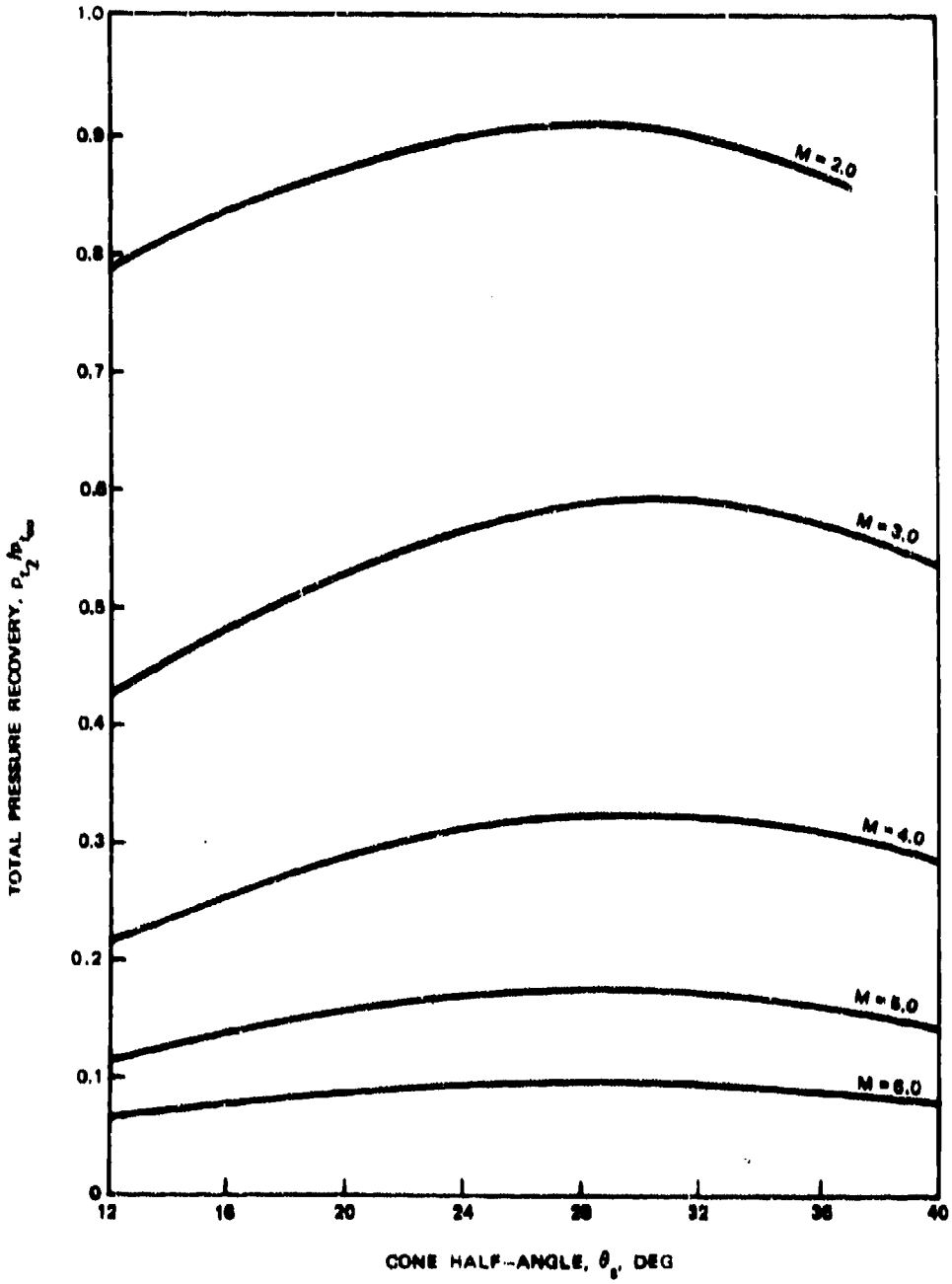

FIGURE 2. Total Pressure Recovery of Single Cone Inlets.

Mach number. This cone angle may be presented as a function of Mach number as in Figure 3. The pressure recovery of the oblique shock inlet may also be increased by internal contraction which reduces the Mach number prior to the normal shock at the throat section. Internal contraction is limited by inlet starting considerations. Finally, a subsonic diffuser section provides further deceleration of the flow.

Since the single oblique shock improved the performance of the inlet, it may be suspected that an additional oblique shock before the normal shock may also be beneficial. This is indeed the case. A double cone or ramp inlet is illustrated in Figure 1d. As in the single oblique shock inlet, there is an optimum combination of deflection angles. Figure 4 presents the total pressure recoveries of various combinations of cone angles for a double cone inlet. The optimum cone angles are shown as a function of Mach number in Figure 5.

Continued improvement in total pressure recovery may be obtained by increasing the number of oblique shocks. Figure 6 demonstrates the total pressure recovery for optimum combinations of cone angles for multiple oblique shocks. The number of shocks, n, includes the terminal normal shock in addition to the oblique shocks. In the limit, the oblique shocks become an isentropic compression shown in Figure 1e. Since a true isentropic compression requires an initial zero slope, the isentropic inlet starts with an initial non-zero slope, either a selected angle or the angle which yields a selected pressure recovery at design conditions. The coordinates of such isentropic surfaces have been calculated for various design Mach numbers. An example for conical inlets is included as Figure 7. In this figure, focal points are indicated for each design Mach number. At the design Mach number, the conical shock from the tip

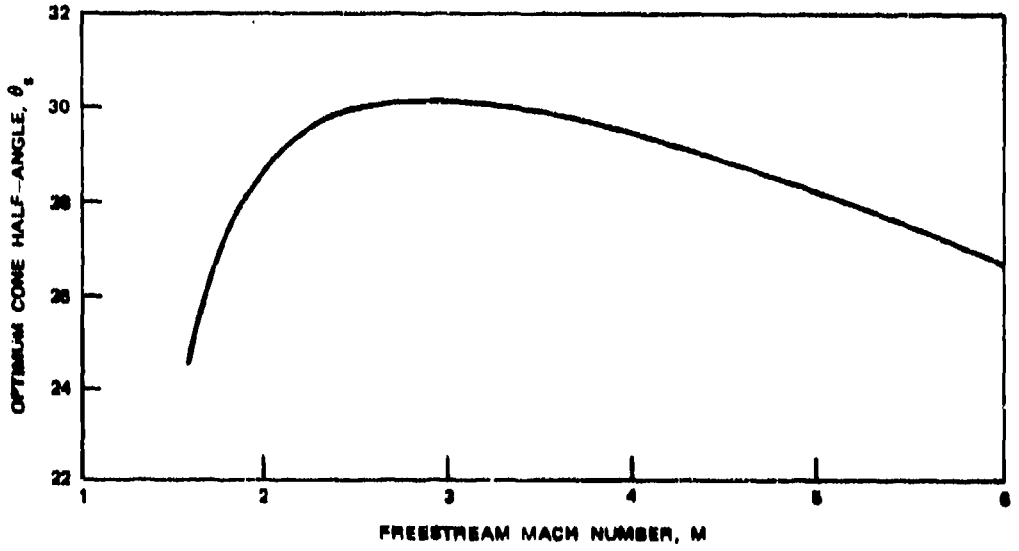

FIGURE 3. Optimum Cone Angle for a Single Cone Inlet.

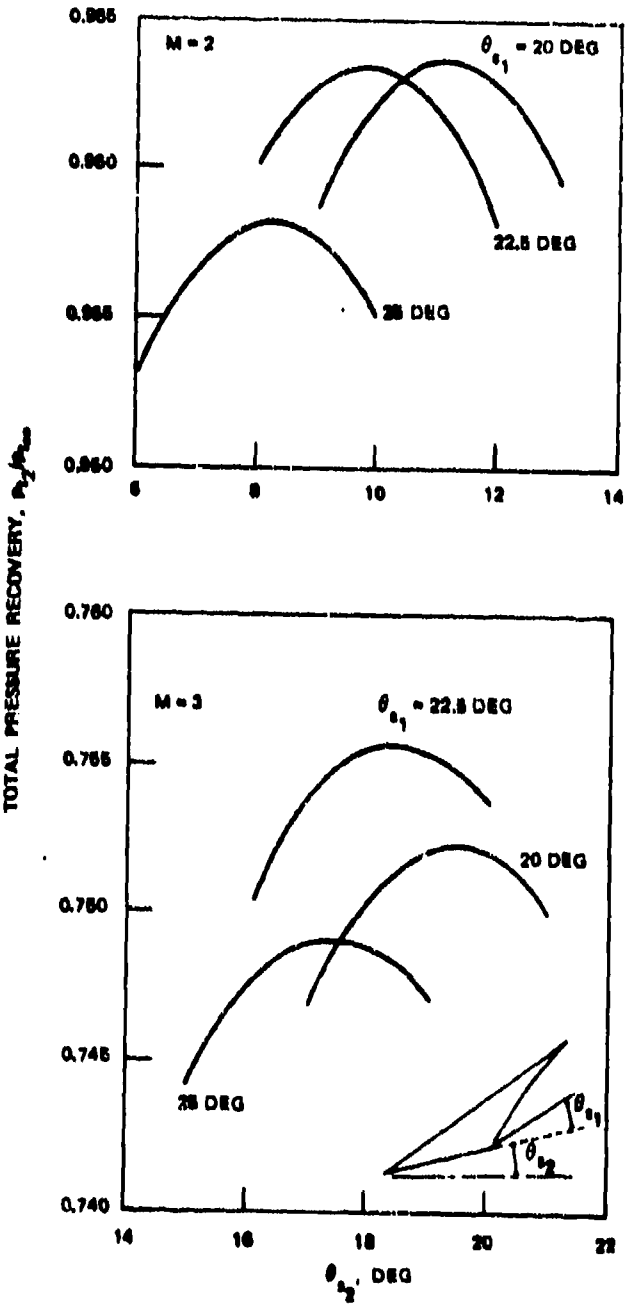

FIGURE 4. Total Pressure Recovery of Double Cone Inlet.

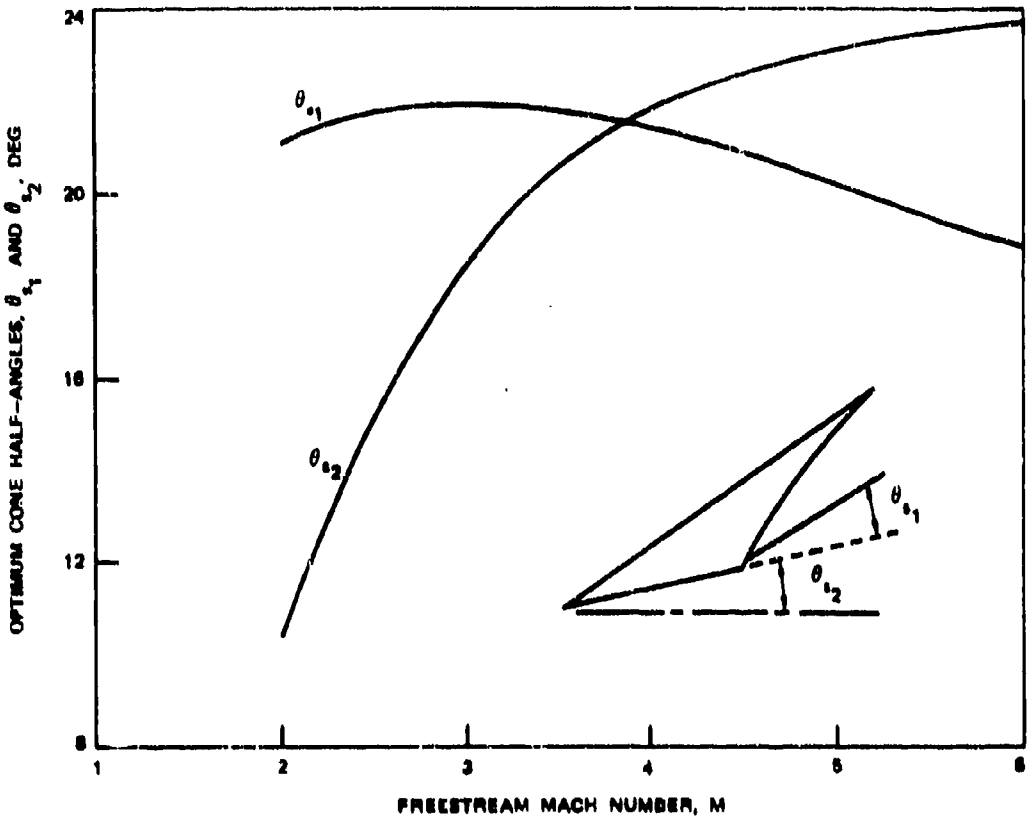

FIGURE 5. Optimum Cone Angles for a Double Cone Inlet.

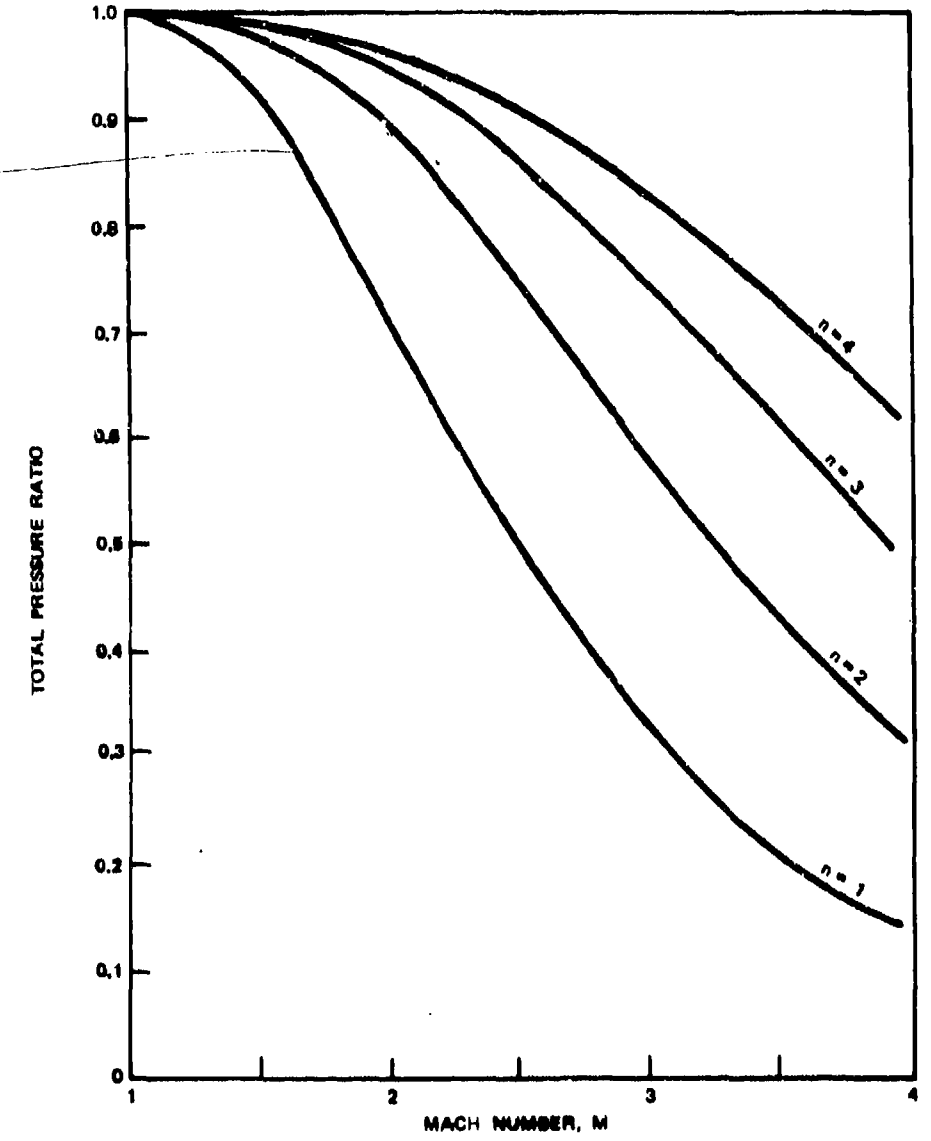

FIGURE 6. Total Pressure Recovery of Multiple Cone Inlets.

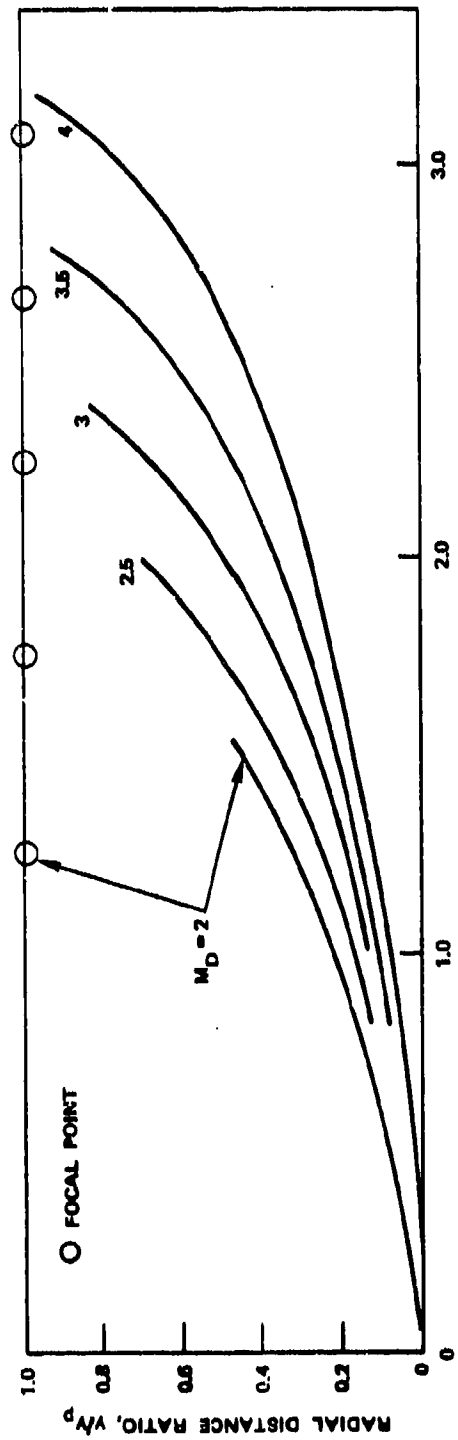

FIGURE 7. Coordinates of Isentropic Cones with 1% Pressure Loss Due to Nose Shock.

and all compression waves generated from the surface coalesce at this point. In practice, this is usually made to be the location of the cowl lip. All dimensions in the figure are ratioed to the radius of the focal point Y_p so that when the cowl diameter is selected, the inlet shape is specified.

The relative performance of air inlets is compared on the basis of three primary figures of merit. These are (1) capture area ratio, (2) total pressure recovery, and (3) drag.

The capture area ratio indicates how much air is delivered to the propulsion system. The mass flow at any point may be written as ρAV where ρ is the density, A is the cross-sectional area, and V is the velocity. When referenced to freestream or 0 (zero) conditions where the density, ρ_0, and velocity, V_0, are readily obtained, the mass flow (which may be measured elsewhere) defines the freestream area of the captured streamtube, A_0. The captured mass flow may be normalized by dividing by the mass flow that could be delivered by the area of the inlet or cowl area, A_c. This mass flow is $\rho_0 A_c V_0$. Thus, the ratio of the actual mass flow to the maximum possible becomes the capture area ratio, A_0/A_c. In addition to the physical meaning, based upon a measured mass flow, the capture area may be determined theoretically by geometrical analysis. Consider a single ramp, two-dimensional inlet as shown in Figure 8. The cowl area, A_c, is simply the cowl height, h_c, multiplied by the inlet width, W. The flow behind the shock is directed parallel to the compression surface at an angle, θ_s. A streamline may be drawn from the cowl lip, parallel to the compression surface, to the intersection with the oblique shock inclined at wave angle, θ_w. Upstream of the shock wave, the flow is horizontal. Thus, the captured streamtube of height, h_0, and width, W, for two-dimensional flow is defined. The capture area ratio, A_0/A_c, is equal to the ratio of heights, h_0/h_c, in this case. Extension to multiple ramps requires only identification of the flow direction behind each shock and tracing the streamline from the cowl back to freestream. An axisymmetric inlet is only slightly more complicated in that the flow is not parallel to the surface but varies between rays. The streamline must be traced from ray to ray to the initial shock. Following this principle, the capture area ratio of any inlet, even a three-dimensional inlet, may be determined by a streamtube trace if the flowfield is known. Mass removal, such as by sidespill or boundary layer bleed, may also be referenced to the possible mass flow to yield an area ratio for each mass removal process.

The second figure of merit has been alluded to in the description of the inlets. The total pressure recovery is a direct measure of the maximum pressure which can be achieved in the combustion chamber and hence of the thrust developed.

There are nine possible modes of operation of an inlet resulting from combinations of three possibilities for each of two independent variables. These nine modes are illustrated in Figure 9. First, an inlet may operate above, at, or below the design Mach number. This is presented in the vertical sequence in the figure. Typically, the design Mach number is the Mach number at which the oblique shock of the inlet

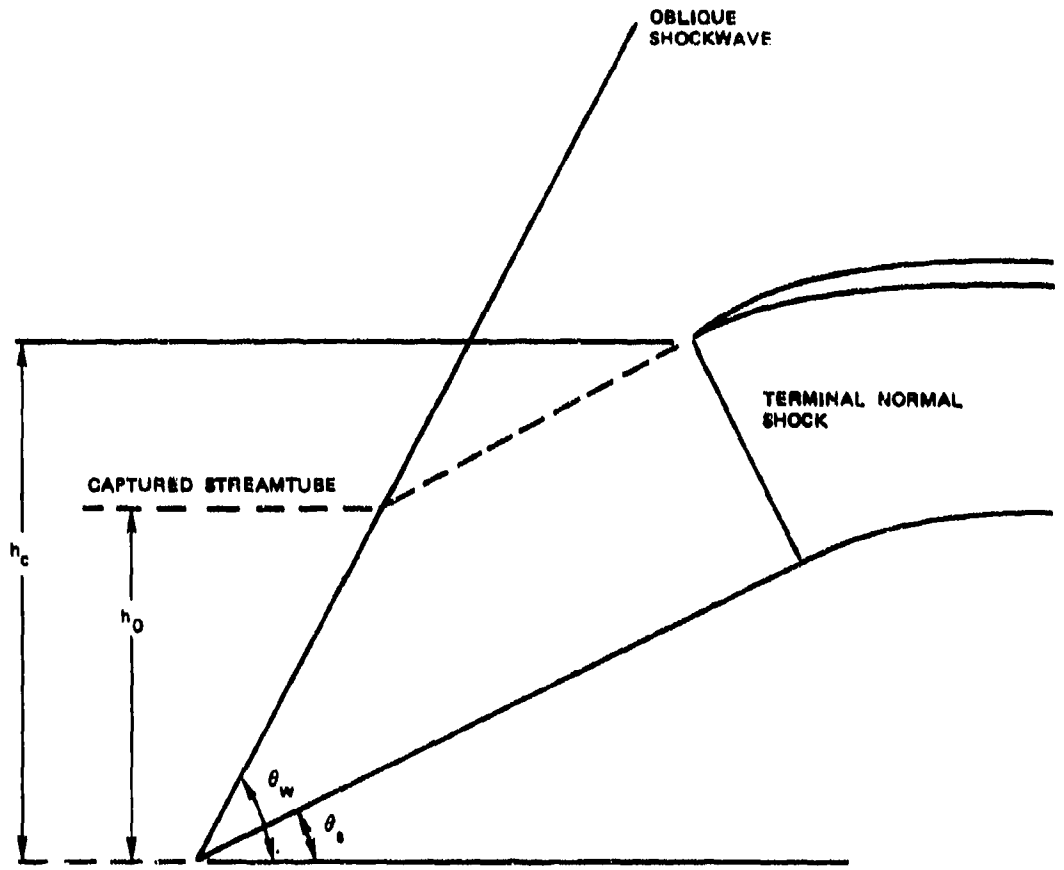

FIGURE 8. Geometrical Determination of Capture Area Ratio.

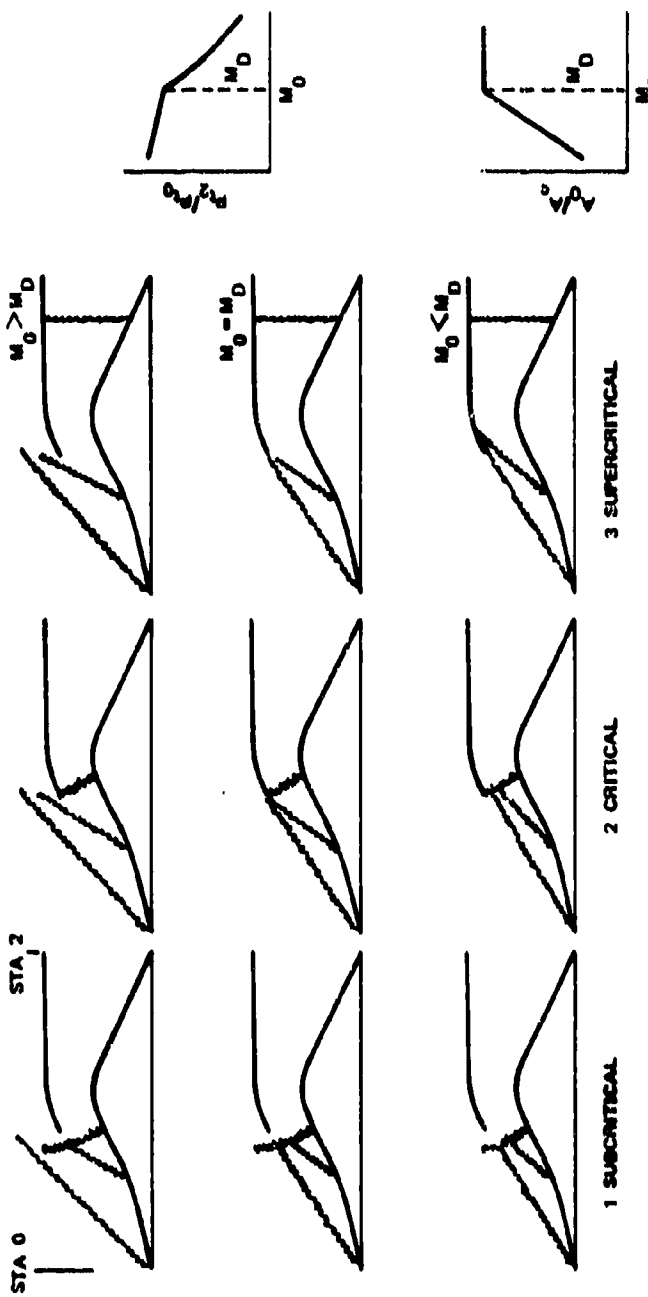

FIGURE 9. Modes of Inlet Operation.

intersects the cowl lip. For multiple shock inlets, the ramp contour is designed so that all shocks coalesce at the cowl lip. Since the shock angle for constant deflection decreases with increasing Mach number, the shock passes above the cowl below the design Mach number and enters the cowl above design Mach number. The effect of Mach number on total pressure recovery and capture area ratio are illustrated on the right side of the figure. Total pressure recovery typically decreases with increasing Mach number, slowly below design and more rapidly above. Often a sharp break in the curve may be noted at the design Mach number. Below design, analysis of a two-dimensional inlet is straightforward in the manner previously described. Above design, analysis is complicated by the non-uniform conditions at the cowl lip plane. Part of the flow has passed through the oblique shock system with a loss of total pressure and velocity and a change in direction. The remainder of the flow at the cowl lip plane is still in the undeflected freestream condition. An analytical model should include some averaging technique to obtain mean conditions at the cowl lip plane for gross inlet behavior. The capture area increases with Mach number below design. Above design Mach number, conditions at the cowl lip are freestream conditions. Since the flow is not deflected, the area of the captured streamtube is the same as the inlet area and the capture area theoretically equals 1.0. The change in operation appears as a sharp break in the capture area curve at the design Mach number.

The other variable of inlet operation is whether the inlet is critical, supercritical, or subcritical. These conditions are illustrated in the horizontal sequence of Figure 9. In the critical condition, the terminal normal shock is at the cowl lip plane of an external compression inlet or at the throat of a mixed external-internal compression inlet. In the supercritical condition, the terminal normal shock is downstream of the critical position, occurring in the subsonic diffuser. Due to supersonic expansion, the terminal shock occurs at a higher Mach number than at the throat, and the total pressure recovery is less. Since the external shock system is unchanged, the capture area ratio remains the same as at critical. In the subcritical condition, the terminal normal shock occurs upstream of the critical position, on the compression surface. This shock location results in a reduction in mass flow or capture area ratio. Depending upon the design of the compression surface, subcritical total pressure recovery may be greater than, equal to, or less than critical recovery. The sequence is summarized in the graph at the bottom of Figure 9, with 1 representing a subcritical condition, 2 critical, and 3 supercritical. As may be observed from the figure, the critical condition may be defined as the condition of maximum pressure recovery at the maximum capture area ratio. The location of the terminal normal shock is determined by the combustor temperature and therefore fuel flow to the combustor. With increased temperature, a higher total pressure is required for the same mass flow rate. To achieve higher total pressure, the shock moves toward the critical position. For further combustor temperature increases, the inlet delivers less mass by subcritical operation, thus reducing the pressure recovery requirements.

The primary concern in testing inlets is the determination of the critical condition. It is generally assumed that the inlet may be easily operated supercritically for less total pressure recovery. In subcritical operation, an instability known as

"diffuser buzz" may occur. During buzz the shock position is unstable, oscillating from supercritical to subcritical operation, possibly to a detached position. This oscillation is accompanied by static pressure oscillations throughout the propulsion system. To avoid the onset of buzz, propulsion systems are designed to avoid the unstable region. For aircraft turbojet engines, where a variable geometry inlet is economically feasible, the inlet configuration is adjusted at each flight condition to maintain near critical or slightly subcritical operation to obtain maximum pressure recovery. This may be achieved by change of ramp angles for a two-dimensional inlet, by change of centerbody location for an axisymmetric inlet, or by varying the bleed flow. Subcritical operation has the additional advantage of providing relatively undistorted flow, desirable for a turbojet compressor. For a fixed-geometry inlet, typical of ramjet application, the inlet is operated supercritically. The inlet is designed with a pressure margin or maximum pressure recovery less than critical. This acts as a safety factor to assure that the inlet will not achieve critical condition, much less an unstable subcritical condition.

The third figure of merit is the performance cost of the inlet, the drag. There are several types of drag attributed to the inlet. There is wave drag associated with the cowl shape and on the cowl lip. For two-dimensional inlets with sideplates, there is a corresponding sideplate lip and wave drag. For inlets installed on the aft portion of a vehicle, a boundary layer diverter is provided to raise the inlet above the vehicle boundary layer so that it does not ingest the low pressure recovery air. This is usually a wedge-shaped structure. There is a drag associated with the diverter; and an optimum diverter height may be found by trading off pressure recovery gains with increased drag. Mass removal processes of bleed and sidespill also have momentum losses and hence drag associated with them. Finally, there is the additive drag of an inlet.

The term additive drag was originally defined by Ferri and Nucci (Ref. 3). A mathematical description of additive drag has been presented by Sibulkin (Ref. 4). First, consider a simple ramjet engine in accelerated flight at zero angle-of-attack, as shown in Figure 10a. The net propulsive thrust is the resultant sum of the axial components of the pressure and friction forces. The net internal thrust, $F_{n,i}$, may be evaluated from the momentum change between the entrance, Station 1, and the exit, Station e.

$$F_{n,i} = F_e - F_1 \tag{2-1}$$

where F_j = stream thrust at $j \equiv \dot{m}V_j + A_j(p_j - p_0)$. Thus, the net propulsive thrust, F_p, is equal to the net internal thrust minus the external drag forces, F_d.

$$F_p = F_{n,i} - F_d \tag{2-2}$$

In practice, engine performance is usually determined from freestream and exit conditions instead of from inlet entrance conditions. Thus, referring to Figure 10b, which includes the streamtube from 0 to 1, the net thrust, F_n, due to momentum change between Stations 0 and e is:

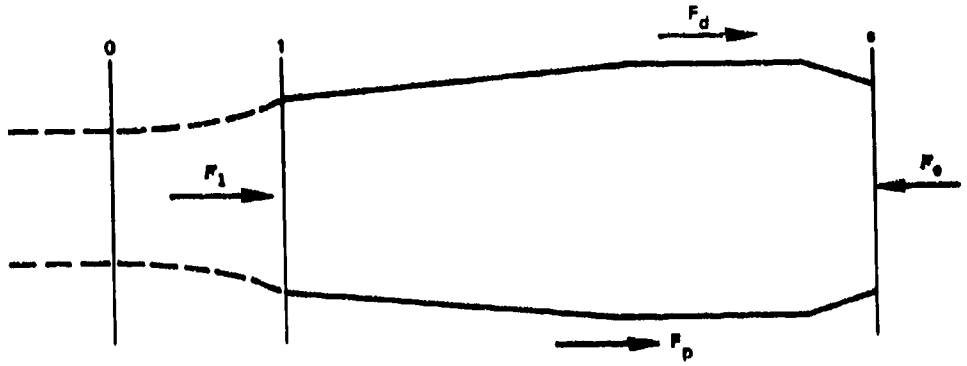

(a) USING STATIONS 1 AND e.

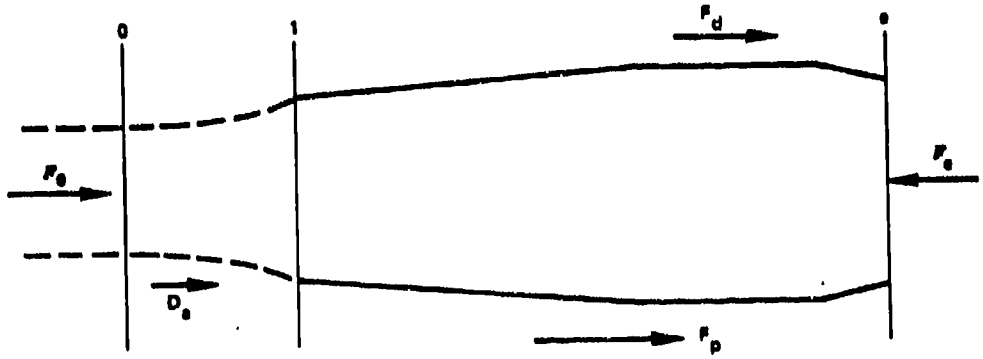

(b) USING STATIONS 0 AND e.

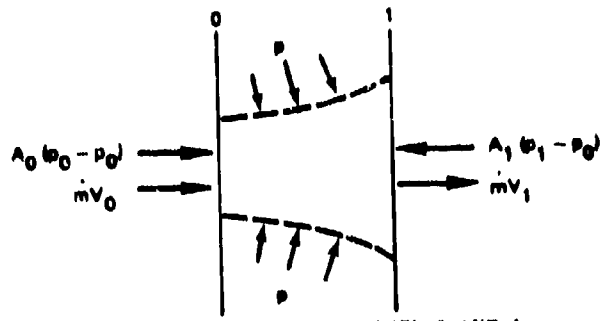

(c) ON STREAMTUBE BETWEEN 0 AND 1.

FIGURE 10. Forces Acting on a Ramjet Engine in Accelerated Flight (Open Nose Inlet).

$$F_n = F_e - F_0 \tag{2-3}$$

In this case, however,

$$F_p \neq F_n - F_d$$

since the momentum change between Stations 0 and 1 has not been considered. This momentum change may be considered as an additional drag force, D_a, called additive drag. Thus,

$$F_p = F_n - F_d - D_a \tag{2-4}$$

which defines additive drag. Comparing Equations 2-1 and 2-4 yields

$$D_a = F_n - F_{n,i} = F_1 - F_0 \tag{2-5}$$

or

$$D_a = \dot{m}V_1 + A_1(p_1 - p_0) - \dot{m}V_0 \tag{2-6}$$

Considering the streamtube from 0 to 1 as indicated in Figure 10c,

$$\int_{\text{Sta 0}}^{\text{Sta 1}} (p - p_0)dA_x - A_1(p_1 - p_0) = -\dot{m}V_0 + \dot{m}V_1 \tag{2-7}$$

where dA_x = axial projection of surface area, or from Equation 2-6,

$$D_a = \int_{\text{Sta 0}}^{\text{Sta 1}} (p - p_0)dA_x \tag{2-8}$$

This integral form of the equation is applicable to other geometries. Evaluation of the momentum terms results in a slightly different form of additive drag for each situation. Mount (Ref. 5) presents the following equation for both the axisymmetric and two-dimensional oblique shock inlets shown in Figure 11.

$$D_a = \int_{\text{Sta 0}}^{\text{Sta 1}} (p - p_0)dA_x = \left[\frac{\dot{w}}{g}V_1 + (p_1 - p_0)A_1\right]\cos\theta$$

$$- \frac{\dot{w}}{g}V_0 + (\bar{p}_s - p_0)A_s \tag{2-9}$$

where $\bar{p}_s$ is the average pressure acting on the compression surface, A_s.

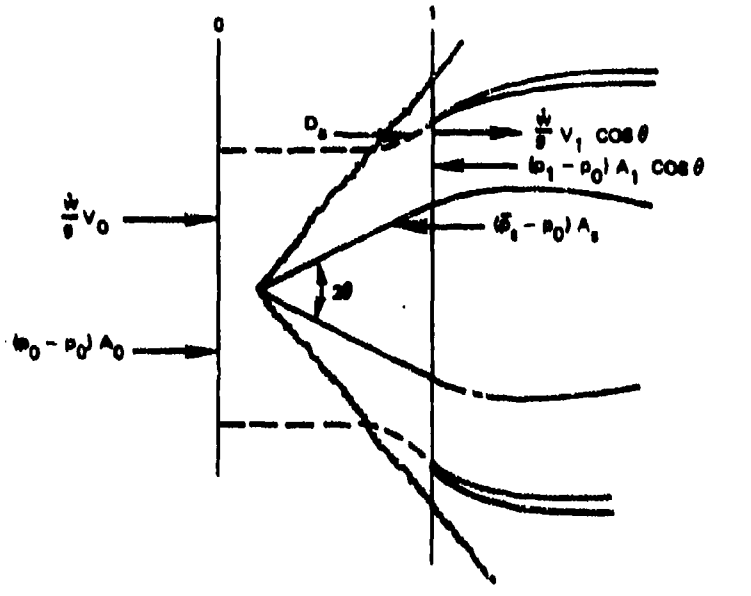

(a) AXISYMMETRIC INLET

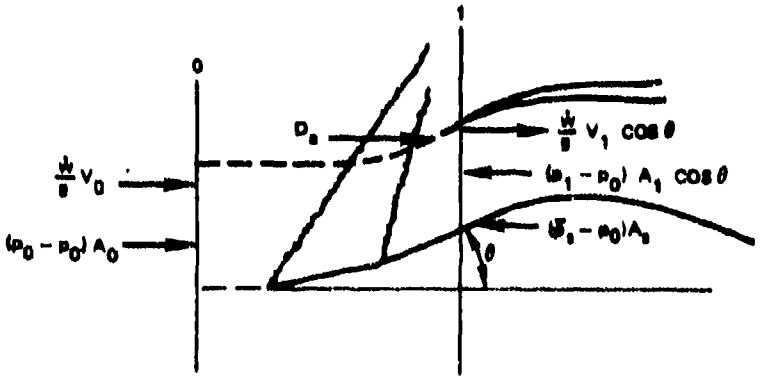

(b) TWO DIMENSIONAL INLET

FIGURE 11. Forces on Oblique Shock Inlets.

This differs from the relation for the open nose inlet, Equation 2-6, by the addition of the term $(\bar{p}_s - p_0)A_s$, which is the pressure force on the compression surface, and by a correction term of $\cos\theta$ to the exit momentum to account for a non-axial exit.

Additive drag appears to be only a bookkeeping term. Its physical significance may be seen by considering the boundary of the captured streamtube to be replaced

by a functionless sheet of solid material. No flow may pass through the sheet and since it conforms to the shape of the streamtube, the flowfield remains undistubed. The pressure forces acting on this extended cowl are easily visualized. Removal of this extension does not change the flow and, hence, the momentum through the inlet system. Distortion of the cowl extension would alter the flowfield and result in a different pressure distribution.

Additive drag occurs in two situations. When the inlet is operating critically or supercritically, at or above the design Mach number, the leading edge shock is at or within the cowl lip. Up to the cowl lip, the flow is undisturbed. Hence, the flow area does not change, and the additive drag is zero for purely two-dimensional flow. With subcritical operation, the terminal normal shock occurs on the compression surface and subsonic flow occurs behind the shock. Osmon (Ref. 6) has considered subcritical additive drag in the transonic region. He employed Moeckel's (Ref. 7) method for prediction of the plane shock shape. This equation was modified to account for lateral spillage; various coefficients were adjusted to fit experimental data. With a determination of the terminal shock shape and position, the pressures behind the various shocks were used to determine subcritical additive drag.

The second condition of additive drag is supercritical additive drag. In this case, the inlet is operating critically or supercritically below the design Mach number. Supercritical additive drag can be evaluated for simple geometries by means of the pressure integral. Consider the single ramp two-dimensional inlet of Figure 8. The static pressure behind the shock is constunt along the streamline and may be obtained from plane oblique shock relationships. The area over which this pressure acts is simply $(A_c - A_0)$ or $A_c(1 - A_0/A_c)$. For multiple oblique shocks, this process may be repeated for each shock. For axisymmetric inlets, the same approach is applied, numerically integrating across the rays. Sharp and Howe (Ref. 8) have employed this technique for determination of additive drag in an automated procedure for analysis of inlets. For two-dimensional inlets of finite width, there is some lateral spillage. Sideplates may be employed to restrict or eliminate this lateral flow at the expense of increased weight and drag. Sidewalls may also be constructed to provide additional sidewise compression. If a sideplate is designed to contain the entire shock system, there will be no sidespill. Sideplates are typically constructed with the sideplate leading edge as a straight line from the cowl lip to the inlet leading edge. Above design Mach number, there will be no spillage from this type of sideplate. In general, however, there will be lateral spillage from a two-dimensional inlet. This will alter the flowfield and the shape of the captured streamtube. To determine additive drag, the shape of the captured streamtube must be determined. This requires knowledge of the flowfield about the compression surface with lateral spillage.

Chapter 3. PREVIOUS INVESTIGATIONS

Little theoretical work has been performed on the problem of sidespill in two-dimensional inlets. This is partially due to the relatively recent emphasis on two-dimensional inlets; most of the previous inlet studies had been directed toward axisymmetric inlets. In addition, most inlet investigations are primarily experimental. Preliminary performance estimates are determined by a combination of theoretical and empirical techniques. Wind tunnel tests are then performed to verify the performance estimates and to select various design features such as bleed system, design, boundary layer diverter height, and installation effects.

INVESTIGATION OF CARRIERE AND LEYNAERT

Carriere and Leynaert (Ref. 9) have considered the problem of mass flow in two-dimensional inlets. No attempt has been made to determine the effects on additive drag. Consider a single ramp inlet with ramp angle, ψ, as shown in Figure 12. The

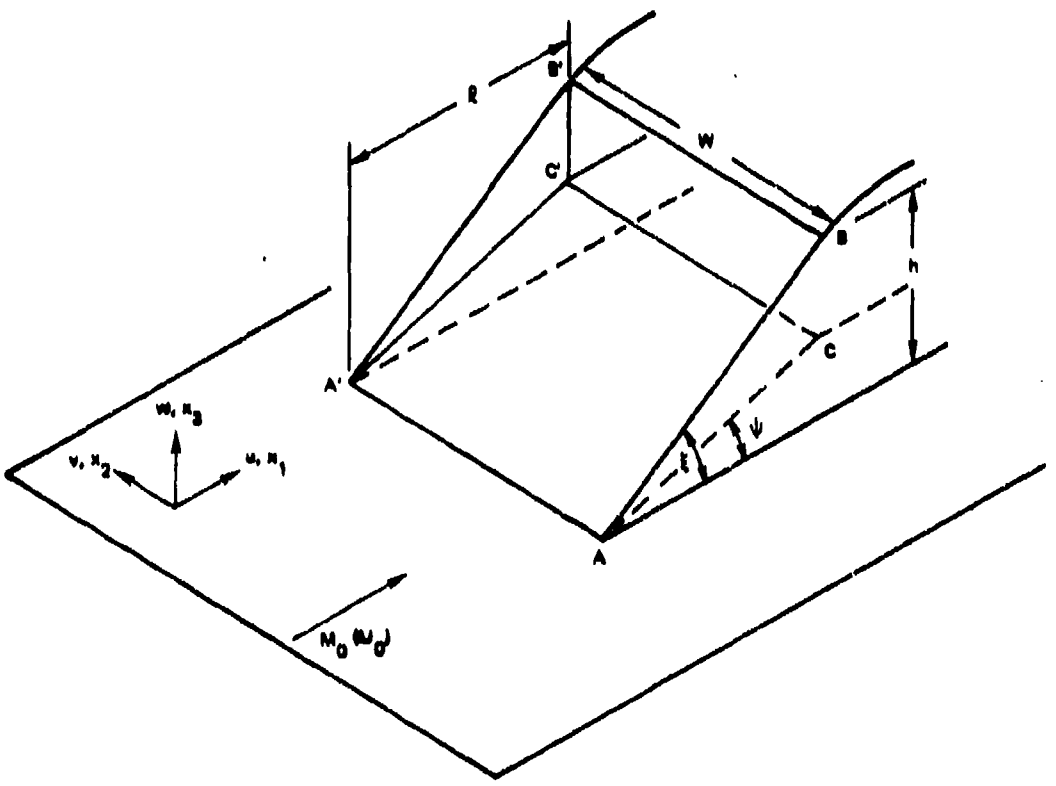

FIGURE 12. Two-Dimensional Inlet Nomenclature.

inlet has two lateral sidewalls with leading edges, AB and A'B', at an angle ξ. It is assumed that the ramp angle, ψ, is small and that the shock waves are comparable to Mach waves. This permits the use of linearized theory.

Three possible situations may be assumed a priori depending upon the value of the parameter $\beta W/\ell$, where β is the cotangent of the Mach angle, μ, and is equal to $\sqrt{M^2 - 1}$. The parameter $\beta W/\ell$ characterizes the lateral aspect ratio of the inlet and is the ratio of the width of the inlet to the radius of the Mach cone at the inlet entrance station. The three possibilities are illustrated in Figure 13. The Mach cones may be completely separate or may overlap. If the overlap occurs within the boundaries of the inlet or $1 < \beta W/\ell < 2$, the sidespill is unaffected and remains the same as the separated case. For narrow inlets where $\beta W/\ell < 1$, the Mach cone generated by one edge influences the flow at the opposite edge.

Consider a uniform approach flow with velocity components:

$$\begin{aligned} u_1 &= U_0 \\ u_2 &= 0 \\ u_3 &= 0 \end{aligned} \tag{3-1}$$

After a small perturbation such as that imposed by the inlet ramp, the velocity components are

$$\begin{aligned} u_1 &= U_0 + u' \\ u_2 &= v' \\ u_3 &= w' \end{aligned} \tag{3-2}$$

or normalizing by U_0

$$\begin{aligned} u_1 &= U_0(1 + u) \\ u_2 &= U_0 v \\ u_3 &= U_0 w \end{aligned} \tag{3-3}$$

In small perturbation theory, it is assumed that the perturbation components are small or

$$u, v, w \ll 1$$

Considering the inlet in Figure 12, the flow enters the inlet through the region BCB'C' of surface $A = W(h - \psi\ell)$ by geometry. The mass flow, $\dot{m}$, after linearization by small perturbations is

$$\dot{m} = \iint_A \rho(1 + u)U_0 \, dA \tag{3-4}$$

where ρ is the mass density and dA an element of the control surface.

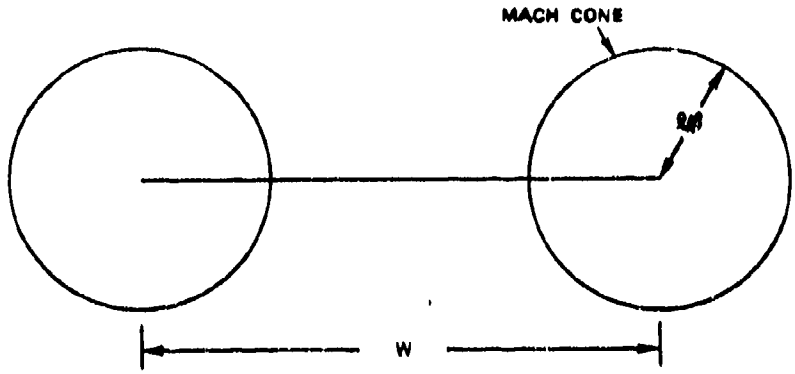

(a) $\beta W/\ell > 2$

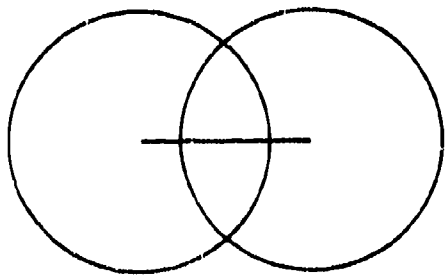

(b) $1 < \beta W/\ell < 2$

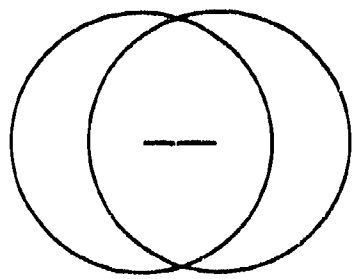

(c) $\beta W/\ell < 1$

FIGURE 13. Possible Inlet Flow Situations.

The local density, ρ, may be related to freestream density, ρ_0, by Mach number functions:

$$\frac{\rho}{\rho_0} = \frac{(1 + \frac{\gamma - 1}{2} M_0^2)^{1/\gamma - 1}}{(1 + \frac{\gamma - 1}{2} M^2)^{1/\gamma - 1}} \tag{3-5}$$

The local Mach number, M, may be written in terms of perturbation velocities

$$M^2 = [(U_0 + u')^2 + v'^2 + w'^2]/a^2 \tag{3-6}$$

$$M^2 = (U_0^2 + 2U_0 u')/a^2 \text{ to first order}$$

the speeds of sound are related by temperature ratios

$$\frac{a^2}{a_0^2} = \frac{\gamma R T}{\gamma R T_0} = \frac{T}{T_0} = \frac{1 + \frac{\gamma - 1}{2} M_0^2}{1 + \frac{\gamma - 1}{2} M^2} \tag{3-7}$$

Substituting a^2 into Equation 3-6

$$M^2 = \frac{U_0^2 + 2U_0 u'}{a_0^2} \frac{1 + \frac{\gamma - 1}{2} M^2}{1 + \frac{\gamma - 1}{2} M_0^2} \tag{3-8}$$

$$M^2 = M_0^2(1 + 2u) \frac{1 + \frac{\gamma - 1}{2} M^2}{1 + \frac{\gamma - 1}{2} M_0^2}$$

Solving for M^2

$$M^2 = \frac{M_0^2(1 + 2u)}{1 - 2u \frac{\gamma - 1}{2} M_0^2}$$

Thus,

$$1 + \frac{\gamma - 1}{2} M^2 = \frac{1 + \frac{\gamma - 1}{2} M_0^2}{1 - 2u \frac{\gamma - 1}{2} M_0^2} \tag{3-9}$$

or

$$\frac{1+\frac{\gamma-1}{2}M_0^2}{1+\frac{\gamma-1}{2}M^2} = 1 - 2u\frac{\gamma-1}{2}M_0^2 \tag{3-10}$$

From Equation 3-5

$$\frac{\rho}{\rho_0} = (1 - 2u\frac{\gamma-1}{2}M_0^2)^{1/\gamma-1} \tag{3-11}$$

Expanding with a binomial expansion to first order:

$$\frac{\rho}{\rho_0} = 1 - uM_0^2 \tag{3-12}$$

Thus Equation 3-4 may be written

$$\dot{m} = \rho_0 U_0 \iint_A (1+u)(1-uM_0^2)dA \tag{3-13}$$

$$\dot{m} = \rho_0 U_0 \iint_A [1 + u(1 - M_0^2)]\,dA \text{ to first order}$$

Since $\beta_0^2 = M_0^2 - 1$, Equation 3-13 becomes

$$\dot{m} = \rho_0 U_0 \iint_A (1 - \beta_0^2 u)dA \tag{3-14}$$

Thus, the flow rate entering the inlet may be determined once the distribution of the axial perturbation velocity, u, is found.

Consider the pure two-dimensional or ∞ case. For a weak two-dimensional wave where the flow is deflected through angle ψ*

$$u^\infty = \frac{u'}{U_0} \approx -\psi/\sqrt{M_0^2 - 1} = -\psi/\beta_0 \tag{3-15}$$

* Refer to Section 4-7, "Weak Oblique Shocks," in *Elements of Gasdynamics*, by H. W. Liepmann and A. Roshko. New York, N.Y., John Wiley & Sons, Inc., 1962, pp. 92-93.

Substituting into Equation 3-14

$$\dot{m}^{\infty} = \rho_0 U_0 \iint_A (1 + \psi\beta_0) dA$$

$$\dot{m}^{\infty} = \rho_0 U_0 (1 + \psi\beta_0) A \tag{3-16}$$

The entrance area, A, has been determined by geometry to be

$$A = W(h - \psi\ell) \tag{3-17}$$

Since $h/\ell = \tan \xi$

$$A = Wh(1 - \psi \cot \xi) \tag{3-18}$$

Thus Equation 3-16 becomes

$$\dot{m}^{\infty} = \rho_0 U_0 Wh[1 - \psi(\cot \xi - \beta_0) - \psi^2 \beta_0 \cot \xi] \tag{3-19}$$

Carriere and Leynaert present this equation only to first order:

$$\dot{m}^{\infty} = \rho_0 U_0 Wh[1 - \psi(\cot \xi - \beta_0)] \tag{3-20}$$

The ignored term, however, is not negligible. Consider, for example, the case of a 10-degree ramp and a 19.6-degree sidewall at a freestream Mach number of 1.96. The term $\psi^2 \beta_0 \cot \xi$ is equal to 0.144 which is not negligible as compared to the other terms. The value of $\dot{m}^{\infty}/\rho_0 U_0 Wh$ is determined to be 0.660 using Equation 3-19 and 0.804 using Equation 3-20. Thus, neglecting the second order term appears to be incorrect.

Carriere and Leynaert present all results relative to the two-dimensional result, $\dot{m}^{\infty}$. Calculations by Fenain by the method of homogeneous flows are cited without reference; and the following results are presented without proof.

a. With lateral plates and $\beta_0 W/\ell > 1$

$$\frac{\dot{m} - \dot{m}^{\infty}}{\dot{m}^{\infty}} = 2\frac{\psi}{\pi}\frac{\ell}{W}\frac{k^2 K'^2 - E'^2}{k' E'} \tag{3-21}$$

where

$$k = \beta_0 \tan \xi$$

$$k' = \sqrt{1 - k^2}$$

K', E' = Complete elliptic integrals of the first and second kind, respectively of modulus k'

b. Without lateral plates and:

1. $\beta_0 W/\ell = k_1 \geq 1$

$$\frac{\dot{m} - \dot{m}^\infty}{\dot{m}^\infty} = -\frac{\psi}{\pi}\frac{\ell}{W}\left[k' + \frac{\sin^{-1} k}{k}\right] \tag{3-22}$$

2. $k' \leq k_1 \leq 1$

$$\frac{\dot{m} - \dot{m}^\infty}{\dot{m}^\infty} = -\frac{\psi}{\pi}\frac{\ell}{W}\left[k' + \frac{\sin^{-1} k}{k} - \frac{(1 - k_1)^2}{k}\frac{\pi}{2}\right] \tag{3-23}$$

3. $k_1 < k' \leq 1$

$$\frac{\dot{m} - \dot{m}^\infty}{\dot{m}^\infty} = -\frac{\psi}{\pi}\frac{\ell}{W}\left[k' + \frac{\sin^{-1} k}{k} - \sqrt{k'^2 - k_1^2} - \frac{(1 + k_1)^2}{k}\sin^{-1}\frac{k}{k_1} + 2k_1 \cos^{-1}\frac{k_1}{k'} + \frac{2k_1}{k}\sin^{-1}\frac{kk_1}{k'\sqrt{1 - k_1^2}}\right] \tag{3-24}$$

Note that for a selected inlet height and Mach number, all of these results have the form $m - m^\infty/m^\infty$ = constant times $(\psi/\pi)(\ell/W)$ which is expected for linearized theory.

Application of these equations has revealed that the equations cannot be evaluated when the cowl angle, ξ, is greater than the Mach angle, μ. Physically, this would occur when the Mach wave from the leading edge enters the cowl. This observation suggests that no distinction has been made between a Mach wave angle and the actual shock wave. This is considered to be in error since there is a significant difference between the Mach wave angle and the angle of a shock wave even for small ramp angles.

HOMOGENEOUS CONICAL FLOW

The method of homogeneous conical flows may be applied to the problem of spillage of two-dimensional inlets. Pawlikowski (Ref. 10) has employed this method to determine perturbation velocities and spillage on the compression ramp of the inlet. Milne-Thomson (Ref. 11) presents a basic discussion of conical flow. He employs this method to determine perturbation velocities on various airfoils. Since Milne-Thomson is primarily concerned with aerodynamic forces, he uses these velocities to determine lifting pressures. The analysis of Milne-Thomson will be described here as an aid to understanding and as a contrast to the investigation of Pawlikowski. Later, the velocity solution of Milne-Thomson will be applied to the spillage problem.

Conical flow is a flow pattern in which the state of the flow is the same at every point along a ray drawn from an origin or vertex. Thus, conditions depend only on the direction of the ray, but not on the distance along it. This means that any property is a homogeneous function of degree zero in x, y, z, and depends only on the ratio of x:y:z. A conical boundary condition implies conical flow. Since the edge of an inlet compression ramp imposes a conical boundary condition, the conical flow analysis may be applied to the inlet flowfield.

For small perturbations in the coordinates of Figure 14, u, v, $w \ll V$, and neglecting squares and products, the perturbation equation for supersonic flow is

$$-(M_\infty^2 - 1)\frac{\partial^2 S}{\partial x^2} + \frac{\partial^2 S}{\partial y^2} + \frac{\partial^2 S}{\partial z^2} = 0 \tag{3-25}$$

where S may be any of the quantities: velocity potential, Φ, perturbation velocity components u, v, or w, pressure, p, or density, ρ.

Equation 3-25 may be rewritten as

$$-\cot^2 \mu \frac{\partial^2 S}{\partial x^2} + \frac{\partial^2 S}{\partial y^2} + \frac{\partial^2 S}{\partial z^2} = 0 \tag{3-26}$$

since $\cot \mu = \sqrt{M^2 - 1}$

Substituting $X = ix \tan \mu$, Equation 3-26 reduces to the Laplace equation

$$\frac{\partial^2 S}{\partial X^2} + \frac{\partial^2 S}{\partial y^2} + \frac{\partial^2 S}{\partial z^2} = 0 \tag{3-27}$$

In spherical polar coordinates as defined in Figure 15,

$$X = R_1 \cos \omega$$
$$y = R_1 \cos \theta \sin \omega$$
$$z = R_1 \sin \theta \sin \omega$$

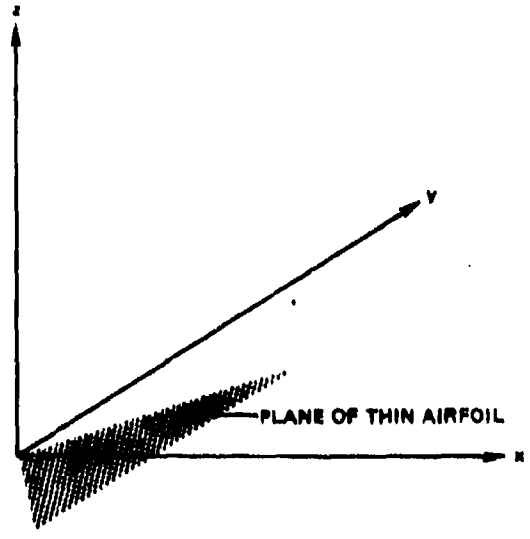

FIGURE 14. Definition of Axes.

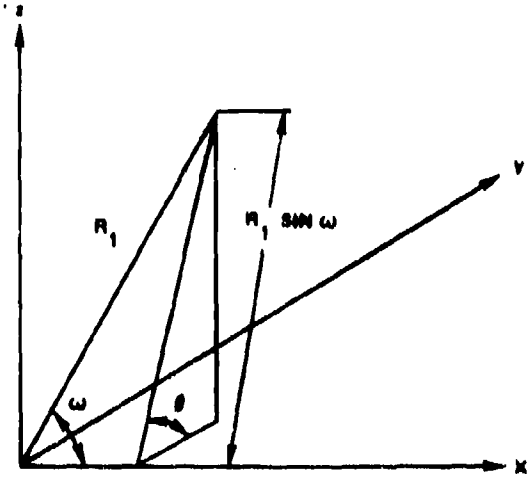

FIGURE 15. Transformation from Cartesian to Spherical Coordinates.

Laplace's equation becomes

$$\frac{\partial}{\partial R_1}\left(R_1^2 \frac{\partial S}{\partial R_1}\right) + \frac{1}{\sin \omega} \frac{\partial}{\partial \omega}\left(\sin \omega \frac{\partial}{\partial \omega}\right) + \frac{1}{\sin^2 \omega} \frac{\partial^2 S}{\partial \theta^2} = 0 \tag{3-28}$$

When S is independent of R_1, as in conical flow, Equation 3-28 becomes

$$\frac{1}{\sin \omega} \frac{\partial}{\partial \omega}\left(\sin \omega \frac{\partial S}{\partial \omega}\right) + \frac{1}{\sin^2 \omega} \frac{\partial^2 S}{\partial \theta^2} = 0 \tag{3-29}$$

By substituting

$$\chi = \log \tan 1/2\omega \tag{3-30}$$

$$\frac{\partial S}{\partial \omega} = \operatorname{cosec} \omega \frac{\partial S}{\partial \chi} = \frac{1}{\sin \omega} \frac{\partial S}{\partial \chi}$$

Equation 3-29 becomes

$$\frac{\partial^2 S}{\partial \chi^2} + \frac{\partial^2 S}{\partial \theta^2} = 0 \tag{3-31}$$

This has the general real-valued solution*

$$S = F(\chi + i\theta) + \bar{F}(\chi - i\theta) \tag{3-32}$$

where F is an arbitrary twice differentiable function.

$$\tan 1/2\omega = \frac{\sin \omega}{1 + \cos \omega} \tag{3-33}$$

$$e^{\chi + i\theta} = e^{\chi} e^{i\theta} = e^{i\theta} \tan 1/2\omega = (\cos \theta + i \sin \theta)\left(\frac{\sin \omega}{1 + \cos \omega}\right)$$

$$e^{\chi + i\theta} = \frac{\cos \theta \sin \omega + i \sin \theta \sin \omega}{1 + \cos \omega}$$

from definition of polar coordinates

$$e^{\chi + i\theta} = \frac{y + iz}{X + R_1} \tag{3-34}$$

* The most *general* solution is $S = F(\chi + i\theta) + G(\chi - i\theta)$ but the most general *real-valued* solution is given in Equation 3-32.

Thus $\chi + i\theta$ is a function of $(y + iz)/(X + R_1)$ and from Equation 3-32, the general real-valued solution of Laplace's equation of zero degree is S_0 where

$$S_0 = f_1\left(\frac{y + iz}{X + R_1}\right) + \bar{f}_1\left(\frac{y - iz}{X + R_1}\right) \tag{3-35}$$

where f_1 denotes an arbitrary function. Since $R_1^2 = X^2 + y^2 + z^2$ or

$$R_1 = \sqrt{y^2 + z^2 - x^2 \tan^2 \mu}$$

$$X + R_1 = ix \tan \mu + \sqrt{y^2 + z^2 - x^2 \tan^2 \mu}$$

$$X + R_1 = i(x \tan \mu + R_2)$$

where

$$R_2^2 = x^2 \tan^2 \mu - y^2 - z^2 \tag{3-36}$$

since

$$\frac{y + iz}{X + R_1} = (-i)\frac{y + iz}{x \tan \mu + R_2} \tag{3-37}$$

The general real-valued solution of degree zero of Equation 3-25 is

$$S_0 = f\left(\frac{y + iz}{x \tan \mu + R_2}\right) + \bar{f}\left(\frac{y - iz}{x \tan \mu + R_2}\right) \tag{3-38}$$

where f is an arbitrary twice differentiable function. This solution applies to all points such that R_2^2 is positive. This is all points within the Mach cone

$$y^2 + z^2 = x^2 \tan^2 \mu \tag{3-39}$$

Introducing Busemann's (Ref. 12) complex variable, $e = x \tan \mu + R_2$, the general solution becomes

$$S_0 = f(e) + \bar{f}(\bar{e}) \tag{3-40}$$

Introducing the dimensionless variables, r, s, s*, which satisfy

$$s = r\cos\theta = \frac{y}{x\tan\mu} \tag{3-41}$$

$$s^* = r\sin\theta = \frac{z}{x\tan\mu}$$

then

$$\epsilon = \frac{s + is^*}{1 + (1 - s^2 - s^{*2})^{1/2}} = \frac{r(\cos\theta + i\sin\theta)}{1 + (1 - r^2)^{1/2}} = Re^{i\theta} \tag{3-42}$$

where

$$R = \frac{r}{1 + (1 - r^2)^{1/2}} = \frac{1 - (1 - r^2)^{1/2}}{r} \tag{3-43}$$

If the point $re^{i\theta}$ is marked in an Argand diagram called the physical plane and the point $Re^{i\theta}$ marked in another, the ϵ plane as in Figure 16, the points correspond to a mapping in which points of a ray from the origin at angle θ from the real axis in the ϵ plane. This mapping is not conformal. From Equation 3-43 it may be noted that $R = 0$ at the origin $r = 0$. On the circumference of the circles $R = 1$ when $r = 1$. R is complex outside the circle $r > 1$. Thus, a Mach circle may be referred to interchangeably in the physical or ϵ planes.

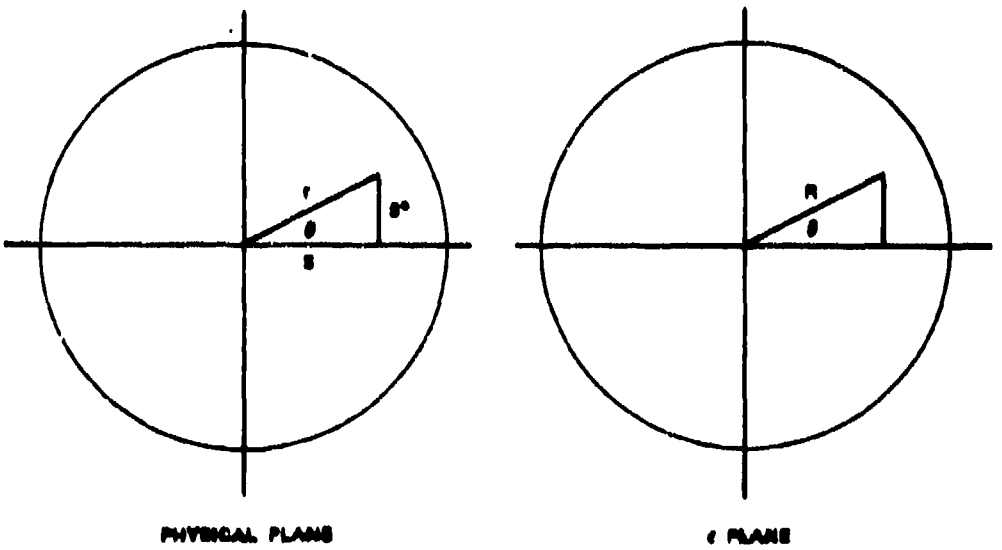

FIGURE 16. Transformation from Physical Plane to ϵ Plane.

In Equation 3-40 the general real-valued solution of the linearized equation was found to be the form $f(e) + \bar{f}(\bar{e})$. Since the perturbation velocity components u, v, and w are solutions of this type, it follows that they are the real parts of functions of the complex variable e and complex velocity components may be written

$$\begin{aligned} U(e) &= u + iu^* \\ V(e) &= v + iv^* \\ W(e) &= w + iw^* \end{aligned} \tag{3-44}$$

where u*, v*, and w* are also real. Since

$$\begin{aligned} u^* - iu &= -iU(e) \\ v^* - iv &= -iV(e) \\ w^* - iw &= -iW(e) \end{aligned}$$

The components u*, v*, and w* are perturbation velocity components of some other conical flow.

The complex velocity components are related by the compatibility relationships

$$\frac{U'}{2e \tan \mu} = \frac{V'}{-(1+e^2)} = \frac{W'}{-i(1-e^2)} \tag{3-45}$$

The derivation of the compatibility relationships is included in Appendix A.

To determine the flowfield about an airfoil, some terms and nomenclature must first be defined. An edge may be leading, trailing, or axial which Milne-Thomson denotes as L, T, and A. If a line drawn parallel to the freestream velocity vector enters the airfoil when it crosses an edge, the edge is called a leading edge. If the line leaves the airfoil as it crosses the edge, the edge is trailing. If the edge is parallel to the freestream velocity vector, it is axial. In addition, an edge may be termed subsonic, sonic, or supersonic, depending upon the normal component of the freestream velocity. A subsonic edge will fall within the Mach cone while a supersonic edge will fall outside. A sonic edge corresponds with the Mach cone. Milne-Thomson denotes this by subscripts i, s, and o for inside, sonic, and outside. Thus, for example, an intersection may be denoted L_oT_i, indicating a leading edge outside the Mach cone and a trailing edge inside. For an axial edge, the subscript is dropped since it must be subsonic.

To determine boundary conditions, the physical situation is reduced to a Mach circle in the physical plane. Consider a L_oL_o airfoil oriented at a small angle of attack, α, to freestream velocity, as shown in Figure 17A. The edges ℓ_1 and ℓ_2 are at angles δ_1 and δ_2, respectively, to the axis and intersect an arbitrary plane, P, perpendicular to the axis at points L_1 and L_2. The intersections with the plane P are shown in Figure 17b with corresponding identification. With supersonic edges, two

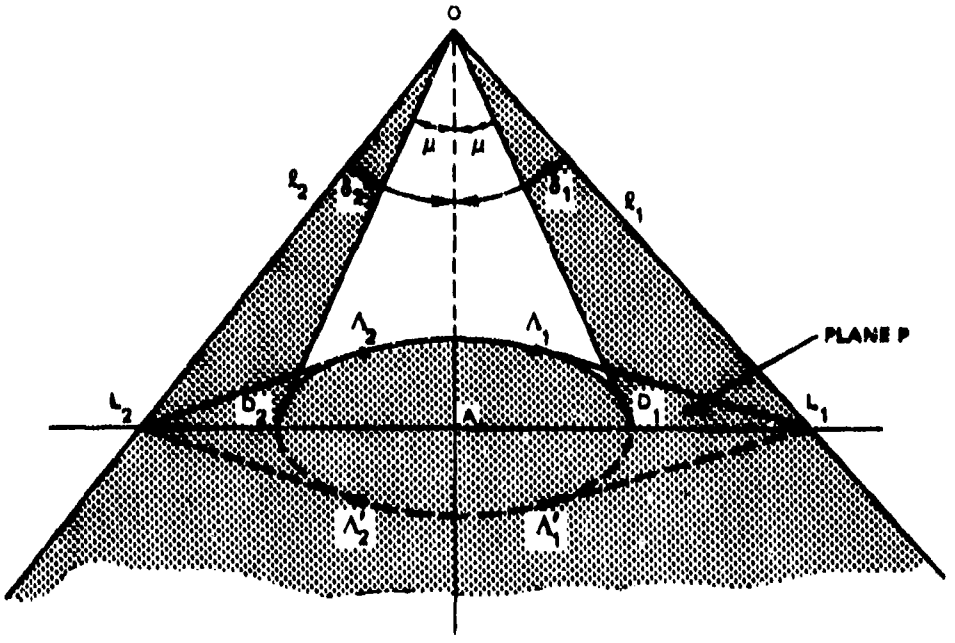

(a)

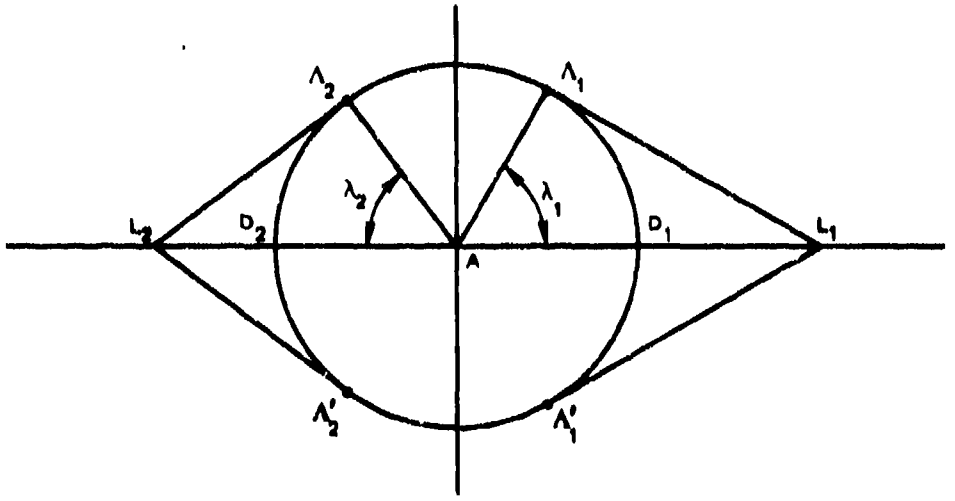

(b)

FIGURE 17. (a) Physical Representation of L_0L_0 Airfoil; (b) L_0L_0 Airfoil on Physical Plane P.

planes may be drawn from the edges tangent to the cone at points Λ and Λ'. The points at which the Mach cone intersects the plane of the airfoil are denoted D_1 and D_2. The angles between the tangency points and the plane of the airfoil are denoted by λ.

$$\cos \lambda_1 = \frac{A\Lambda_1}{AL_1} = \frac{A\Lambda_1}{OA} \frac{OA}{AL_1} = \tan \mu \cot \delta_1 \tag{3-46}$$

Similarly, $\cos \delta_2 = \tan \mu \cot \delta_2$.

The physical significance of the tangent planes may be realized by considering each point on the leading edge as a generator of a Mach cone as shown in Figure 18.

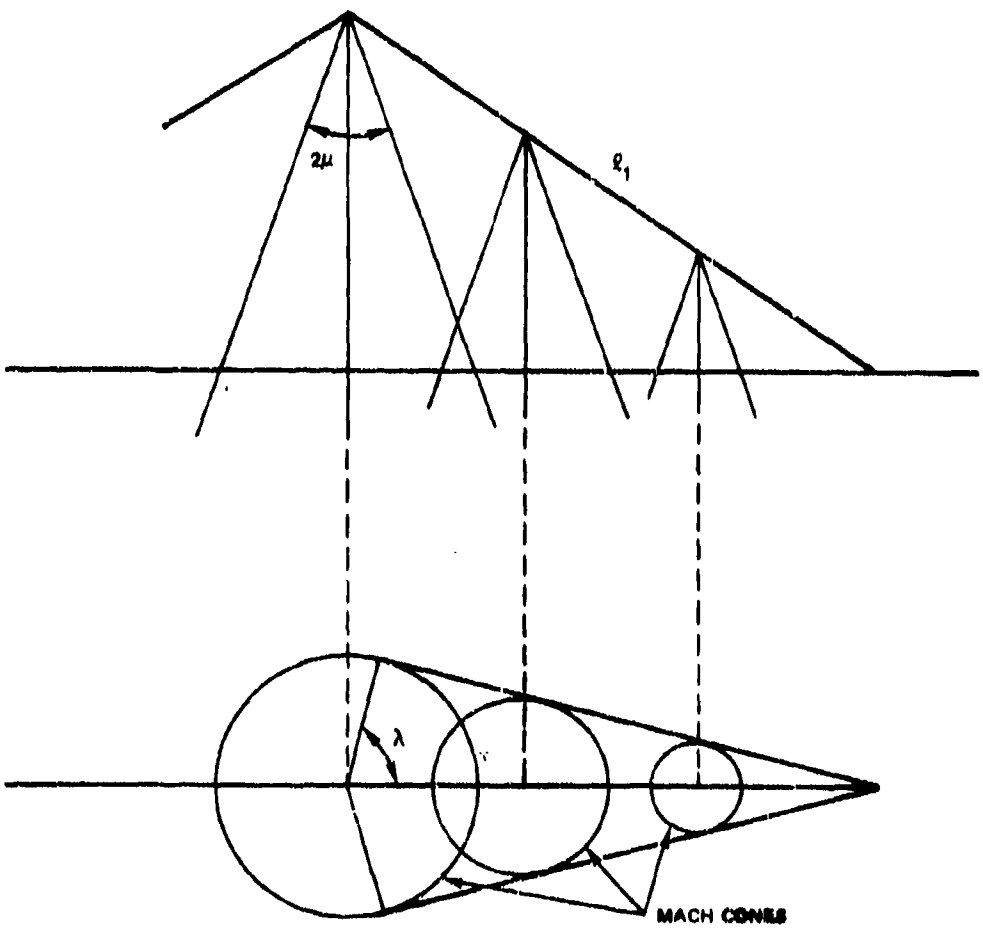

FIGURE 18. Definition of Region Where Two-Dimensional Boundary Conditions Apply.

The planes formed by these cones are the planes $\Lambda_1 L_1$ and $\Lambda_1' L_1$. Thus, these planes define the region of influence of the airfoil where the perturbation velocities are defined by two-dimensional flow. Therefore, the streamwise components of the perturbation velocities in Figure 17 are:

$u = u_1$ on arc $D_1\Lambda_1$
$u = - u_1$ on arc $D_1\Lambda_1'$
$u = u_2$ on arc $D_2\Lambda_2$
$u = - u_2$ on arc $D_2\Lambda_2'$
$u = 0$ on arc $\Lambda_1\Lambda_2$
$u = 0$ on arc $\Lambda_1'\Lambda_2'$

where u_1 and u_2 are appropriate two-dimensional perturbation velocities

The case of an L_0T_1 airfoil is shown in Figure 19a. Since the leading edge does not intersect the plane of the Mach circle, the ray is extended to intersect at point L'. Also, since the trailing edge is inside the Mach cone, the tangent planes are not present. This case results in the Mach circle representation of Figure 19b. The perturbation velocities are:

$u = u_0$ on arc $D_2\Lambda$
$u = - u_0$ on arc $D_2\Lambda'$
$u = 0$ on arc $\Lambda' D_1\Lambda$

These cases illustrate the essential representation for other cases.

The basic problem in conical flow is to find a function, $f(\epsilon)$, analytic within the Mach circle, γ, whose real part takes on specified values on the circumference. Since a point on the circumference can be specified by the angle θ from the real axis, the real part of $f(\epsilon)$ must take on the value $F(\theta)$ on the circumference where $F(\theta)$ is given. For a point σ on the circumference

$$\sigma = e^{i\theta} \tag{3-47}$$

or

$$\theta = (\log \sigma)/i \tag{3-48}$$

Thus,

$$F(\theta) = F[(\log \sigma)/i] = g(\sigma) \tag{3-49}$$

where the function $g(\sigma)$ is likewise known. The real part of $f(\epsilon)$ is $1/2f(\epsilon) + 1/2\bar{f}(\bar{\epsilon})$.

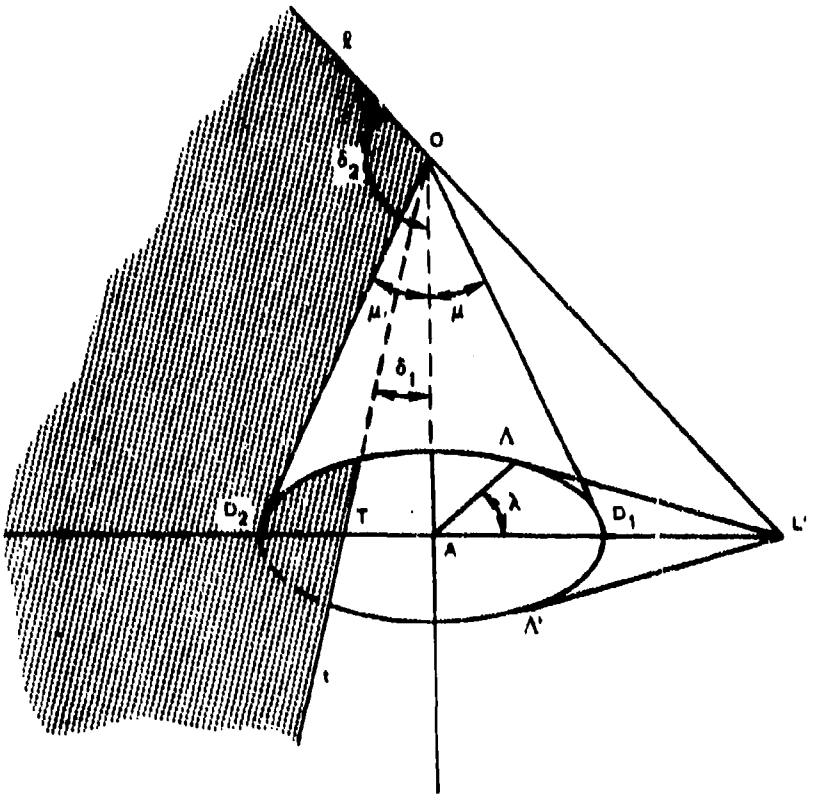

(a)

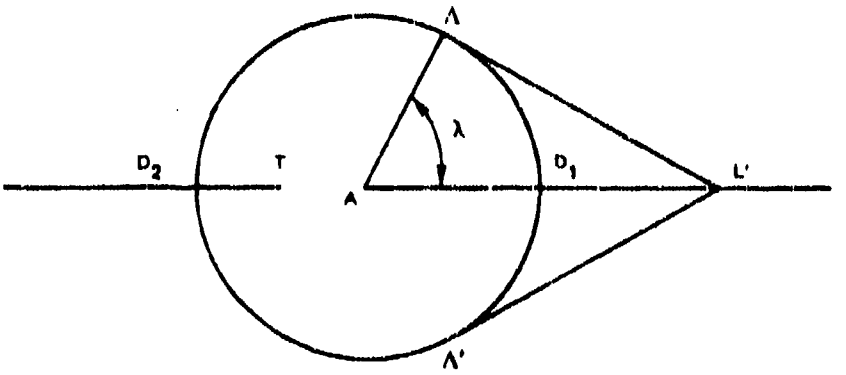

(b)

FIGURE 19. (a) Physical Representation of L_0T_1 Airfoil; (b) L_0T_1 Airfoil on Physical Plane.

On the circumference

$$\epsilon = \sigma \text{ and } \bar{\sigma} = e^{-i\theta} = 1/\sigma$$

therefore

$$f(\sigma) + \bar{f}(1/\sigma) = 2g(\sigma) \tag{3-50}$$

Multiplying this equation by $d\sigma/2\pi i(\sigma - \epsilon)$ and integrating around the Mach circle, γ

$$\frac{1}{2\pi i}\int_\gamma \frac{f(\sigma)d\sigma}{\sigma - \epsilon} + \frac{1}{2\pi i}\int_\gamma \frac{\bar{f}(1/\sigma)d\sigma}{\sigma - \epsilon} = \frac{1}{\pi i}\int_\gamma \frac{g(\sigma)d\sigma}{\sigma - \epsilon} \tag{3-51}$$

By Cauchy's formula, the first integral is $f(\epsilon)$. The second integral may be evaluated by the residue theorem. Since $f(\epsilon)$ has been assumed analytic within the Mach circle, it may be expanded in an infinite series.

$$f(\epsilon) = a_0 + a_1\epsilon + a_2\epsilon^2 + \cdots$$

Thus

$$\bar{f}(1/\sigma) = \bar{a}_0 + \bar{a}_1/\sigma + \bar{a}_2/\sigma^2 + \cdots \tag{3-52}$$

By Cauchy's residue theorem

$$\frac{1}{2\pi i}\int_\gamma \frac{\bar{a}_0 d\sigma}{\sigma - \epsilon} = \bar{a}_0 = \bar{f}(0) \tag{3-53}$$

and

$$\frac{1}{2\pi i}\int_\gamma \frac{\bar{a}_n d\sigma}{\sigma^n(\sigma - \epsilon)} = 0 \text{ for } n > 0 \tag{3-54}$$

That is, the residue is the appropriate term of the Laurent's series. Thus, from Equation 3-51

$$f(\epsilon) + \bar{f}(0) = \frac{1}{\pi i}\int_\gamma \frac{g(\sigma)d\sigma}{\sigma - \epsilon} \tag{3-55}$$

In many applications, $g(\sigma)$ is constant over arcs of the circumference. Consider for example that $g(\sigma) = u_0$ from $\theta = -\lambda$ to $+\lambda$ and is zero on the rest of the circumference. Then,

$$\frac{1}{\pi i}\int_{\gamma}\frac{g(\sigma)d\sigma}{\sigma - \epsilon} = \frac{u_0}{\pi i}\left[\log(\sigma - \epsilon)\right]_{\sigma=\bar{\epsilon}_1}^{\sigma=\epsilon_1} \tag{3-56}$$

for $\epsilon_1 = e^{i\lambda}$ and $\bar{\epsilon}_1 = e^{-i\lambda}$.

Therefore,

$$f(\epsilon) = -\bar{f}(0) + \frac{u_0}{\pi i}\left[\log(\epsilon_1 - \epsilon) - \log(\bar{\epsilon}_1 - \epsilon)\right] \tag{3-57}$$

$\bar{f}(0)$ is a constant determined by other information. For $f(\epsilon) = u_0$ when $\epsilon = 1$ or $\theta = 0$, then

$$u_0 = -\bar{f}(0) + \frac{u_0}{\pi i}\left[\log(\epsilon_1 - 1) - \log(\bar{\epsilon}_1 - 1)\right]$$

which gives*

$$\bar{f}(0) = u_0\lambda/\pi$$

The same principle can be used to determine a function $f(\epsilon)$ analytic within a semicircle of unit radius where $f(\epsilon)$ is real-valued on the diameter and the real part of $f(\epsilon)$ takes given values on the semicircle. To solve this problem, the circle is complete by reflection as shown in Figure 20. The function $f(\epsilon)$ and its reflection are determined to be complex conjugates. This reduces the problem to the one just solved.

* This result is based on the convention that the branch cut is on the negative real axis and that all angles thus may take on value between $-\pi$ and π.

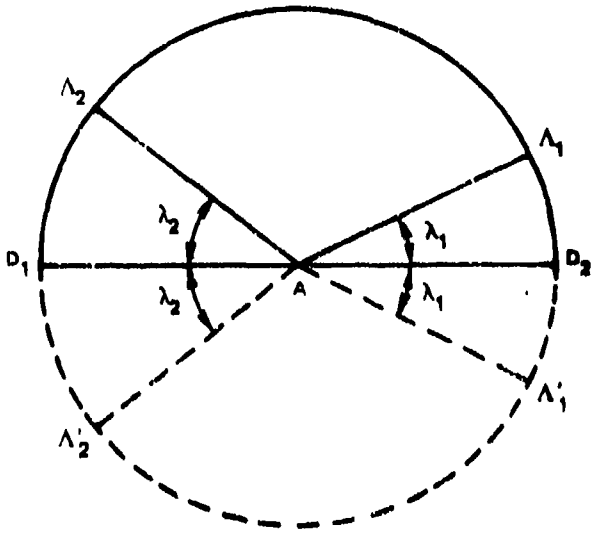

FIGURE 20. Reflection of Semi-Circle.

To investigate the flowfield of a two-dimensional inlet, the model of a rectangular airfoil may be employed. This is equivalent to a L_0A airfoil in Milne-Thomson's notation. The physical situation is shown in Figure 21a, while the projection in the ϵ plane is shown in Figure 21b. The boundary conditions are also included in the figure. On arc $D\Lambda$, the perturbation velocity, u, is equal to the two-dimensional perturbation velocity $u_0 = \alpha V \tan \mu \operatorname{cosec} \lambda$. For $\delta = \pi/2$, u_0 is equal to $\alpha V \tan \mu$. On the lower arc $D\Lambda'$, u is $-u_0$. On the surface of the airfoil AD, the imaginary component u^* of the complex perturbation velocity, U, is zero. Consider an airfoil at angle of attack, α. For small angles where $\sin \alpha = \alpha$ and $\cos \alpha = 1$, the freestream velocity may be considered as having velocity components V, 0, and αV in the coordinates of Figure 14. On the surface, since the air cannot flow through the airfoil, $w + \alpha V = 0$. From the compatibility relationship of Equation 3-45,

$$\frac{U'}{2\epsilon \tan \mu} = - \frac{W'}{i(1 - \epsilon^2)}$$

$$W' = - \frac{i(1 - \epsilon^2)}{2\epsilon \tan \mu} V'$$

$$d(w + iw^*) = - i \frac{(1 - \epsilon^2)}{2\epsilon \tan \mu} d(u + iu^*) \qquad (3\text{-}58)$$

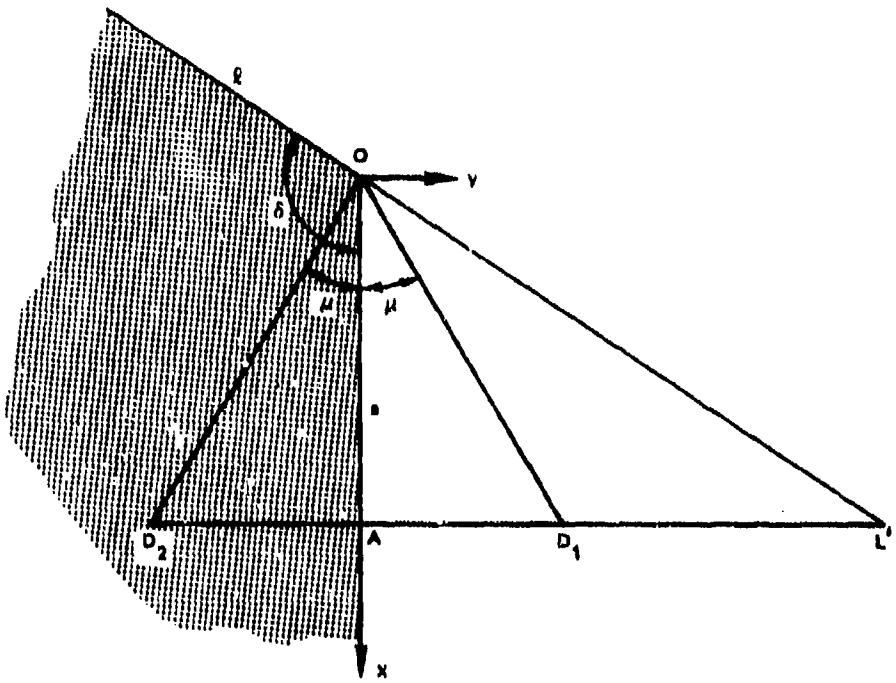

(a)

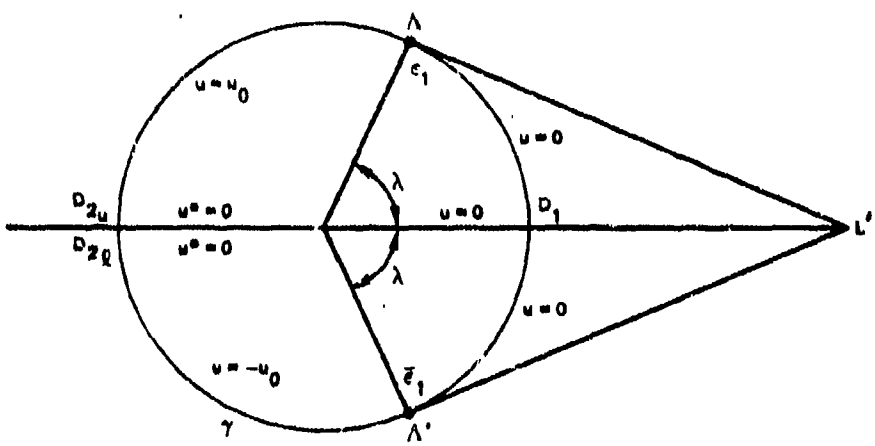

(b)

FIGURE 21. (a) Physical Representation of L_0A Airfoil; (b) L_0A Airfoil in Physical Plane.

On the surface of the airfoil, ϵ is real and hence $(1 - \epsilon^2)/2\epsilon \tan \mu$ is real. Collecting the real terms of Equation 3-58,

$$dw = -i^2 \frac{(1 - \epsilon^2)}{2\epsilon \tan \mu} du^*$$

Since $w = -\alpha V$ = constant, $dw = 0$. Therefore, $du^* = 0$ or u^* = constant. Without loss of generality, the constant may be considered to be zero so that

$$u^* = 0$$

and

$$u = U(\epsilon)$$

on the airfoil surface.

To solve the problem of the L_0A airfoil, define $\nu^2 = \epsilon$ mapping the Mach circle, γ, on a semi-circle in the ν plane which is completed by reflection as shown in Figure 22. If σ is a point on the circumference, γ'

$$U(\sigma) + \bar{U}(1/\sigma) = 2u(\sigma) \tag{3-59}$$

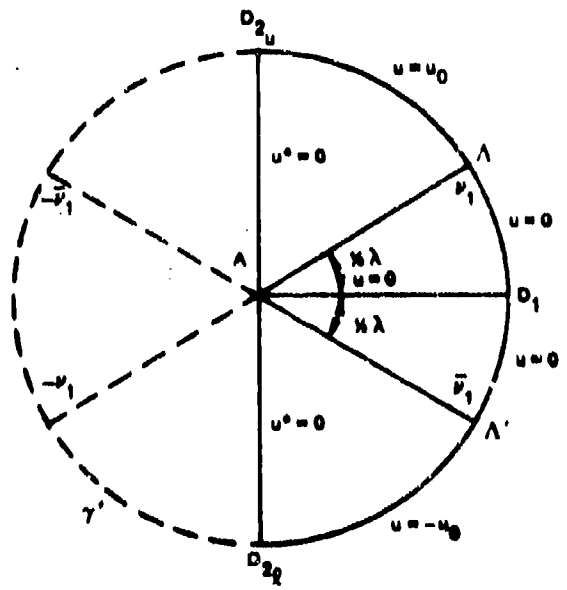

FIGURE 22. L_0A Airfoil in ν Plane.

As shown previously, this leads to

$$U(\nu) + \overline{U}(0) = \frac{2u_0}{2\pi i}\int_{\nu_1}^{-\bar{\nu}_1} \frac{d\sigma}{\sigma - \nu} - \frac{2u_0}{2\pi i}\int_{-\nu_1}^{\bar{\nu}_1} \frac{d\sigma}{\sigma - \nu} \tag{3-60}$$

Since $u = u^* = 0$ at $\nu = 0$, $U(0) = 0$, and hence $\overline{U}(0) = 0$, which yields:

$$U(\nu) = -\frac{iu_0}{\pi} \log \frac{(\nu_1 + \nu)(\bar{\nu}_1 + \nu)}{(\nu_1 - \nu)(\bar{\nu}_1 - \nu)} \tag{3-61}$$

Since Milne-Thomson is concerned with the pressure forces on the airfoil, he does not determine the other perturbation velocity components.

EXTENSION OF THEORY

The compatibility relationships may be employed to determine these other components. Equation 3-61 may be rewritten

$$U(\nu) = -\frac{iu_0}{\pi} [\log (\nu_1 + \nu) + \log (\bar{\nu}_1 + \nu) - \log (\nu_1 - \nu) - \log (\bar{\nu}_1 - \nu)] \tag{3-62}$$

The compatibility relations are:

$$\frac{U(e)'}{2e \tan \mu} = -\frac{V(e)'}{(1 + e^2)} = -\frac{W(e)'}{i(1 - e^2)}$$

In terms of the variable ν where $\nu^2 = e$

$$U(e)' = \frac{dU(e)}{de} = \frac{dU(\nu)}{d\nu}\frac{d\nu}{de} = U(\nu)'\frac{d\nu}{de}$$

Similarly

$$V(\nu)' = V(\nu)' \frac{d\nu}{de}$$

$$W(e)' = W(\nu)' \frac{d\nu}{de}$$

Thus the compatibility relationships become

$$\frac{U(\nu)'}{2e \tan \mu} \frac{d\nu}{de} = -\frac{V(\nu)'}{(1+e^2)} \frac{d\nu}{de} = -\frac{W(\nu)'}{i(1-e^2)} \frac{d\nu}{de}$$

or dividing by $\frac{d\nu}{de}$

$$\frac{U(\nu)'}{2e \tan \mu} = -\frac{V(\nu)'}{(1+e^2)} = -\frac{W(\nu)'}{i(1-e^2)} \tag{3-63}$$

In terms of ν

$$\frac{U'}{2\nu^2 \tan \mu} = -\frac{V'}{(1+\nu^4)} = -\frac{W'}{i(1-\nu^4)} \tag{3-64}$$

Thus,

$$V' = -\frac{(1+\nu^4)}{2\nu^2 \tan \mu} U' \tag{3-65}$$

and

$$W' = -\frac{i(1-\nu^4)}{2\nu^2 \tan \mu} U' \tag{3-66}$$

From Equation 3-62

$$U' = -\frac{iu_0}{\pi}\left[\frac{1}{\nu_1+\nu} + \frac{1}{\bar{\nu}_1+\nu} + \frac{1}{\nu_1-\nu} + \frac{1}{\bar{\nu}_1-\nu}\right] \tag{3-67}$$

Using the compatibility Equation 3-65,

$$V' = \frac{iu_0}{\pi} \frac{(1+\nu^4)}{2\nu^2 \tan \mu}\left[\frac{1}{\nu_1+\nu} + \frac{1}{\bar{\nu}_1+\nu} + \frac{1}{\nu_1-\nu} + \frac{1}{\bar{\nu}_1-\nu}\right]$$

$$V' = \frac{iu_0}{2\pi \tan \mu}\left(\frac{1}{\nu^2}+\nu^2\right)\left[\frac{1}{\nu_1+\nu} + \frac{1}{\bar{\nu}_1+\nu} + \frac{1}{\nu_1-\nu} + \frac{1}{\bar{\nu}_1-\nu}\right] \tag{3-68}$$

Integrating and simplifying yields:

$$V = \frac{iu_0}{2\pi \tan \mu}\left[-\frac{2}{\nu_1 \nu} - \frac{2}{\bar{\nu}_1 \nu} + \frac{1}{\nu_1^2}\log\left(\frac{\nu_1 + \nu}{\nu}\right) + \frac{1}{\bar{\nu}_1^2}\log\left(\frac{\bar{\nu}_1 + \nu}{\nu}\right)\right.$$

$$- \frac{1}{\nu_1^2}\log\left(\frac{\nu_1 - \nu}{\nu}\right) - \frac{1}{\bar{\nu}_1^2}\log\left(\frac{\bar{\nu}_1 - \nu}{\nu}\right) - 2\nu_1 \nu - 2\bar{\nu}_1 \nu + \nu_1^2 \log(\nu_1 + \nu)$$

$$\left. + \bar{\nu}_1^2 \log(\bar{\nu}_1 + \nu) - \nu_1^2 \log(\nu_1 - \nu) - \bar{\nu}_1^2 \log(\bar{\nu}_1 - \nu)\right] + C \qquad (3\text{-}69)$$

where C is the constant of integration.

To evaluate the constant of integration, the boundary condition $v = 0$ at $\nu = 1 + 0i = 1$ is employed. Recognizing that $\bar{\nu}_1 = 1/\nu_1$ and $\nu_1 = 1/\bar{\nu}_1$ and evaluating at $\nu = 1$

$$V = \frac{iu_0}{2\pi \tan \mu}\left\{-4\nu_1 - 4\bar{\nu}_1\right.$$

$$+ \bar{\nu}_1^2 [\log(\nu_1 + 1) - \log(\nu_1 - 1) + \log(\bar{\nu}_1 + 1) - \log(\bar{\nu}_1 - 1)]$$

$$\left. + \nu_1^2 [\log(\bar{\nu}_1 + 1) - \log(\bar{\nu}_1 - 1) + \log(\nu_1 + 1) - \log(\nu - 1)]\right\} + C$$

or

$$V = \frac{iu_0}{2\pi \tan \mu}\left\{-4(\nu_1 + \bar{\nu}_1) + (\nu_1^2 + \bar{\nu}_1^2)\log\frac{(\nu_1 + 1)(\bar{\nu}_1 + 1)}{(\nu_1 - 1)(\bar{\nu}_1 - 1)}\right\} + C \qquad (3\text{-}70)$$

In the general case,

$$\nu_1 = a + bi$$

and

$$\bar{\nu}_1 = a - bi$$

where a and b are real constants.

Substituting the general values for ν_1 and $\bar{\nu}_1$ and recognizing that since ν_1 is on the circle γ', $a^2 + b^2 = 1$, Equation 3-70 becomes:

$$V = \frac{iu_0}{2\pi \tan \mu}\left[-8a + (2a^2 - 2b^2)\log\frac{1 + a}{1 - a}\right] + C$$

The physical perturbation velocity v is the real part of the complex perturbation velocity V.

For $0 \leq a \leq 1$, the semicircle in the ν plane which represents the circle γ in the ϵ plane and is the physical part of the problem, the term $1 + a/1 - a$ is always real and positive. The singularity at $a = 1$ corresponds to a physical situation where the angle between the extension of the leading edge of the airfoil and the axial edge is equal to the Mach angle. This is the limit where the model of an L_0A airfoil may be applied. Since the function $1 + a/1 - a$ is always real and positive in the region of interest, the angle that the function makes with the real axis, which is the principal value of the imaginary component of the logarithm, is zero. Thus, the only real part of the complex perturbation velocity occurs in the constant of integration. Since $v = 0$, at $\nu = 1$, the real part of the constant is zero and the imaginary part may be ignored since it will not be required in determining the physical perturbation velocities.

Hence, for the purpose of evaluating the physical perturbation velocity,

$$V = \frac{iu_0}{2\pi \tan \mu}\left[-\frac{2}{\nu_1 \nu} - \bar{\nu}_1\frac{2}{\nu} + \frac{1}{\nu_1^2}\log\left(\frac{\nu_1 + \nu}{\nu}\right) + \frac{1}{\bar{\nu}_1^2}\log\left(\frac{\bar{\nu}_1 + \nu}{\nu}\right)\right.$$

$$-\frac{1}{\nu_1^2}\log\left(\frac{\nu_1 - \nu}{\nu}\right) - \frac{1}{\bar{\nu}_1^2}\log\left(\frac{\bar{\nu}_1 - \nu}{\nu}\right) - 2\nu_1\nu - 2\bar{\nu}_1\nu + \nu_1^2\log(\nu_1 + \nu)$$

$$\left. + \bar{\nu}_1^2\log(\bar{\nu}_1 + \nu) - \nu_1^2\log(\nu_1 - \nu) - \bar{\nu}_1^2\log(\bar{\nu}_1 - \nu)\right] \qquad (3\text{-}71)$$

From the compatibility relationships, as shown in Equation 3-66:

$$W' = -\frac{i(1 - \nu^4)}{2\nu^2 \tan \mu}U'$$

$$W' = -\frac{1}{2\tan\mu}\left(-\frac{iu_0}{\pi}\right)\left(\frac{1 - \nu^4}{\nu^2}\right)\left[\frac{1}{\nu_1 + \nu} + \frac{1}{\bar{\nu}_1 + \nu} + \frac{1}{\nu_1 - \nu} + \frac{1}{\bar{\nu}_1 - \nu}\right] \qquad (3\text{-}72)$$

Integrating as before

$$W = -\frac{u_0}{2\pi \tan \mu}\left[-\frac{2}{\nu_1 \nu} - \frac{2}{\bar{\nu}_1 \nu} + 2\nu_1 \nu + 2\bar{\nu}_1 \nu + \frac{1}{\nu_1^2} \log\left(\frac{\nu_1 + \nu}{\nu}\right)\right.$$

$$+ \frac{1}{\bar{\nu}_1^2} \log\left(\frac{\bar{\nu}_1 + \nu}{\nu}\right) - \frac{1}{\nu_1^2} \log\left(\frac{\nu_1 - \nu}{\nu}\right) - \frac{1}{\bar{\nu}_1^2} \log\left(\frac{\bar{\nu}_1 - \nu}{\nu}\right) - \nu_1^2 \log(\nu_1 + \nu)$$

$$\left. - \bar{\nu}_1^2 \log(\bar{\nu}_1 + \nu) + \nu_1^2 \log(\nu_1 - \nu) + \bar{\nu}_1^2 \log(\bar{\nu}_1 - \nu)\right] + C \qquad (3\text{-}73)$$

where C is the constant of integration.

For the boundary condition at $\nu = 1$, $w = 0$

$$W = -\frac{u_0}{2\pi \tan \mu}[\bar{\nu}_1^2 \log(\nu_1 + 1) + \nu_1^2 \log(\bar{\nu}_1 + 1) - \bar{\nu}_1^2 \log(\nu_1 - 1)$$

$$- \nu_1^2 \log(\bar{\nu}_1 - 1) - \nu_1^2 \log(\nu_1 + 1) - \bar{\nu}_1^2 \log(\bar{\nu}_1 + 1) + \nu_1^2 \log(\nu_1 - 1)$$

$$+ \bar{\nu}_1^2 \log(\bar{\nu}_1 - 1)] + C$$

$$W = -\frac{u_0}{2\pi \tan \mu}\left\{(\nu_1^2 - \bar{\nu}_1^2)\left[\log \frac{(\nu_1 - 1)(\bar{\nu}_1 + 1)}{(\nu_1 + 1)(\bar{\nu}_1 - 1)}\right]\right\} + C$$

for $\nu_1 = a + bi$ and $\bar{\nu}_1 = a - bi$

$$W = -\frac{u_0}{2\pi \tan \mu}\left\{4abi\,[\log(-1)]\right\} + C$$

$$W = -\frac{u_0}{2\pi \tan \mu}\left\{4abi\,[\log|1| + i\pi]\right\} + C$$

$$W = \frac{2ab u_0}{\tan \mu} + C$$

The physical perturbation velocity w is the real part of the complex perturbation velocity W

$$w = \frac{2ab u_0}{\tan \mu} + C'$$

where C' is the real part of constant C.

Since $w = 0$ at $\nu = 1$

$$C' = -\frac{2abu_0}{\tan \mu}$$

Hence

$$W = -\frac{u_0}{2\pi \tan \mu}\left[-\frac{2}{\nu_1 \nu} - \frac{2}{\bar{\nu}_1 \nu} + 2\nu_1 \nu + 2\bar{\nu}_1 \nu + \frac{1}{\nu_1^2} \log\left(\frac{\nu_1 + \nu}{\nu}\right) + \frac{1}{\bar{\nu}_1^2} \log\left(\frac{\bar{\nu}_1 + \nu}{\nu}\right)\right.$$

$$- \frac{1}{\nu_1^2} \log\left(\frac{\nu_1 - \nu}{\nu}\right) - \frac{1}{\bar{\nu}_1^2} \log\left(\frac{\bar{\nu}_1 - \nu}{\nu}\right) - \nu_1^2 \log(\nu_1 + \nu) - \bar{\nu}_1^2 \log(\bar{\nu}_1 + \nu)$$

$$\left. + \nu_1^2 \log(\nu_1 - \nu) + \bar{\nu}_1^2 \log(\bar{\nu}_1 - \nu)\right] - 2\frac{abu_0}{\tan \mu} \qquad (3\text{-}74)$$

These expressions for perturbation velocities have been evaluated around and within the circle γ' for an arbitrary value of $\nu_1 = 0.8 + 0.6i$ which corresponds to $\delta = 116$ degrees at $M = 2$. The physical perturbation velocities on the circle γ' are presented in Figure 23. The magnitudes and signs of the perturbation velocities are determined by the equations without requiring separate determinations of the two-dimensional perturbation velocities v_0 and w_0. Consider the physical situation of the thin plate at positive angle of attack. The two-dimensional perturbation in the direction of the flow would be negative on the lower surface as the velocity is reduced from the freestream value. On the upper surface, an expansion results in a higher velocity or positive perturbation. The vertical velocity perturbation, w, will have the same magnitude and direction on both upper and lower surfaces and will be negative or downward for positive angle of attack. The sideward velocity, v, may be expected to change direction on the upper and lower surfaces and to be positive or outward with sweepback toward the axial edge. For the case of no sweepback, $\delta = 90$ degrees, the two-dimensional perturbation v_0 is zero. Thus, the perturbation velocity v is zero everywhere on the circle γ'. However, due to the imaginary component, v has non-zero values within the circle.

The perturbation velocities v and w each have a singularity at the point $\nu = 0$ which corresponds to the axial edge. This is due to the term $2/\nu_1 \nu + 2/\bar{\nu}_1 \nu$ whose real and imaginary components approach ∞ as ν approaches zero. There appears to be an additional contribution from terms of the form $\log[(\nu_1 \pm \nu)/\nu]$. As ν approaches zero, the real part of the logarithm, which is equal to the log of the amplitude, approaches ∞. However, examination of the equations for perturbation velocities reveals that each of these terms may be combined with a similar term to be of the form $\log[(\nu_1 + \nu)/(\nu_1 - \nu)]$. This term approaches $\log(1)$ as ν approaches zero. The term $2/\nu_1 \nu + 2/\bar{\nu}_1 \nu$, however, still causes a singularity at $\nu = 0$.

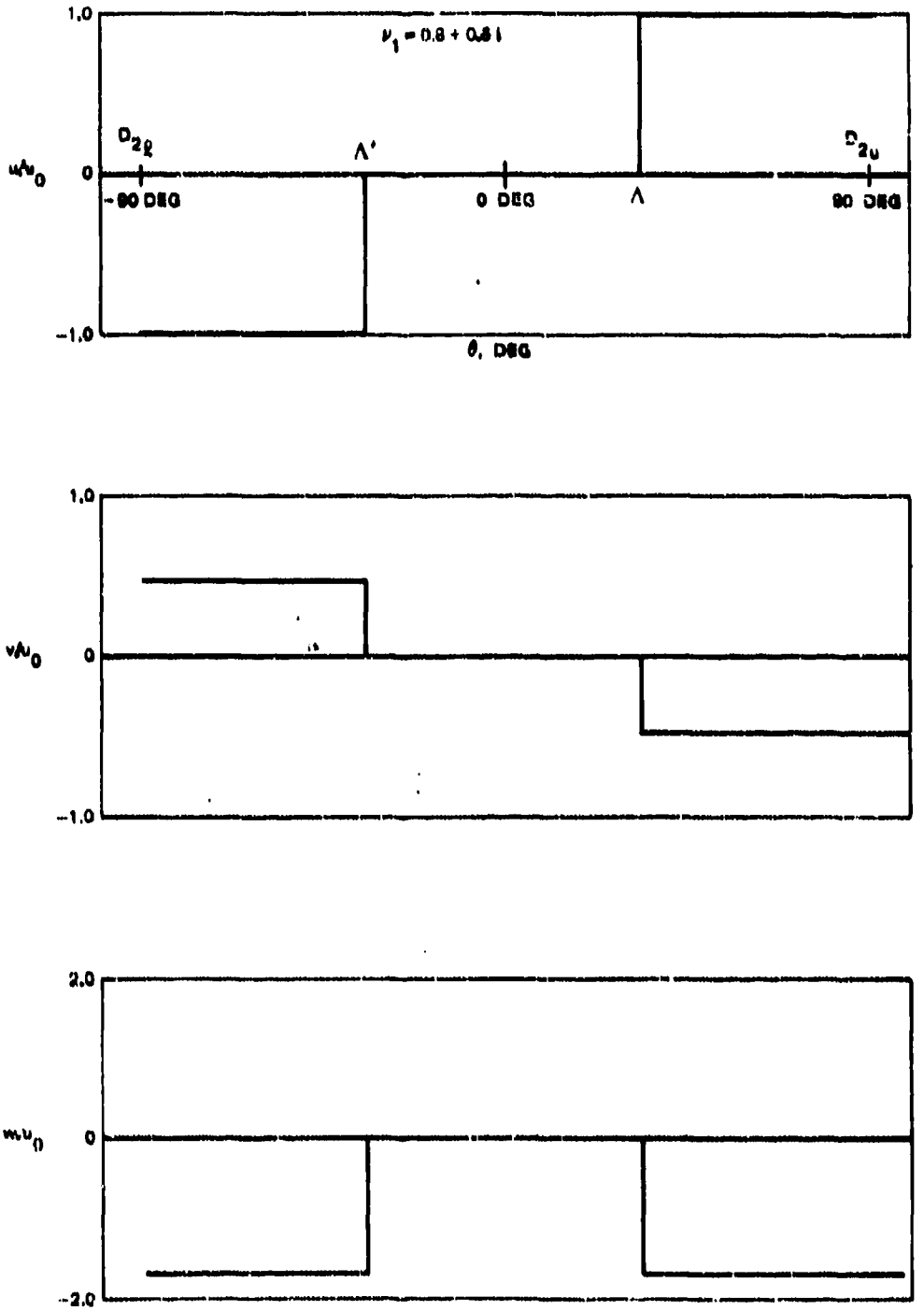

FIGURE 23. Perturbation Velocities on Circle γ'.

The physical perturbation velocities are shown in Figure 24 as functions of location in the ν plane for the arbitrary value of $\nu_1 = 0.8 + 0.6i$. The singularities in v and w are apparent for small values of radius.

There are also singularities when ν equals ν_1 or $\bar{\nu}_1$. At this point, the terms in perturbation velocities v and w of the forms $\log [(\nu_1 - \nu)/\nu]$ or $\log (\nu_1 - \nu)$ become $\log (0)$ which cannot be evaluated. In addition, the perturbation velocity u has a singularity at ν_1 and $\bar{\nu}_1$ due to the term $\log (\nu_1 + \nu)(\bar{\nu}_1 + \nu)/(\nu_1 - \nu)(\bar{\nu}_1 - \nu)$ which approaches $\log (\infty)$.

Finally, singularities exist in perturbation velocity u on the circle γ'. The velocity u is proportional to the imaginary component of a logarithm. The principal value is the angle of the argument of the logarithm. The real part of the argument is negative while the imaginary part is zero. Due to round-off error, the imaginary part has a very small but non-zero value which may be either positive or negative. Thus, the angle is evaluated as plus or minus π radians. This singularity causes no practical problem in evaluation of velocities since this will occur only when the point in question is exactly on the circle γ'.

Chapter 4. STREAMTUBE CALCULATIONS

To evaluate the amount of sidespill and the additive drag of a two-dimensional inlet, a trace of the captured streamtube was employed. The velocities within the conical flow region can be calculated by Equations 3-62, 3-71, and 3-74. Within the two-dimensional flow region, the perturbation velocities are also known. To determine the captured streamtube, a numerical calculation of streamlines from the inlet cowl was performed. A computer program was written in FORTRAN V for the Univac 1110 computer. This program is listed in Appendix C and a flow chart is presented in Figure 25. The numerical computer solution was selected for several reasons. The repetitive nature of the calculations in tracing the streamlines from the cowl to freestream permits the application of a computer to this problem. This permits the use of small incremental distances to accurately portray the streamtube. Determination of additive drag is also performed on the computer by numerically integrating the pressures over the surface of the streamtube. In addition, the computer simplifies the solution of the complicated and complex equations of the conical perturbation velocities. Once a variable has been identified as a complex variable, the equations in FORTRAN are written as with real variables. Arithmetic equations are performed using the complex variables. Functions such as square roots and logarithms must be identified as complex functions. Hand calculation of perturbation velocities are tedious and prone to error.

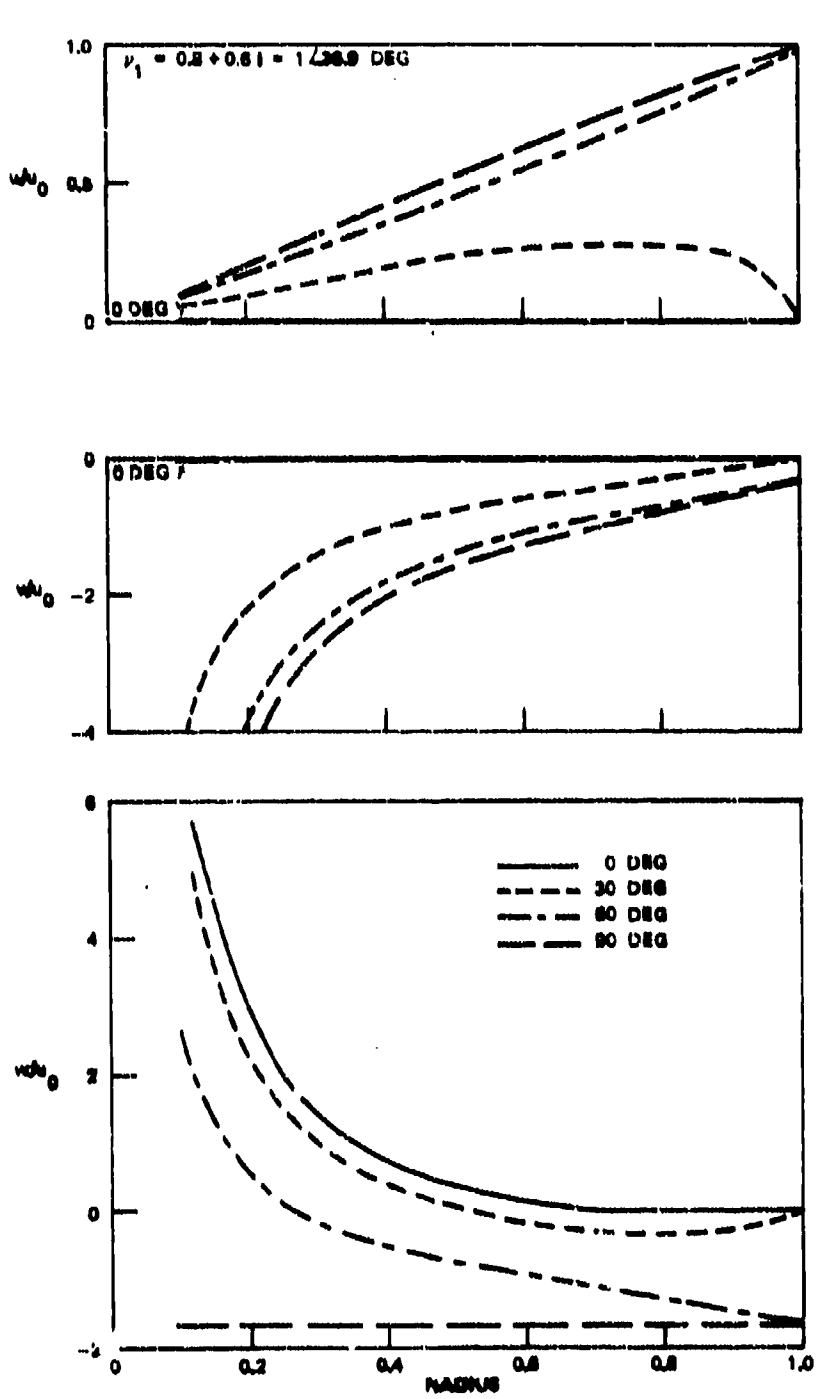

FIGURE 24. Perturbation Velocities, ν_1 = 0.8 + 0.6i.

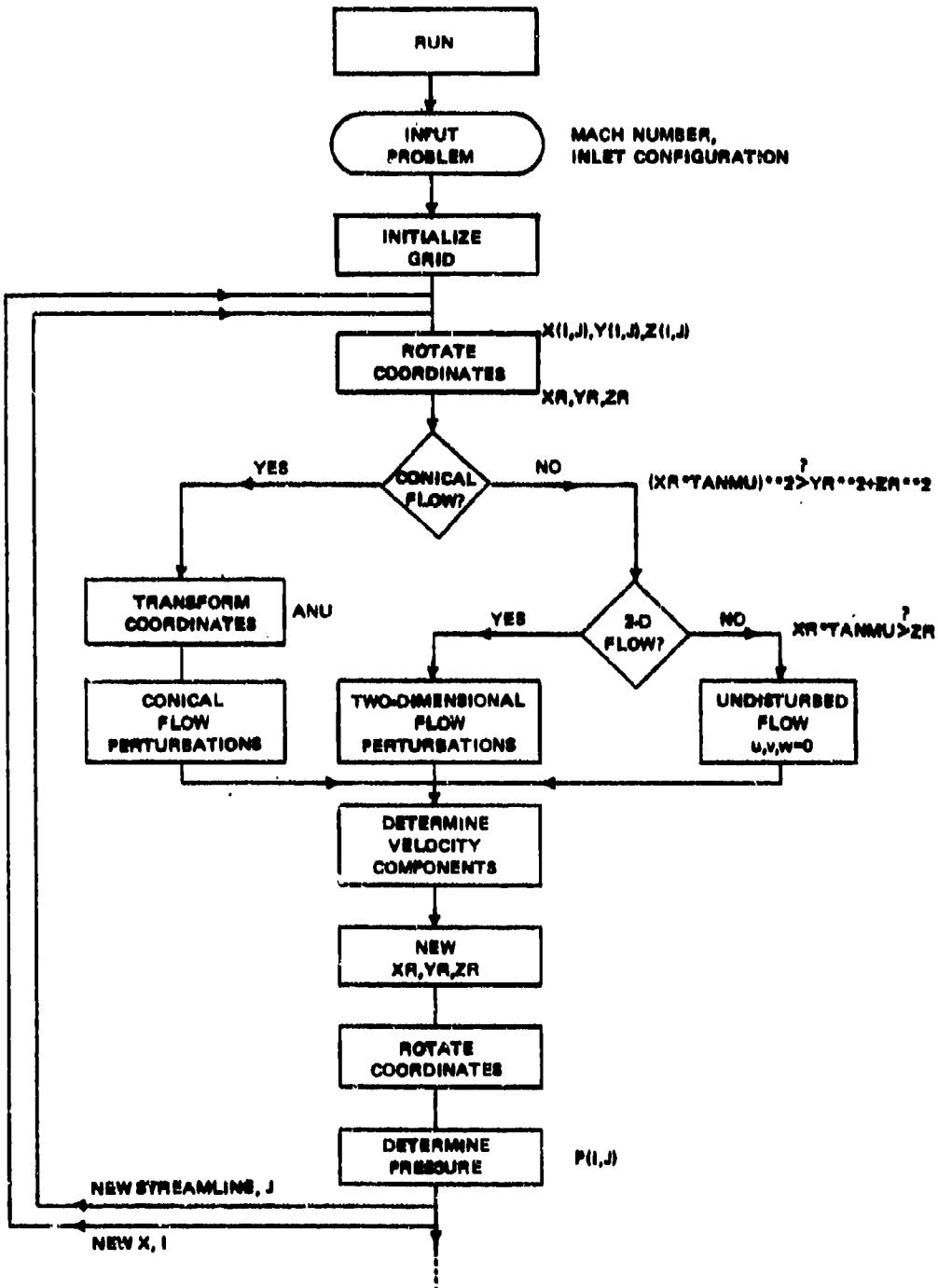

FIGURE 25. Flow Chart of Streamtube Tracing Computer Program.

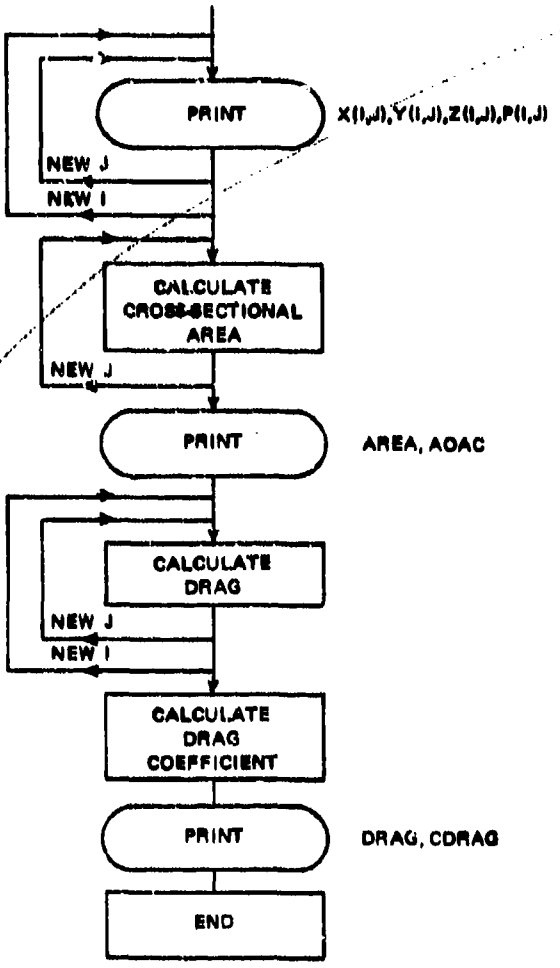

FIGURE 25. (Contd.).

DESCRIPTION OF COMPUTER PROGRAM

To determine the perturbation velocities at any point, the inlet ramp is represented as a thin airfoil in the xy plane at a negative angle of attack α. This is accomplished by a rotation transformation of the ramp and cowl coordinates. The rotation changes the freestream velocity components to V, 0, $-\alpha V$. The two-dimensional perturbation components are:

$$u_0 = \alpha V \tan \mu \operatorname{cosec} \lambda \qquad (4\text{-}1)$$

where $\cos \lambda = \tan \mu \cot \delta$

$$v_0 = \alpha V \tan \mu \cot \delta \operatorname{cosec} \lambda$$
$$w_0 = \alpha V$$

Derivation of these velocity components is included in Appendix D.

Both the conical and two-dimensional shocks may be represented as Mach waves in the rotated coordinate system. For small angles and Mach numbers, the two-dimensional shock angle is approximately equal to the Mach angle plus the deflection angle as illustrated in Figure 26. The conical shock wave angle is approximately equal to the Mach wave angle measured from the axis, over the same range of Mach number and conical deflections as shown in Figure 27.

To trace the streamtube, initial points are selected around the cowl lip and sideplate leading edge. At the side edge of the ramp, there are singularities in both v and w. To avoid this, two points were chosen in the neighborhood of the singularity, one on the vertical sideplate and one on the ramp surface slightly within the inlet. From the latter point the vertical velocity is zero and the streamline is constrained to the ramp surface. Thus, this defines the lower edge of the streamtube. The presence of the singularity also makes it necessary to employ small differences in axial location for the streamline trace in this region. A large difference results in a vertical change such that the streamline is projected through the ramp.

In order to calculate perturbation velocities, a determination must first be made of the type of flow existing at any point. Three types of flow were considered: conical flow, two-dimensional flow, and undisturbed flow. The square of the physical radius $y^2 + z^2$ is compared with the square of the radius of Mach cone, $x^2 \tan^2 \mu$, to determine if a given point is within the cone and hence in the region of conical flow. If the point is in this region, the position is recalculated in the form of Busemann's complex variable, ϵ, and then by the complex square root, as ν. The conical perturbation components are then evaluated.

If the point in question is outside the cone, the angle $\tan^{-1} z/x$ is compared with the Mach angle, μ. If the angle is less than μ, the point is within the region of two-dimensional flow, and the perturbation velocities are two-dimensional components. If the angle is greater than μ, the perturbation components are zero.

Once the perturbation velocity components have been determined, they are added to the freestream velocity yielding the local velocity at each point. The velocity vector is projected an incremental distance upstream to a new set of spatial coordinates. A rotational transformation converts the streamline coordinates back to the physical coordinate system for printing. This procedure is repeated for each streamline and then for a new series of incremental distances until the streamtube is determined back to the inlet ramp leading edge. The order of calculation could have

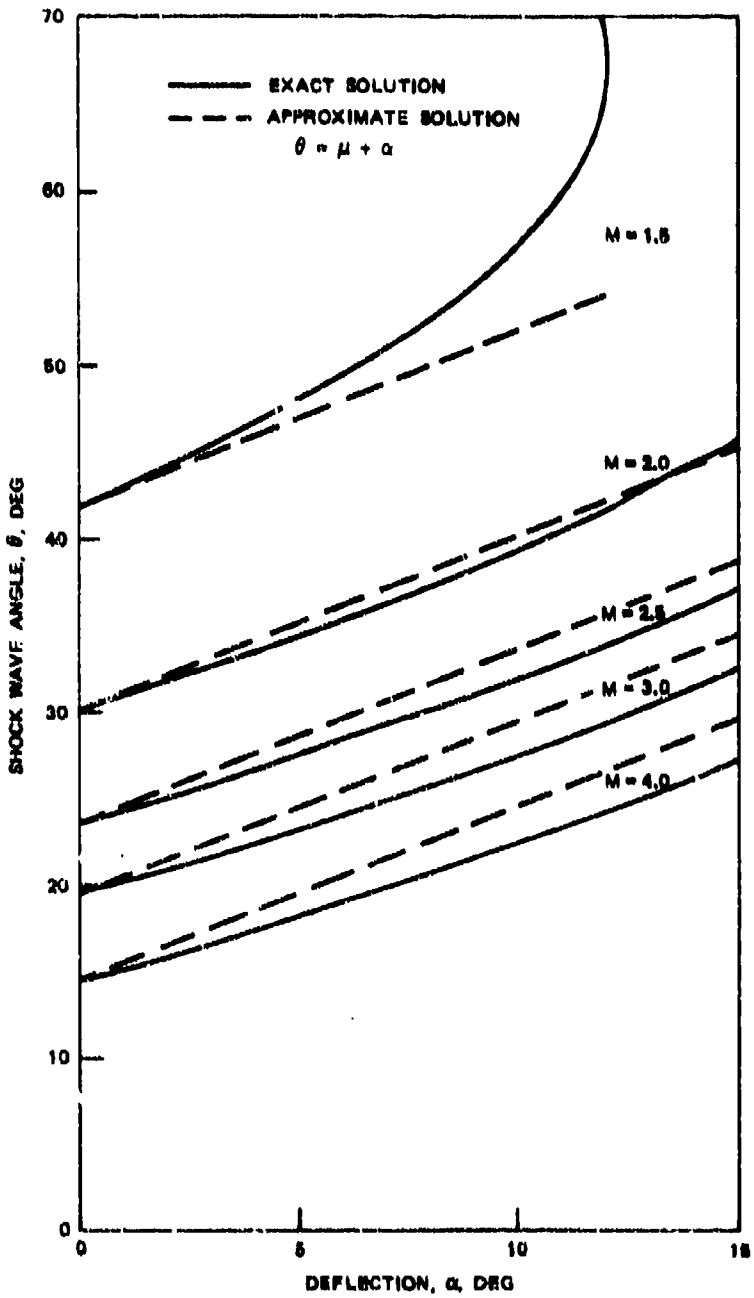

FIGURE 26. Approximation for Two-Dimensional Shock Waves.

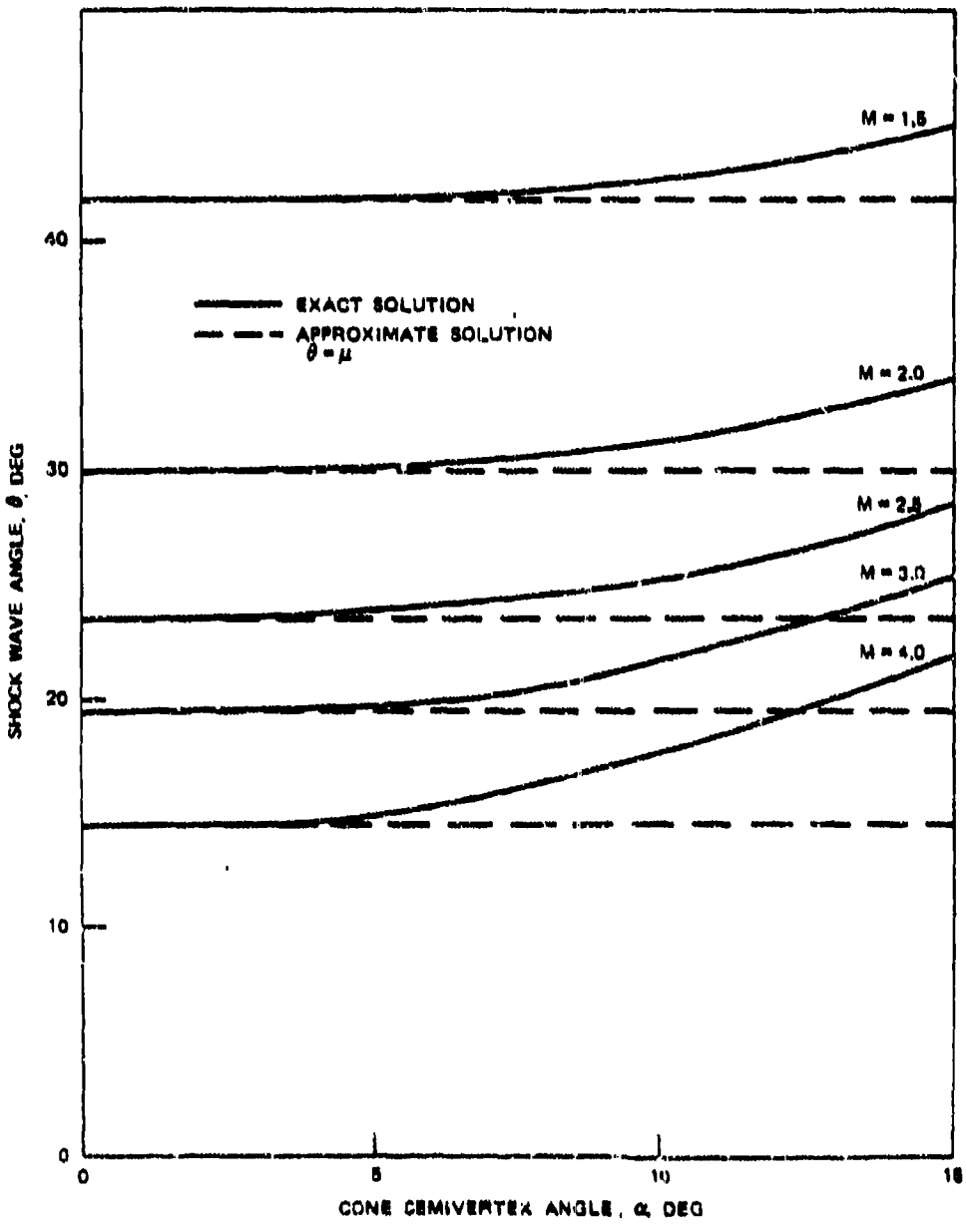

FIGURE 27. Approximation for Conical Shock Waves.

been different such that each streamline was traced to the leading edge before a new streamline was examined. The procedure chosen yields data groupings of cross sections at approximately constant axial stations.

The static pressures are evaluated at each point. From the perturbation velocity components, the local velocity components are determined. For simplicity, all velocities have been ratioed to the freestream velocity, V. Initially, the ratio V/a*, where a* is the speed of sound at sonic conditions, has been determined from the freestream Mach number.

$$V/a^* = \left[\frac{\gamma+1}{2} M^2 \left(1 + \frac{\gamma-1}{2} M^2\right)^{-1}\right]^{1/2} \tag{4-2}$$

Since the compression process is adiabatic, a* remains constant. Thus, when the magnitude of the local velocity, V_ℓ, is determined, the ratio V_ℓ/a^* may also be determined.

$$V_\ell/a^* = (V_\ell/V) \times (V/a^*) \tag{4-3}$$

From the value of V_ℓ/a^*, the ratio of local static to total pressure may be determined*

$$(p/p_t)_\ell = \left[1 - \frac{\gamma-1}{\gamma+1}\left(\frac{V}{a^*}\right)^2\right]^{\gamma/\gamma-1} \tag{4-4}$$

For the calculations herein, it was assumed that $p_{t_\ell} = p_{t_\infty}$ which is reasonable for the small ramp angles and low Mach numbers considered. It would be simple to include the ratio of total pressures across the shock wave.

Once the streamline has been traced upstream to the ramp leading edge, the final cross-sectional area is evaluated by numerical integration and divided by the capture area to yield the mass flow area, A_0/A_c, for both spillage and below design Mach number operation.

Following this, a numerical integration of the static pressures over the streamtube is performed to obtain the additive drag. The static pressure has been calculated at each printed point of the streamtube. A numerically-averaged pressure over the projected area of each element is summed to yield the drag force which determines the additive drag coefficient.

* Refer to Equation 53 in *Equations, Tables, and Charts for Compressible Flow*, by Ames Research Staff. National Advisory Committee for Aeronautics, Moffett Field, Calif., 1953. (NACA Report 1135.)

$$C_{D_a} = \frac{(p - p_o)dA}{qA_{ref}} \approx \frac{\Sigma[(\bar{p}/p_t)_\ell - p_o/p_t]}{(q/p_t)} \frac{\Delta A}{A_{ref}} \tag{4-5}$$

Thus, this computer program has yielded both the mass spillage and the additive drag coefficient from the small perturbation velocity components.

For presentation purposes, the computer program was coupled with a plotting routine, DISSPLA, developed by Integrated Software Systems Corporation. Since plotting routines are generally unique to each computer system, further description and listing of plotting call statements are omitted.

Typical results of the program are included in Figures 28 through 33. The inlet considered has a 10-degree ramp. The cowl is located 10 units of length from the leading edge with a height of 5 units. Inlet width is 10 units. Freestream Mach number is 2.2. The first five plots, Figures 28 through 32, show the shape of the cross section of the streamtube, from the midplane to the axial edge at various longitudinal locations from the cowl lip to the leading edge. Superimposed on these plots are the boundaries of the two-dimensional and conical flow regions to illustrate the analytical model for each portion of the streamtube. At the leading edge, Figure 32, the flow is undisturbed and there are no regions of perturbation. Integration of this cross section yields the mass capture area ratio of the inlet. Figure 33 presents a perspective view of the inlet and streamtube.

PAWLIKOWSKI'S ANALYSIS

At this point, it is worthwhile to examine the investigation of Pawlikowski (Ref. 10). Pawlikowski has performed an analysis of the perturbation velocities similar to that already discussed. To determine the velocities, he employed a technique developed by Lagerstrom (Ref. 13). This method will be described here in the coordinate system of Milne-Thomson shown in Figure 14 rather than in Lagerstrom's notation. Starting from the small perturbation equation,

$$-(M^2 - 1)\frac{\partial^2 S}{\partial x^2} + \frac{\partial^2 S}{\partial y^2} + \frac{\partial^2 S}{\partial z^2} = 0 \tag{4-6}$$

a Mach number of $\sqrt{2}$ is assumed. This reduces the term $M^2 - 1$ to unity. Other Mach numbers are treated by distorting the longitudinal dimension by a Prandtl-Glauert transformation.

The small perturbation equation is further reduced by expressing it in cylindrical polar coordinates. Conical flow is evoked by observing that the flowfield is completely specified if it is known within the Mach circle in the plane $x = 1$. In this

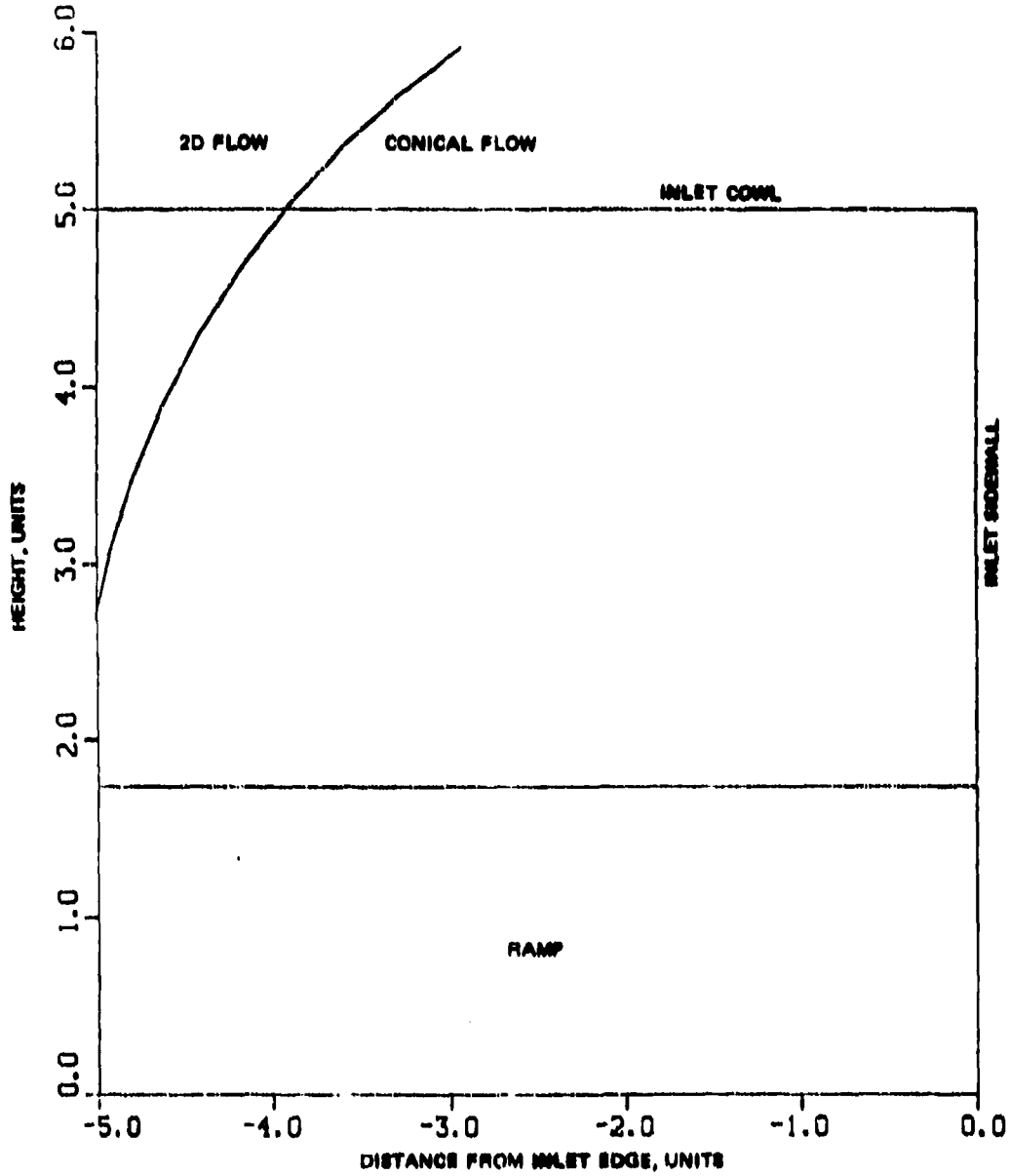

FIGURE 28. Cross Section of Streamtube, x = 10.0.

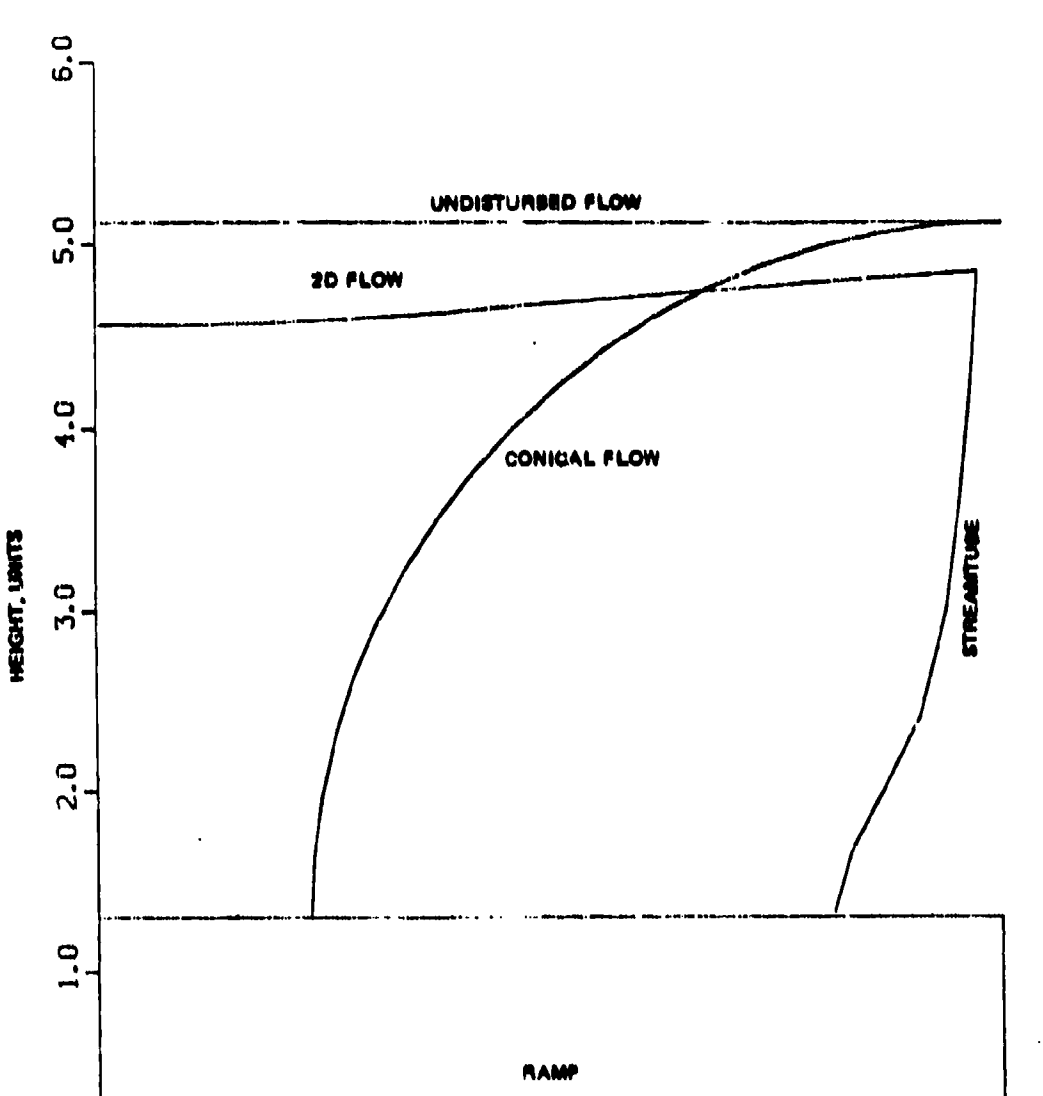

FIGURE 29. Cross Section of Streamtube, x = 7.5.

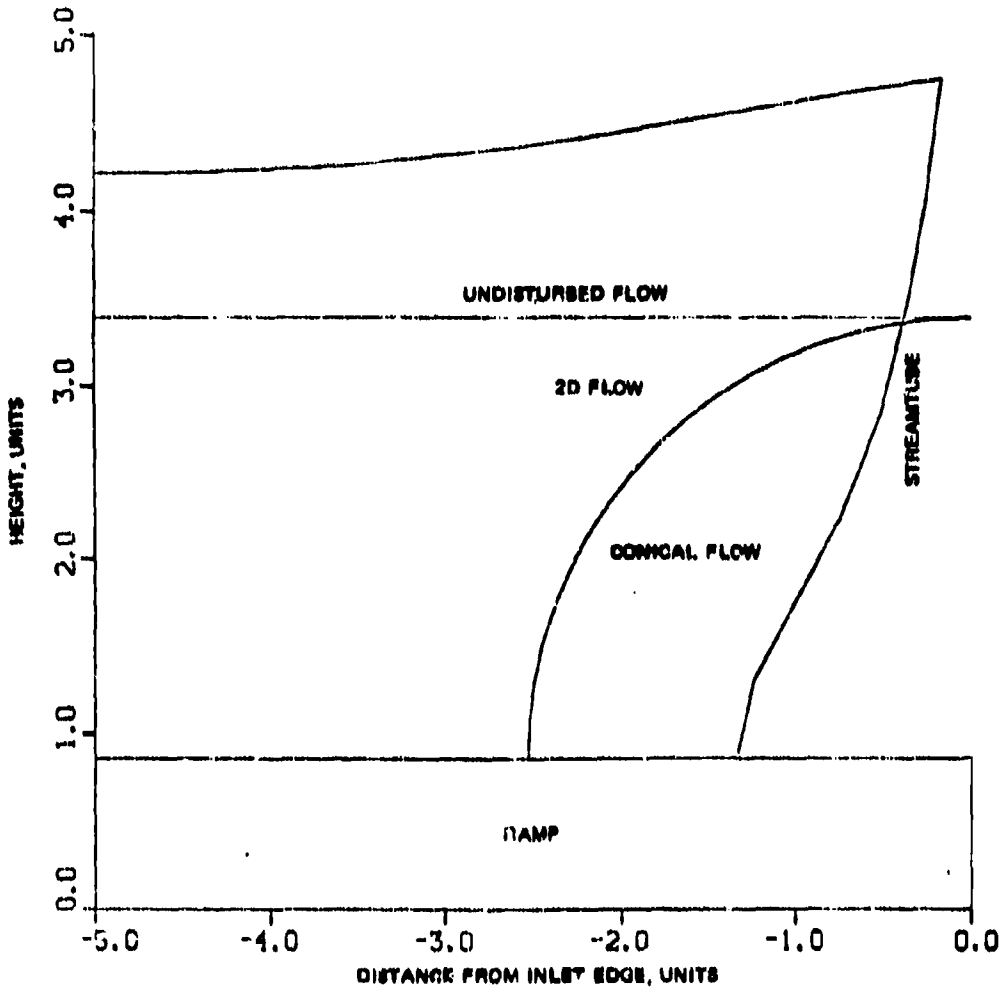

FIGURE 30. Cross Section of Streamtube, x = 5.0.

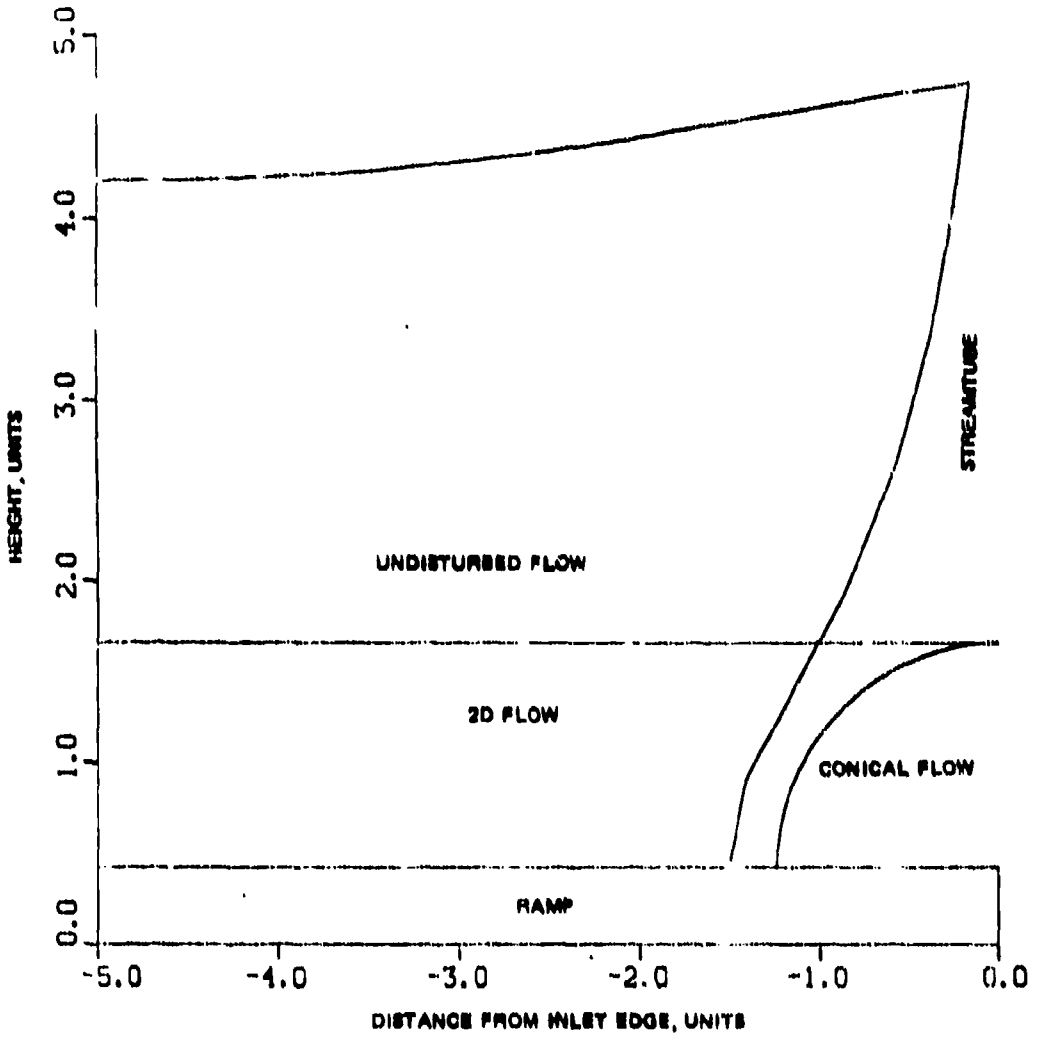

FIGURE 31. Cross Section of Streamtube, x = 2.5.

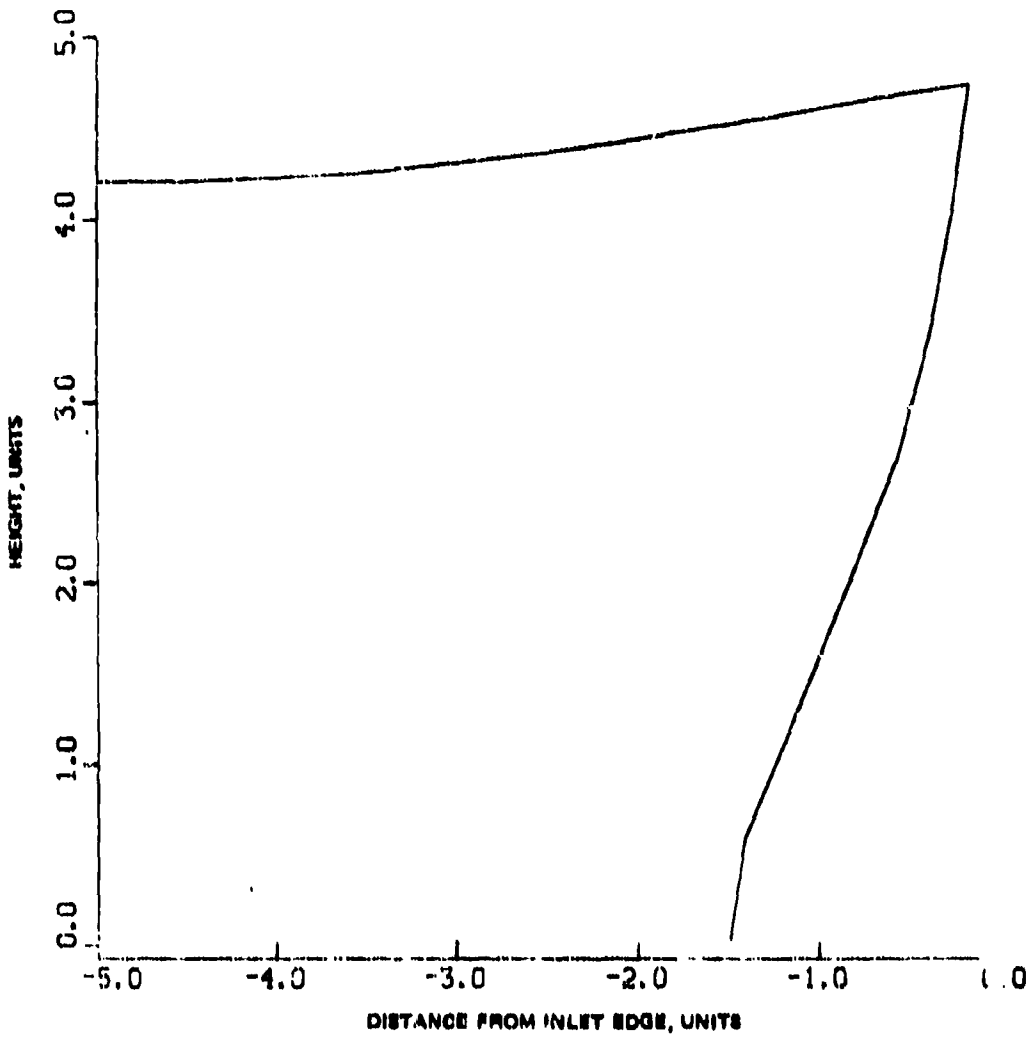

FIGURE 32. Cross Section of Streamtube, x = 0.0.

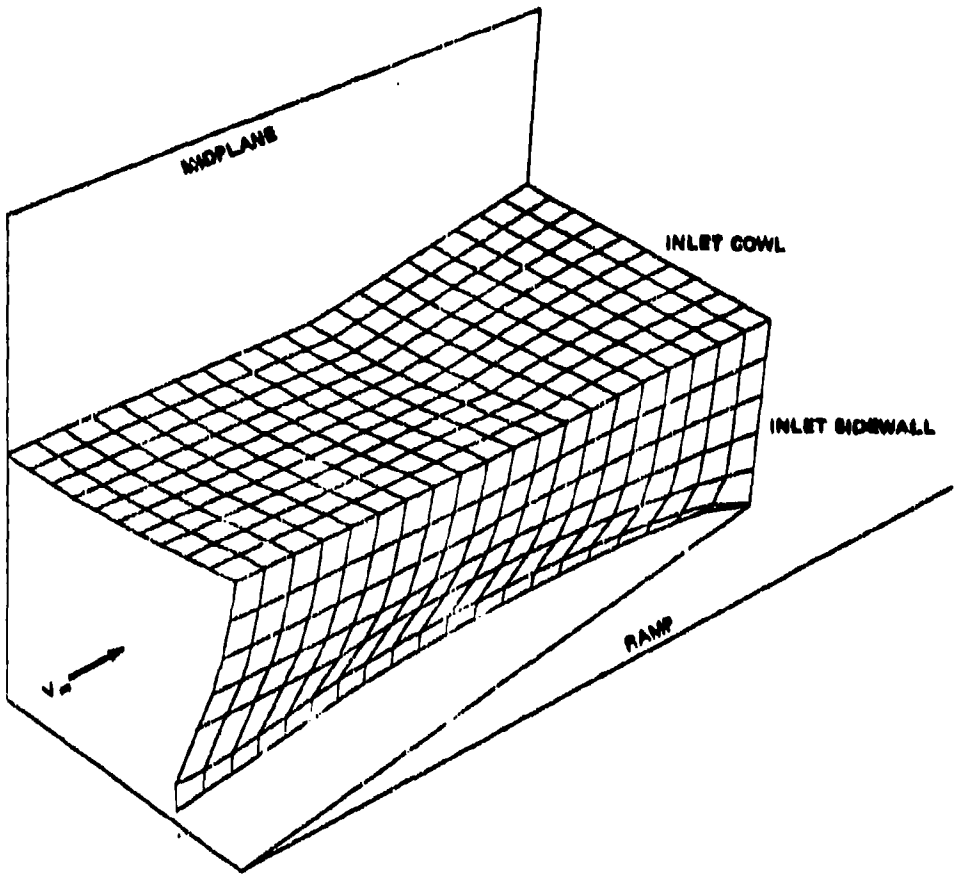

FIGURE 33. Perspective View of Streamtube, M = 2.2, α = 10 Degrees.

plane, with a freestream Mach number of $\sqrt{2}$, the Mach circle has a radius of unity since $\tan \mu = 1$. In the plane $x = 1$, the small perturbation equation may be written:*

$$(\frac{1}{r} - r)\frac{\partial}{\partial r}(r\frac{\partial S}{\partial r}) - r\frac{\partial S}{\partial r} + \frac{1}{r^2}\frac{\partial^2 S}{\partial \theta^2} = 0 \tag{4-7}$$

This may be reduced to Laplace's equation

$$\frac{\partial^2 S}{\partial R^2} + \frac{1}{R}\frac{\partial S}{\partial R} + \frac{1}{R^2}\frac{\partial^2 S}{\partial \theta^2} = 0$$

by a Tschaplygin transformation

$$\epsilon = \frac{1 - \sqrt{1 - r^2}}{r} \tag{4-8}$$

which is identical to Equation 3-43. As in Milne-Thomson's analysis, Busemann's complex variable ϵ, and the compatibility relationships for $M = \sqrt{2}$ or $\tan \mu = 1$ are introduced. At this point, Lagerstrom determines the perturbation velocities. The boundary conditions for a symmetrical thin body in the xy plane are:

$w = w_0$ on the upper surface
$w = -w_0$ on the lower surface
$w = 0$ in the xy plane off the body

Consider a general edge within the Mach cone intersecting the plane $x = 1$ at ϵ_0 (similar to point T in Figure 19). The boundary conditions may be satisfied by the imaginary part of a logarithmic singularity at ϵ_0. Thus, he writes:

$$W = -\frac{iw_0}{\pi}\log(\epsilon - \epsilon_0) + f(\epsilon) \tag{4-9}$$

where $f(\epsilon)$ is analytic at ϵ_0 and purely imaginary on the real axis. From the compatibility relationships, he obtains

$$\frac{dU}{d\epsilon} = -\frac{w_0}{\pi}\left(\frac{2}{\epsilon^2 - 1}\right)\left(\frac{\epsilon}{\epsilon - \epsilon_0}\right) + \frac{2\epsilon}{i(\epsilon^2 - 1)}f'(\epsilon) \tag{4-10}$$

For the special case where the edge is parallel to the flow direction, $\epsilon_0 = 0$ and W has a logarithmic singularity at $\epsilon_0 = 0$ which is represented by $-i(w_0/\pi)\log \epsilon$.

* Equation 1-28 in Reference 13.

The boundary conditions are written for the planar body with axial edge equivalent to the L_oA airfoil. These boundary conditions are shown in Figure 34. The singularities at ϵ_1 and ϵ_2 are also expressed as logarithmic singularities. Combining these with the singularity at the axial edge yields

$$W = \frac{iw_0}{\pi} [\log (\epsilon - \epsilon_1)(\epsilon - \epsilon_2) - \log \epsilon] \tag{4-11}$$

which satisfies the boundary conditions of Figure 34.

Employing the compatibility relationship

$$\frac{dW}{d\epsilon} = \frac{i}{2} \left(\epsilon - \frac{1}{\epsilon}\right) \frac{dU}{d\epsilon}$$

$$\frac{dU}{d\epsilon} = \frac{2w_0}{\pi} \frac{\epsilon}{\epsilon^2 - 1} \left[\frac{1}{\epsilon - \epsilon_1} + \frac{1}{\epsilon - \epsilon_2} - \frac{1}{\epsilon}\right] \tag{4-12}$$

Placing the terms over a common demoninator and simplifying yields:

$$\frac{dU}{d\epsilon} = \frac{2w_0}{\pi} \frac{1}{\epsilon^2 - 1} \left[\frac{\epsilon^2 - \epsilon_1 \epsilon_2}{(\epsilon - \epsilon_1)(\epsilon - \epsilon_2)}\right] \tag{4-13}$$

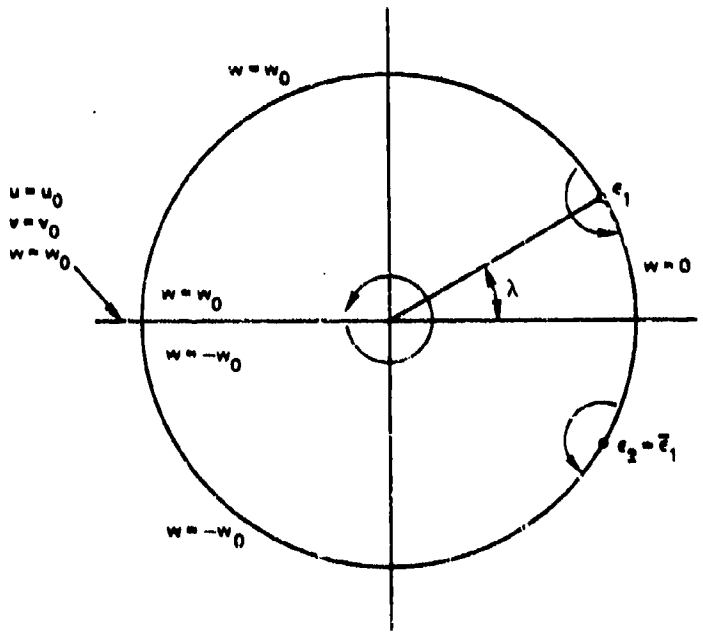

FIGURE 34. Boundary Conditions in ϵ Plane.

Since ϵ_2 is the complex conjugate of ϵ_1 on a circle of radius 1, $\epsilon_1\epsilon_2 = 1$. Thus,

$$\frac{dU}{d\epsilon} = \frac{2w_0}{\pi}\left[\frac{1}{(\epsilon - \epsilon_1)(\epsilon - \epsilon_2)}\right]$$

This may be expanded to yield:

$$\frac{dU}{d\epsilon} = \frac{2w_0}{\pi}\left[\frac{(\epsilon - \epsilon_2) - (\epsilon - \epsilon_1)}{(\epsilon - \epsilon_1)(\epsilon - \epsilon_2)(\epsilon_1 - \epsilon_2)}\right]$$

or

$$\frac{dU}{d\epsilon} = \frac{2w_0}{\pi}\left[\frac{1}{(\epsilon - \epsilon_1)(\epsilon_1 - \epsilon_2)} + \frac{1}{(\epsilon - \epsilon_2)(\epsilon_2 - \epsilon_1)}\right] \tag{4-14}$$

Since

$$\epsilon_1 = e^{i\lambda} = \cos\lambda + i\sin\lambda$$

and

$$\epsilon_2 = e^{-i\lambda} = \cos\lambda - i\sin\lambda,$$

$$\epsilon_1 - \epsilon_2 = 2i\sin\lambda \tag{4-15}$$

Equation 4-14 may be rewritten as

$$\frac{dU}{d\epsilon} = -\frac{iw_0}{\pi\sin\lambda}\left[\frac{1}{\epsilon - \epsilon_1} - \frac{1}{\epsilon - \epsilon_2}\right] \tag{4-16}$$

Integration yields

$$U = \frac{iw_0}{\pi\sin\lambda}\log\frac{\epsilon - \epsilon_2}{\epsilon - \epsilon_1} + C \tag{4-17}$$

The constant of integration, C, is evaluated by the boundary condition at $\epsilon = -1$,

$$u = \mathrm{Re}(U) = u_0 = -\frac{w_0}{\sin\lambda}$$

By geometry, as shown in Figure 35,

$$\mathrm{Re}\left[-i\log\frac{-1 - \epsilon_1}{-1 - \epsilon_2}\right] = \lambda$$

since the imaginary part of the logarithm is the argument.

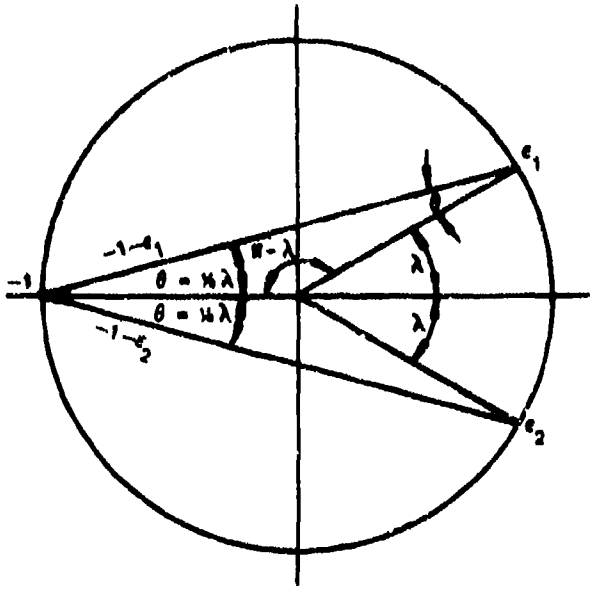

SUMMATION OF ANGLES OF TRIANGLE = π

$2\theta + \pi - \lambda = \pi$

$\theta = \frac{1}{2}\lambda$

FIGURE 35. Geometrical Solution of Constant of Integration.

$$C = -\frac{w_0}{\pi \sin \lambda}[\pi + \lambda] \tag{4-18}$$

and

$$fJ = -\frac{w_0}{\pi \sin \lambda}\left[-i \log \frac{e - e_2}{e - e_1} + \pi + \lambda\right] \tag{4-19}$$

Differentiating this yields:

$$\frac{dU}{de} = \frac{iw_0}{\pi \sin \lambda}\left[\frac{1}{e - e_2} - \frac{1}{e - e_1}\right] \tag{4-20}$$

This is combined with the other compatibility relationship,

$$\frac{dV}{de} = -\frac{1}{2}\left(\frac{e^2 + 1}{e}\right)\frac{dU}{de}$$

to obtain

$$\frac{dV}{de} = -\frac{iw_0}{2\pi \sin \lambda}\frac{e^2 + 1}{e}\left[\frac{-1}{e - e_1} + \frac{1}{e - e_2}\right] \tag{4-21}$$

Equation 4-21 is rewritten as

$$\frac{dV}{de} = -\frac{iw_0}{\pi}\left[-\frac{\cos\lambda}{\sin\lambda}\frac{1}{e-e_1} + \frac{\cos\lambda}{\sin\lambda}\frac{1}{e-e_2} - \frac{1}{e}\right] \tag{4-22}$$

This equivalence is more easily verified by working backwards.

Recognizing that, for the complex conjugates e_1 and e_2,

$$e_1 + e_2 = 2\cos\lambda$$

and

$$e_1 - e_2 = 2i\sin\lambda$$

Equation 4-22 may be written

$$\frac{dV}{de} = -\frac{iw_0}{\pi}\frac{\cos\lambda}{\sin\lambda}\left[-\frac{1}{e-e_1} + \frac{1}{e-e_2} - \frac{i\sin\lambda}{e\cos\lambda}\right]$$

$$\frac{dV}{de} = -\frac{iw_0}{2\pi\sin\lambda}(e_1+e_2)\left[-\frac{1}{e-e_1} + \frac{1}{e-e_2} - \frac{e_1-e_2}{e(e_1+e_2)}\right] \tag{4-23}$$

Placing this expression over a common denominator and simplifying by subtracting and dividing by identical terms yields:

$$\frac{dV}{de} = -\frac{iw_0}{2\pi\sin\lambda}\left[\frac{e_2e^2 + e_1e_2^2 - e_1e^2 - e_1^2e_2}{e(e-e_1)(e-e_2)}\right]$$

$$\frac{dV}{de} = -\frac{iw_0}{2\pi\sin\lambda}\left[\frac{(e^2 + e_1e_2)(e_2 - e_1)}{e(e-e_1)(e-e_2)}\right] \tag{4-24}$$

Since e_2 is the complex conjugation of e_1 on a circle of unity radius,

$$e_1e_2 = 1$$

Hence

$$\frac{dV}{de} = -\frac{iw_0}{2\pi\sin\lambda}\frac{e^2+1}{e}\left[\frac{e_2-e_1}{(e-e_1)(e-e_2)}\right]$$

$$= -\frac{iw_0}{2\pi\sin\lambda}\frac{e^2+1}{e}\left[\frac{(e-e_1)-(e-e_2)}{(e-e_1)(e-e_2)}\right]$$

$$\frac{dV}{de} = -\frac{iw_0}{2\pi \sin\lambda}\frac{e^2+1}{e}\left[-\frac{1}{e-e_1}+\frac{1}{e-e_2}\right]$$

which is identical to Equation 4-21.

Since, from two-dimensional linearized theory shown in Appendix D,

$$v_0 = -u_\infty \cot\delta \operatorname{cosec}\lambda = w_0 \tan\mu \cot\delta \operatorname{cosec}\lambda$$

and

$$\cos\lambda = \tan\mu \cot\delta$$

$$v_0 = w_0 \cos\lambda \operatorname{cosec}\lambda = w_0 \frac{\cos\lambda}{\sin\lambda} \tag{4-25}$$

From this, Equation 4-22 becomes

$$\frac{dV}{de} = -\frac{iv_0}{\pi}\left[-\frac{1}{e-e_1}+\frac{1}{e-e_2}\right]-\frac{w_0}{\pi e} \tag{4-26}$$

Hence, by integration

$$V = -\frac{iv_0}{\pi}\log\frac{e-e_2}{e-e_1}-\frac{w_0}{\pi}\log e + C \tag{4-27}$$

The constant is evaluated as before with the boundary condition that at $e = -1$, $v = \mathrm{Re}(V) = v_0$

since

$$\mathrm{Re}\left[-i\log\frac{-1-e_1}{-1-e_2}\right] = \lambda$$

and

$$\mathrm{Re}[\log -1] = \log|-1| = 0$$

$$C = \frac{v_0}{\pi}[\pi+\lambda] \tag{4-28}$$

Therefore

$$V = \frac{v_0}{\pi}\left[-i\log\frac{e-e_1}{e-e_2}+\pi+\lambda\right]-\frac{w_0}{\pi}\log e \tag{4-29}$$

Thus, the complex perturbation velocities, as far as their contributions to the physical or real components are concerned, have been determined by Lagerstrom for a freestream Mach number of $\sqrt{2}$. These components are further reduced to real velocity components by a geometrical argument.

Consider a general point $\epsilon = Re^{i\theta}$ within the circle of unity radius as shown in Figure 36.

$$\mathrm{Re}[-i \log (\epsilon_1 - \epsilon)] = \arg (\epsilon_1 - \epsilon) = \phi_1$$

$$\mathrm{Re}[-i \log (\epsilon_2 - \epsilon)] = \arg (\epsilon_2 - \epsilon) = \phi_2 \qquad (4\text{-}30)$$

Therefore from Equations 4-19, 4-29, and 4-11

$$u = \mathrm{Re}(U) = \frac{u_0}{\pi} [\phi_2 - \phi_1 + \pi + \lambda]$$

$$v = \mathrm{Re}(V) = \frac{v_0}{\pi} [\phi_2 - \phi_1 + \pi + \lambda] - \frac{w_0}{\pi} \log R$$

$$w = \mathrm{Re}(W) = \frac{w_0}{\pi} [\theta - (\phi_1 + \phi_2)] \qquad (4\text{-}31)$$

Pawlikowski employs these perturbation components to determine the amount of sidespill and the additive drag coefficient. He considers only the crosswise velocity component v,

$$v = \frac{v_0}{\pi} [\phi_2 - \phi_1 + \pi + \lambda] - \frac{w_0}{\pi} \log R \qquad (4\text{-}32)$$

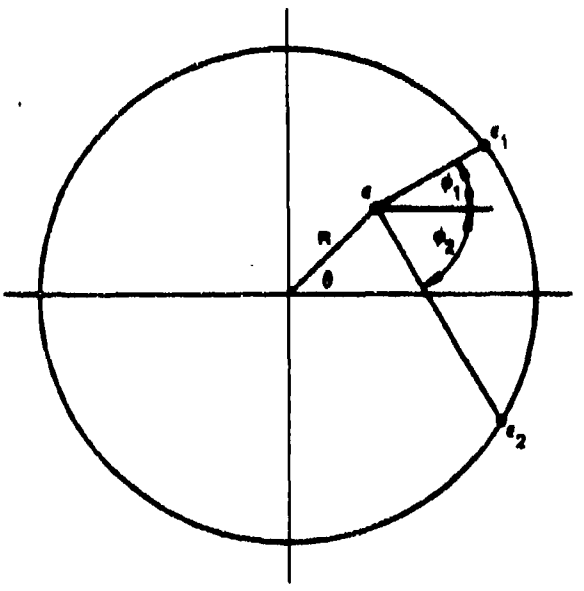

FIGURE 36. Geometrical Interpretation of Perturbation Velocity Components.

Pawlikowski first considers the simple case of an inlet with no leading edge sweepback. For this case, the two-dimensional spanwise velocity component v_0 is zero. Hence, Equation 4-32 reduces to:

$$v = -\frac{w_0}{\pi} \log R \tag{4-33}$$

In physical coordinates this equation may be written as:

$$v = -\frac{w_0}{\pi} \log \frac{1 - \sqrt{1 - r^2}}{r} \tag{4-34}$$

The average velocity $\bar{v}$ between any two radii r_1 and r_2 may be written as

$$\bar{v} = \frac{\int_{r_1}^{r_2} v\,dr}{\int_{r_1}^{r_2} dr} \tag{4-35}$$

From this equation, Pawlikowski obtains:

$$\bar{v} = \frac{w_0}{\pi(r_2 - r_1)} \left[r \log \frac{r}{1 - \sqrt{1 - r^2}} + \sin^{-1} r \right]_{r_1}^{r_2} \tag{4-36}$$

For the case where the Mach cone intersects the cowl of the inlet, integration is performed from $r_2 = 0$ to $r_2 = 1$. For this case,

$$\bar{v} = \frac{w_0}{2}$$

To determine the mass flow rate of spillage, Pawlikowski assumes that the density is constant and may be evaluated from oblique shock relationships. This assumption is questioned in view of the wide variation in crosswise perturbation velocity as demonstrated, for example, in Figure 24. Although this figure is for a ramp with sweepback, there is a singularity at $r = 0$ for any value of ν_1, including $\nu_1 = 1 \angle 45$ deg which represents the ramp without sweepback. Thus, a large variation in local density is expected.

With the assumption of constant density, the mass flow, $\dot{m}$, may be written as:

$$\dot{m} = \rho \bar{v} A_{side} \tag{4-37}$$

where A_{side} is the area bounded by the Mach cone and the cowl, as defined in Figure 37a.

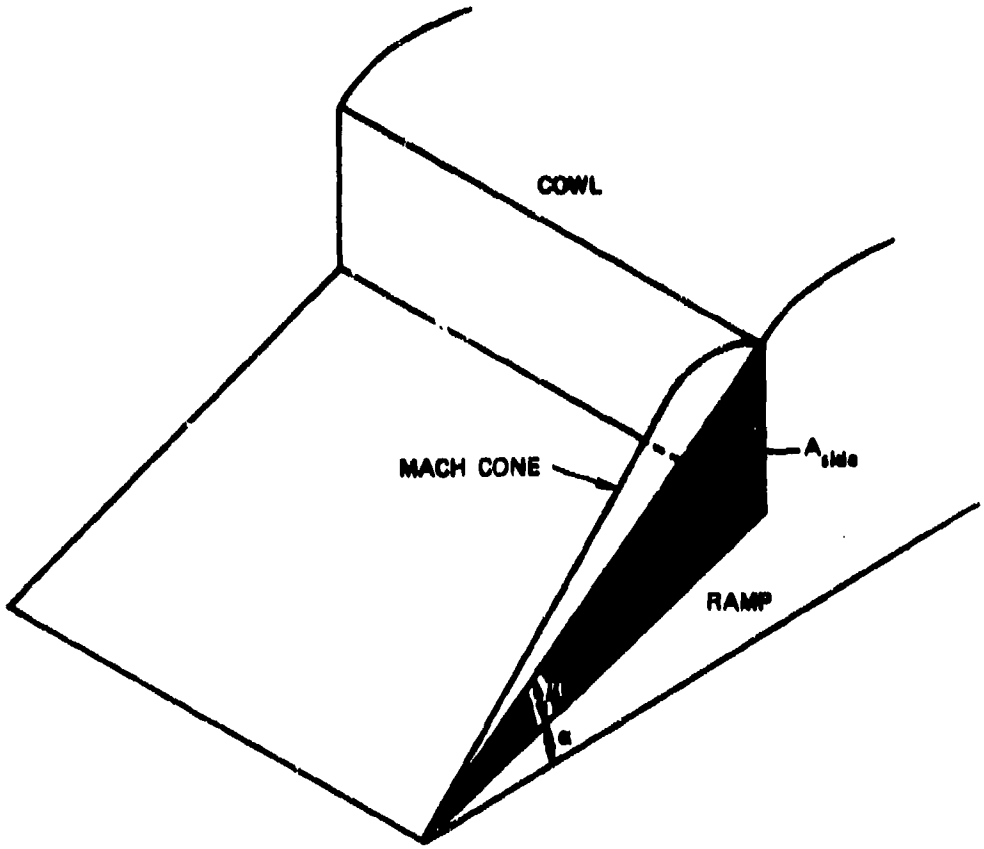

(a)

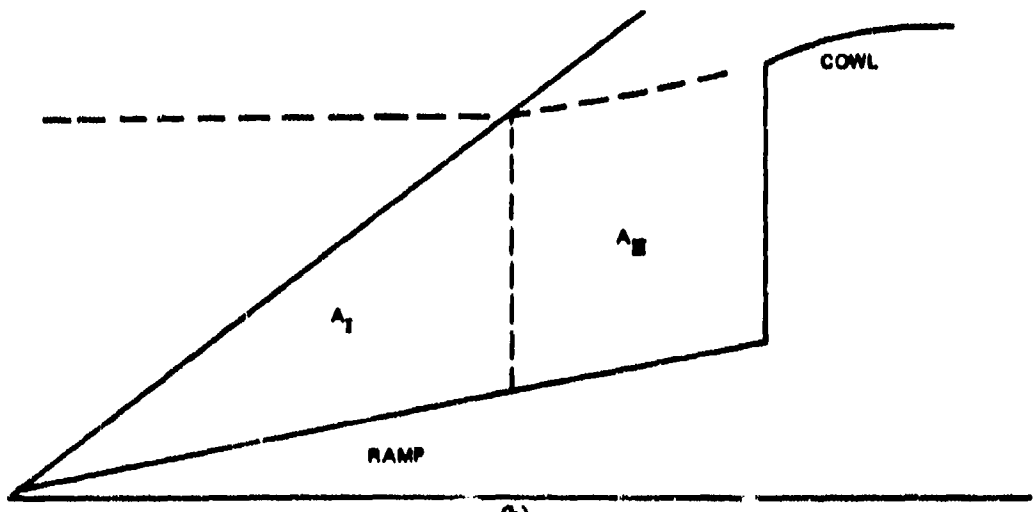

(b)

FIGURE 37. (a) Geometrical Determination of A_{side}; (b) Geometrical Determination of Spillage Areas.

In keeping with standard inlet nomenclature, the spillage mass flow may be expressed as an area of streamtube at freestream condition

$$\dot{m} = \rho_\infty V_\infty A_{OSS}$$

where A_{OSS} is the streamtube area.

Thus

$$\frac{A_{OSS}}{A_{side}} = \frac{\rho}{\rho_\infty} \frac{\bar{v}}{V_\infty} \tag{4-38}$$

From gas dynamic relations across an oblique planar shock,

$$\frac{\rho}{\rho_\infty} = \frac{(\gamma + 1) M^2 \sin^2 \theta_s}{(\gamma - 1) M^2 \sin^2 \theta_s + 2} \tag{4-39}$$

In the more general case, where the Mach cone does not intersect the cowl, as shown in Figure 37b, the area of spillage is separated into two regions. The first region, A_I, is bounded by the Mach cone and is equivalent to the case already described. The second region, A_{II}, is bounded by a streamtube parallel to the ramp surface. The average velocity between each ray may be determined by Equation 4-36 and the average over the area A_{II} is calculated by numerical integration. Thus, the mass spillage for this case may be written as:

$$\frac{A_{OSS}}{A_{side}} = \frac{\rho}{\rho_\infty} \left[\frac{\bar{v}_I A_I}{V_\infty A_{side}} + \frac{\bar{v}_{II} A_{II}}{V_\infty A_{side}} \right] \tag{4-40}$$

Altnough Pawlikowski uses the spillage area, A_{side}, as a reference, any reference area could be employed.

This portion of Pawlikowski's analysis is considered to be in error. He has made an a priori assumption concerning the shape of the captured streamtube. He has assumed that the spillage effect is a small perturbation to the two-dimensional analytical model. Thus, the density is assumed constant and the area of sidespill is the same as the side of the two-dimensional streamtube. The analysis already presented herein has demonstrated that the streamtube resulting from spillage has a complicated, three-dimensional shape. It is difficult to identify the region at the side of the inlet through which spillage occurs. Thus, the assumption of the two-dimensional streamtube is considered to be incorrect.

Pawlikowski then evaluates the additive drag. He states that the additive drag, D_a, may be written approximately as

$$D_a = (p_1 - p_\infty) A_{OSS} \tag{4-41}$$

This result assumes constant static pressure. The area A_{OSS} would be the cross-sectional area at freestream conditions of the spilled streamtube and under these assumptions,

$$D_a = \int (p - p_\infty)\, dA = (p_1 - p_\infty) \int dA = (p_1 - p_\infty) A_{OSS} \tag{4-42}$$

These assumptions are questionable for the same reasons previously discussed when a constant density was assumed. There is a large variation in local velocity which implies variation in local physical properties.

Pawlikowski expresses the additive drag in coefficient form:

$$C_{D_a} = \frac{D_a}{q A_1} \tag{4-43}$$

where A_1 is the inlet area.

From Equation 4-42

$$C_{D_a} = \frac{p_1 - p_\infty}{q} \frac{A_{OSS}}{A_1} \tag{4-44}$$

The first term $p_1 - p_\infty/q$ is the pressure coefficient behind the planar shock wave. Thus, Pawlikowski writes:

$$C_{D_a} = C_p \frac{A_{OSS}}{A_{side}} \frac{A_{side}}{A_1} \tag{4-45}$$

Pawlikowski continues to consider more general inlets, specifically those with leading edge sweepback and yawed side edges. This involves more difficult determinations of the average velocity. However, all of his analysis assumes constant properties and knowledge of the streamtube shape and thus is considered too simplified for correct application.

Chapter 5. APPLICATIONS OF COMPUTER PROGRAM

The computer program for tracing the streamtube and determining the additive drag has been applied to several cases to determine the effect of various inlet configurations and conditions.

COMPARISON WITH EXPERIMENTAL DATA

This computer program has been applied to the analysis of an inlet experimentally investigated by Kemper (Ref. 14). This inlet is illustrated in Figure 38. The inlet is a two-ramp design with an initial ramp angle of 9 degrees and a second ramp angle of 19.75 degrees. A straight sidewall extends from the cowl lip to a point just forward of the second ramp. The inlet mass flow was determined for this case and compared with measured data. To model the inlet analytically, only the first ramp was considered. Above the design Mach number of 2.3, the planar shock from the second ramp is contained wholly within the sidewalls. At Mach numbers below 2.3, the region of the second shock forward of the sidewall is small relative to that of the first shock. Thus, the contribution of the second shock is assumed to be small and has been neglected. The actual inlet employs both sidewall and throat bleed. To account for the bleed mass flow, an estimate of the bleed was determined by means of the automated procedure of Ref. 8. This value was subtracted from the analytical determination of streamtube cross-sectional area to yield a net mass capture area ratio for comparison to measurements with both spillage and bleed. The comparison of capture area ratio is presented in Figure 39. The upper curve is that which would be predicted by two-dimensional analysis without spillage or bleed. Above the design Mach number, the two-dimensional capture area ratio is unity or full capture. Bleed and sidespill reduce this value. The capture area ratio predicted by the present method, modified for bleed, is compared with measured flow rates for two inlets. The two inlets have the same aerodynamic shape but are manufactured by different processes. Inlet 4 is machined from an investment casting while inlet 5 is formed from sheet metal. The agreement of the present method with the data is reasonable. The capture area ratio predicted by Pawlikowski's method is also presented in Figure 39. The value of spillage in addition to the bleed flow was determined by the automated procedure of Ref. 8. The logic of this automated procedure does not permit calculation of spillage at or above the design Mach number of the inlet. Hence, the comparison is limited and no conclusion may be drawn. No determination of additive drag was made in the test, and, hence, no comparison is possible for the predicted value of additive drag.

EFFECT OF INLET DESIGN VARIABLES

The effects of various design variables were examined theoretically by the method described herein. For these studies, a simple single ramp two-dimensional inlet was considered. The baseline inlet is shown in Figure 40. The inlet consists of a 10-degree ramp which is 10 units in length. Since in both conical flow and two-dimensional flow, the flow depends only on direction, the units of length are not essential, only the ratios of lengths. The cowl is 5 units high and the inlet is 10 units in width. The baseline inlet has no leading edge sweepback or sidewalls.

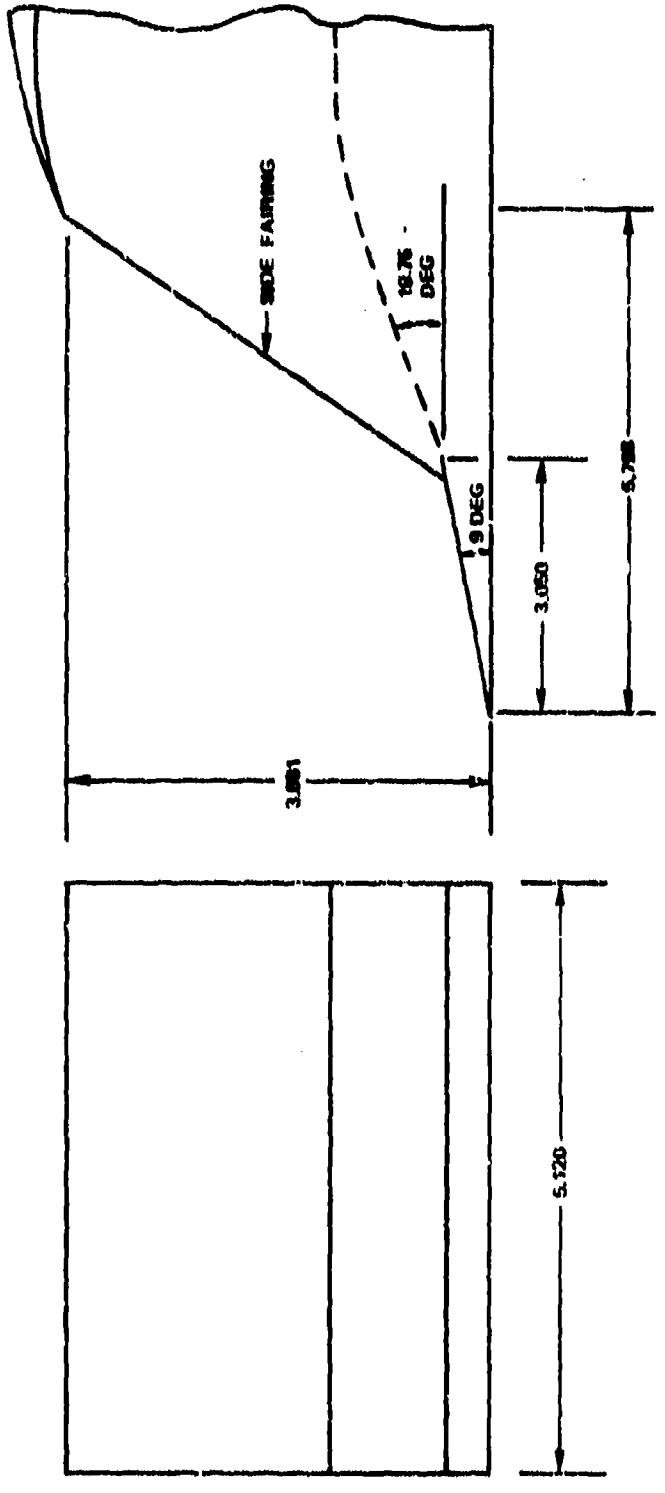

FIGURE 38. Cast Inlet Configuration.

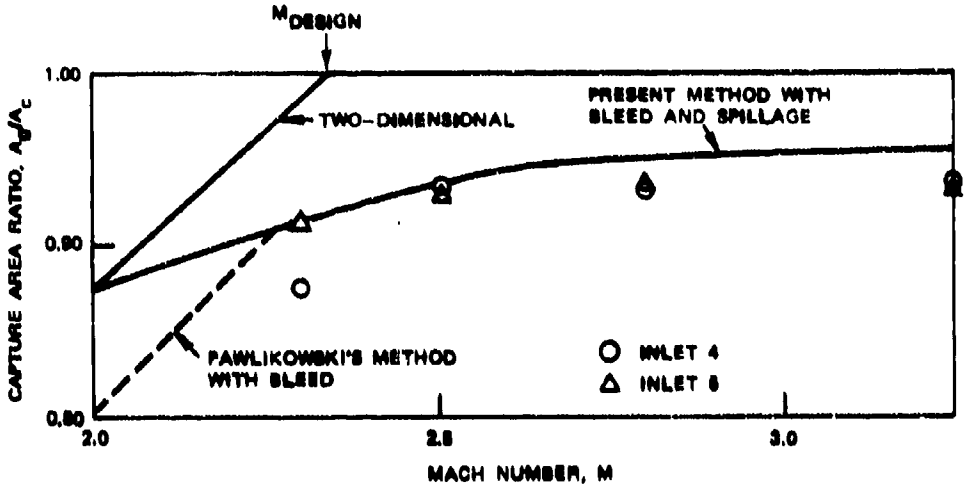

FIGURE 39. Comparison of Theory with Measured Data.

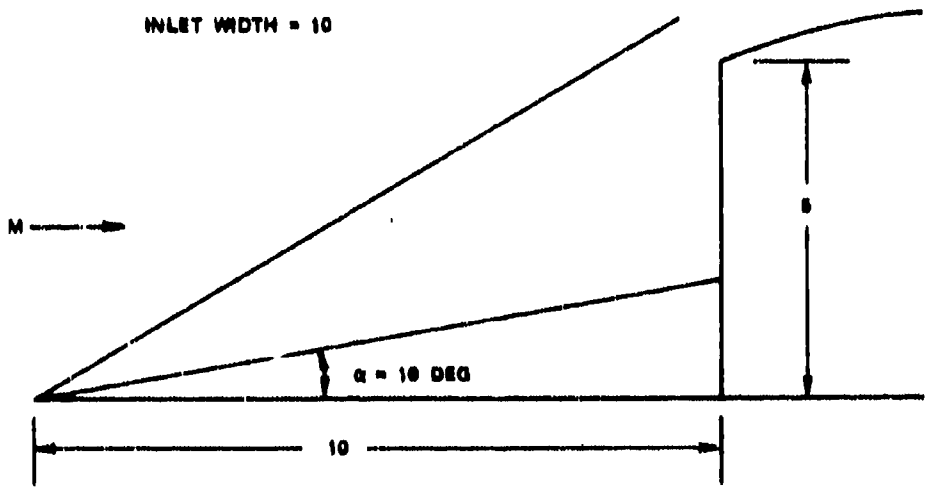

FIGURE 40. Configuration of Baseline Inlet.

Effect of Sidespillage

The results of the three-dimensional analysis described herein were compared to those of a two-dimensional analysis based on linearized theory. The effect of sidespillage on the captured streamtube is illustrated in Figure 41. The case of a 10-degree ramp with the freestream Mach number of 2.5 was considered for this example. The streamtube determined from the three-dimensional analysis is the irregular area ABCD. The upper portion of the streamtube, line AB, results from tracing the streamlines upstream from the top surface of the cowl. Freestream flow

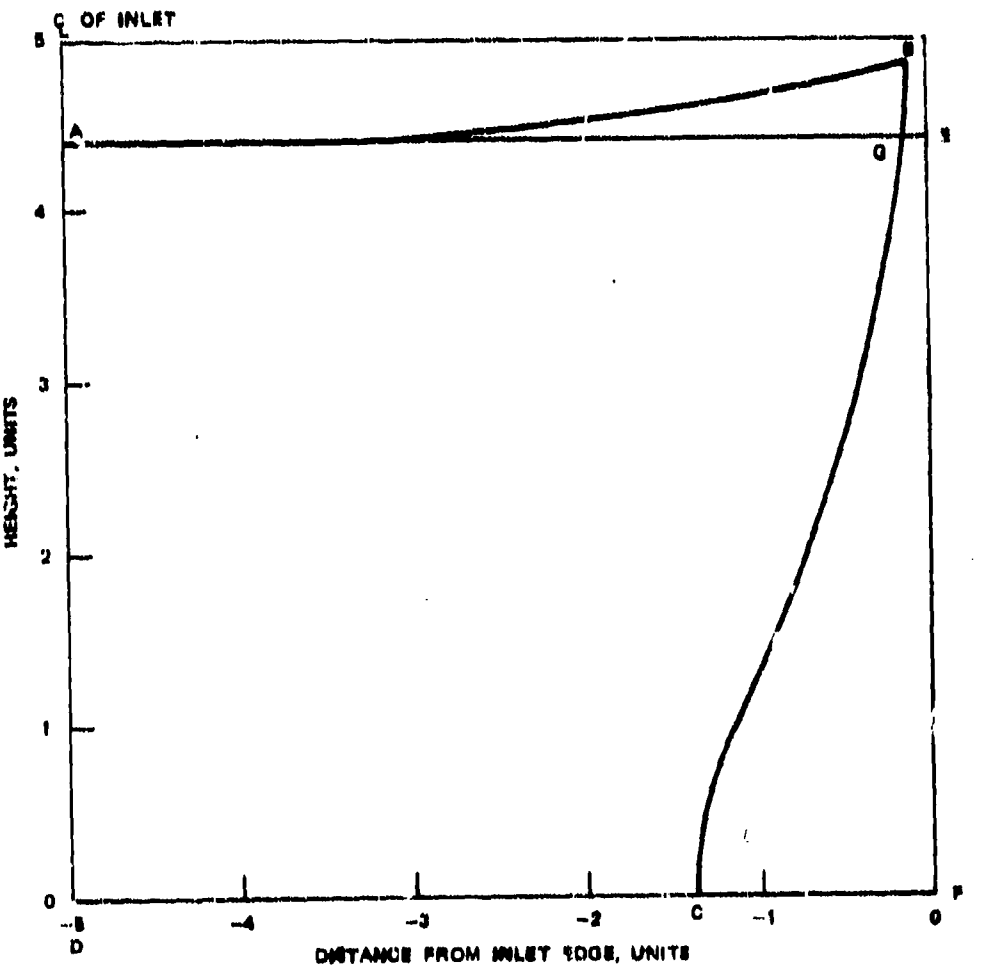

FIGURE 41. Comparison of Captured Streamtubes, M = 2.5, α = 10 Degrees.

which is above this line is spilled over the top of the cowl and is not captured by the inlet. The side portion, line BC, is determined from the side of the inlet. Flow to the right of this line is spilled to the side of the inlet. Corner B originates at the cowl of the inlet and thus divides the flow over the corner from the sidespillage. The rectangle AEFD is the captured streamtube for the two-dimensional model. Note that since the flow is two-dimensional at the midplane of the inlet for this case, the heights of the streamtubes at this point are identical. The excess spillage over the two-dimensional case is the difference between the spillage of area GEFC and the gain of area ABG. It is obvious in this case that there is a loss in capture area due to sidespillage. The difference in capture area ratio is presented for the various Mach numbers in Figure 42 for a ramp angle of 10 degrees. In this case, the net sidespillage is an almost constant 10% over the Mach number range considered. The net sidespillage will vary depending upon the Mach number and inlet geometry.

The effect of sidespillage on the additive drag coefficient for the same case is shown in Figure 43. The effect of sidespillage as revealed by the three-dimensional analysis is a significant decrease in inlet additive drag as compared with that predicted by two-dimensional theory. This results from a combination of three effects. Examination of the pressure forces has revealed that the upper surface of the streamtube is the major contributor to the total drag force. The presence of sidespillage reduces the surface area on the upper surface since some of the flow is spilled. In addition, the deflections on the upper surface of the streamtube are less for conical flow as evidenced by the upper region ABG in Figure 41. This results in reduced local pressures and hence, reduced drag. Finally, the presence of high velocities

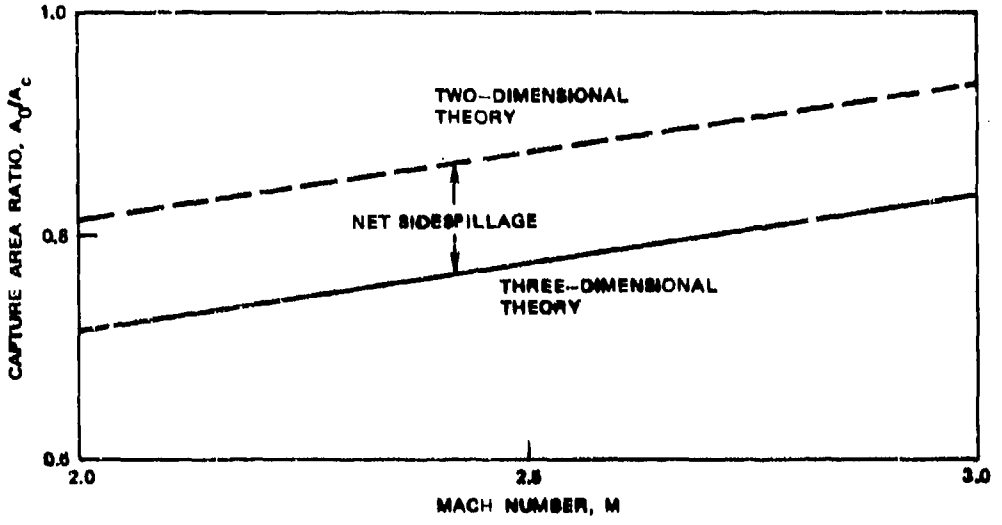

FIGURE 42. Comparison of Capture Area Ratio, α = 10 Degrees.

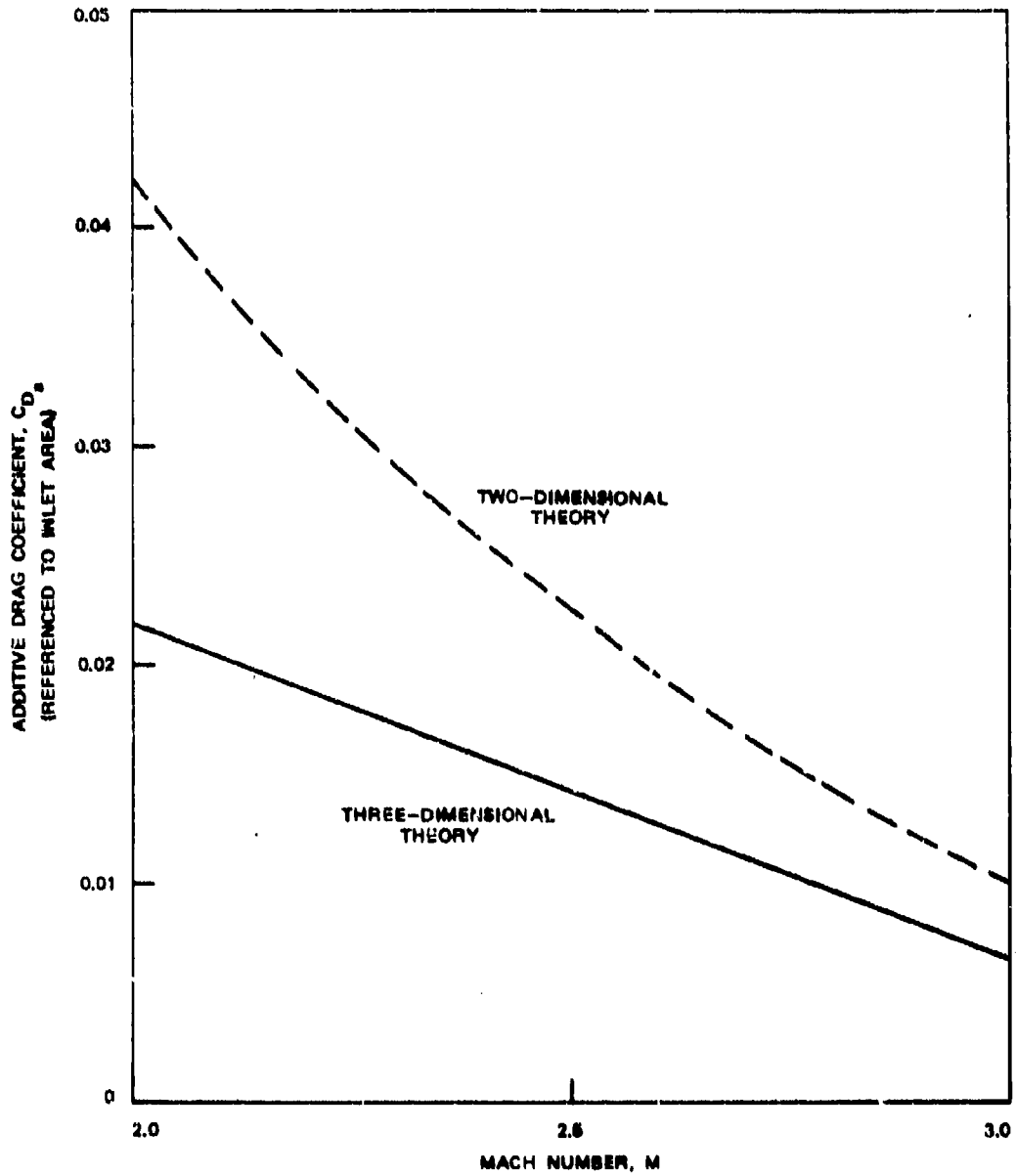

FIGURE 43. Comparison of Additive Drag Coefficient, α = 10 Degrees.

near the side edge of the ramp can result in negative pressure coefficients. In many cases, the side of the streamtube is found to reduce the total drag. The net effect of these three factors is a decrease in additive drag resulting from sidespillage as compared with the two-dimensional model. This result causes doubts about the method of Pawlikowski in which it is assumed a priori that the spillage drag is an additional term to the two-dimensional additive drag.

Effect of Ramp Angle

The first design variable examined was the angle of the inlet ramp. Deflections of 5, 10 and 15 degrees were considered for Mach numbers of 2.0, 2.5, and 3.0. The effect of ramp angle on the inlet capture area ratio is presented in Figure 44. As expected, the capture area ratio decreases with increasing ramp angle for all Mach

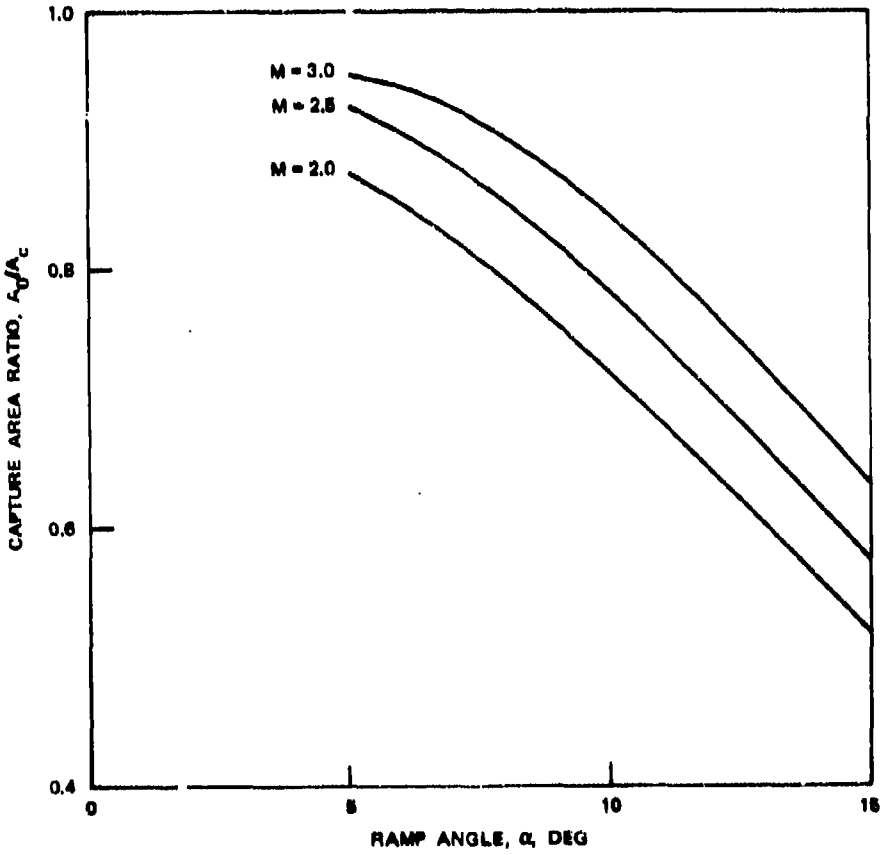

FIGURE 44. Effect of Ramp Angle on Inlet Capture Area Ratio.

numbers. The freestream shapes of the captured streamtubes are shown in Figure 45 for a freestream Mach number of 2.5. Similar trends are observed at the other Mach numbers. As may be noted from the figure, both the spillage over the cowl and the sidespillage are increased with ramp angle, decreasing the capture area ratio.

The effect of ramp angle on additive drag is presented in Figure 46. The additive drag coefficient increases with increasing ramp angle. The additive drag as defined in Equation 2-8 is the integral of the static pressure over the projection of the streamtube exterior. As demonstrated in Figure 45, the capture area decreases with increasing ramp angle or the axially projected area of the streamtube increases. The

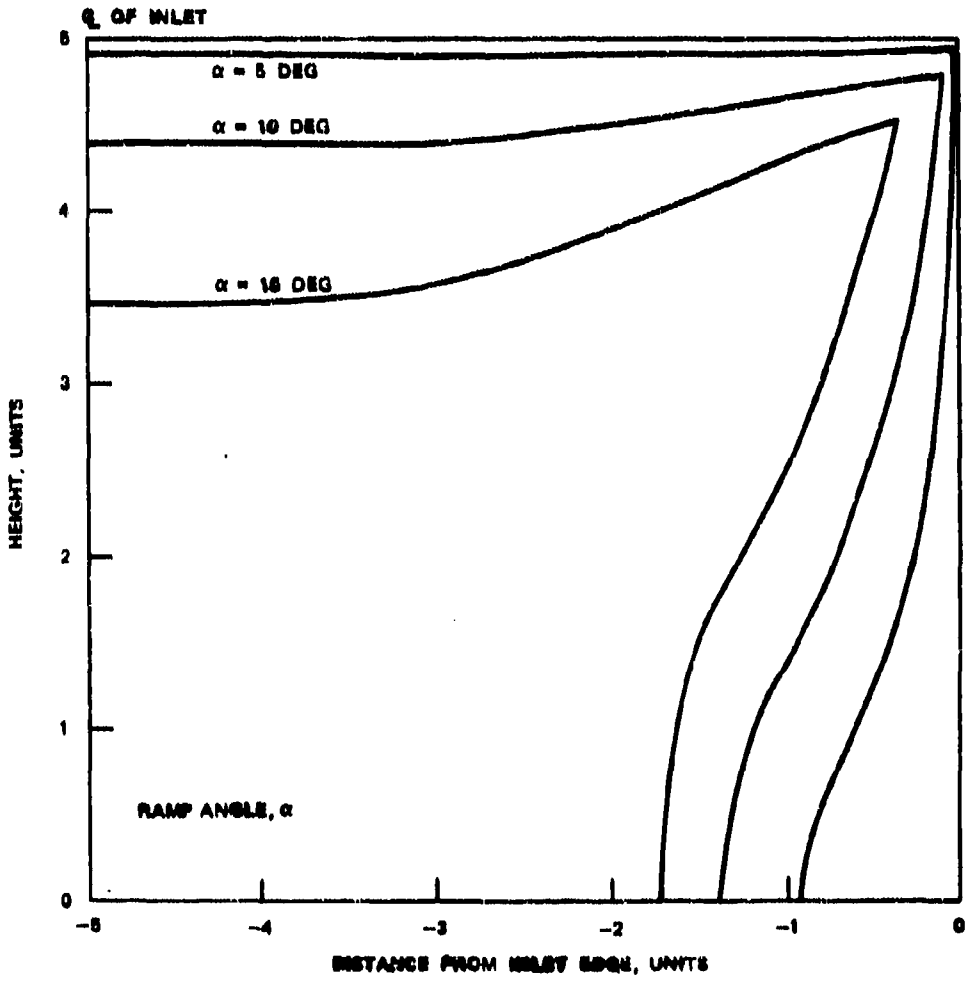

FIGURE 45. Shape of Captured Streamtubes for Various Ramp Angles, M = 2.5.

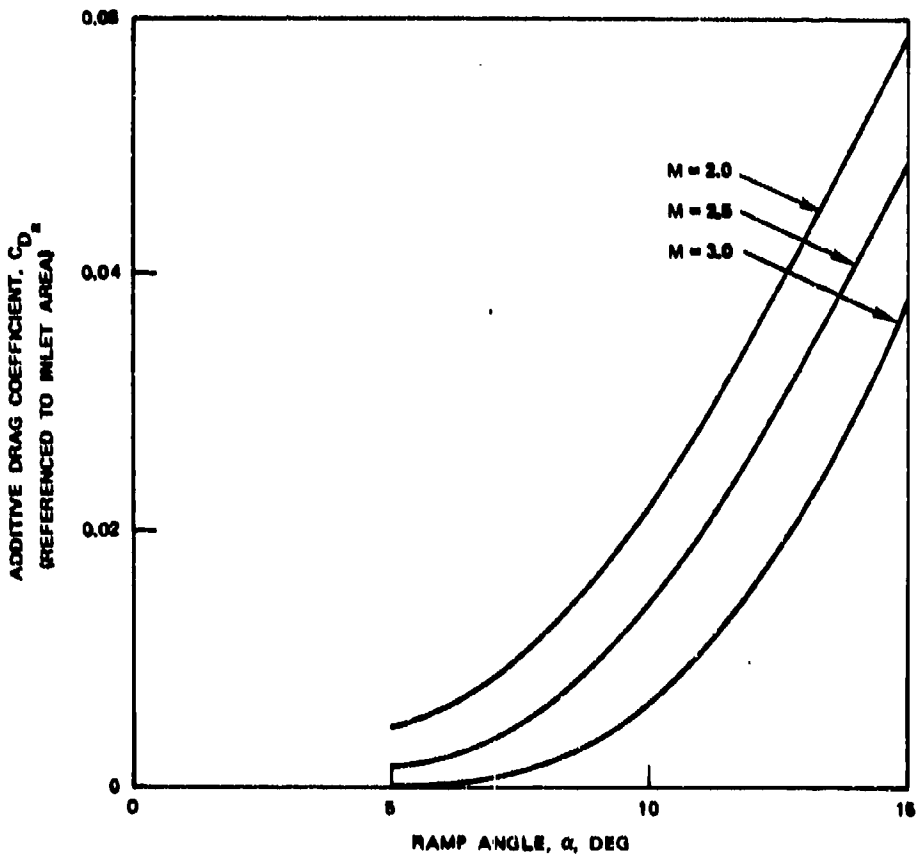

FIGURE 46. Effect of Ramp Angle on Inlet Additive Drag.

increased ramp angle causes greater deceleration or more compression of the flow, increasing the static pressure. Thus, both increased pressure and area combine for an increase in additive drag.

Effect of Mach Number

These same results have been replotted to demonstrate the effects of freestream Mach number. The effect of Mach number on inlet capture area ratio is shown in Figure 47. At a constant ramp angle, the capture area ratio increases with Mach number. As the Mach number increases, the shock wave angle decreases, and the influence of the ramp is exerted over a smaller region. At Mach numbers above the design or "shock-on-lip" Mach number, the shock wave is within the cowl, and there is no spillage over the cowl, only sidespillage. The shapes of the captured streamtubes are

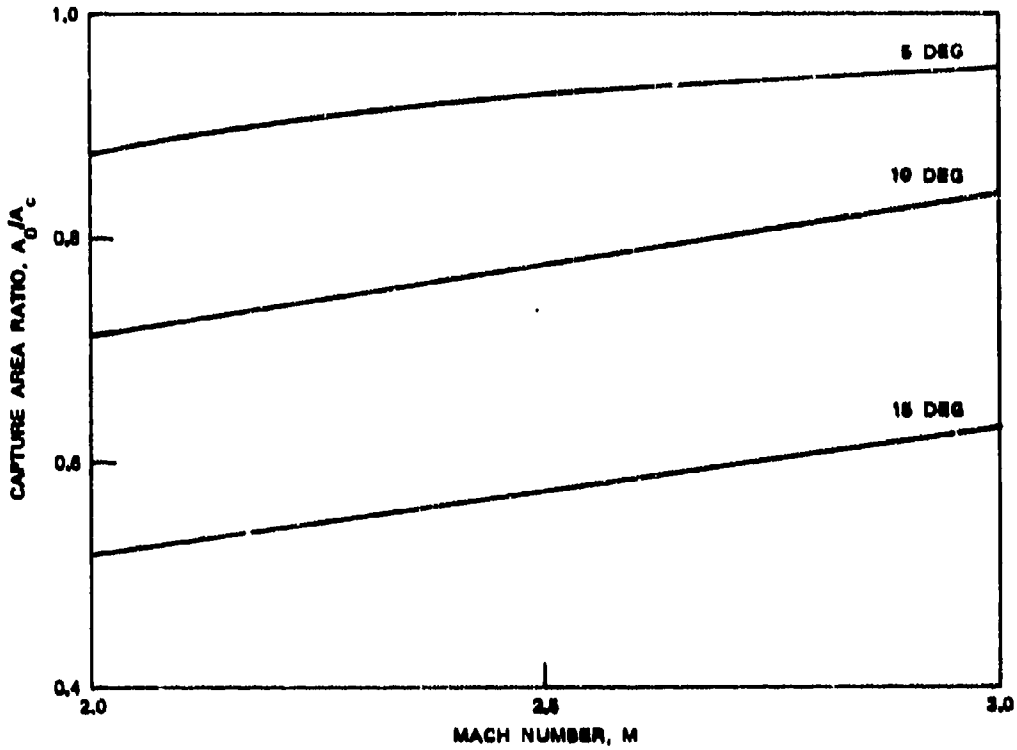

FIGURE 47. Effect of Mach Number on Inlet Capture Area Ratio.

presented in Figure 48 for a ramp angle of 10 degrees. Both spillage over the cowl and sidespillage decrease as the Mach number increases.

The effect of Mach number on additive drag is shown in Figure 49. Additive drag decreases with Mach number. The increasing capture area ratio means that the axially projected area of the streamtube is decreasing with Mach number. Although the pressure behind the shock wave increases with Mach number, the pressure coefficient which is defined as the difference from freestream pressure divided by the freestream dynamic pressure, decreases with Mach number. Thus, both contributions to the additive drag coefficient decrease with Mach number resulting in a decreasing additive drag coefficient (not necessarily decreasing additive drag).

Effect of Sidewalls

Sidewalls are often added to two-dimensional inlets to reduce the amount of sidespillage. An analysis was performed to investigate the effects of various sidewalls on inlet capture area ratio and additive drag. In initialization of the computer program,

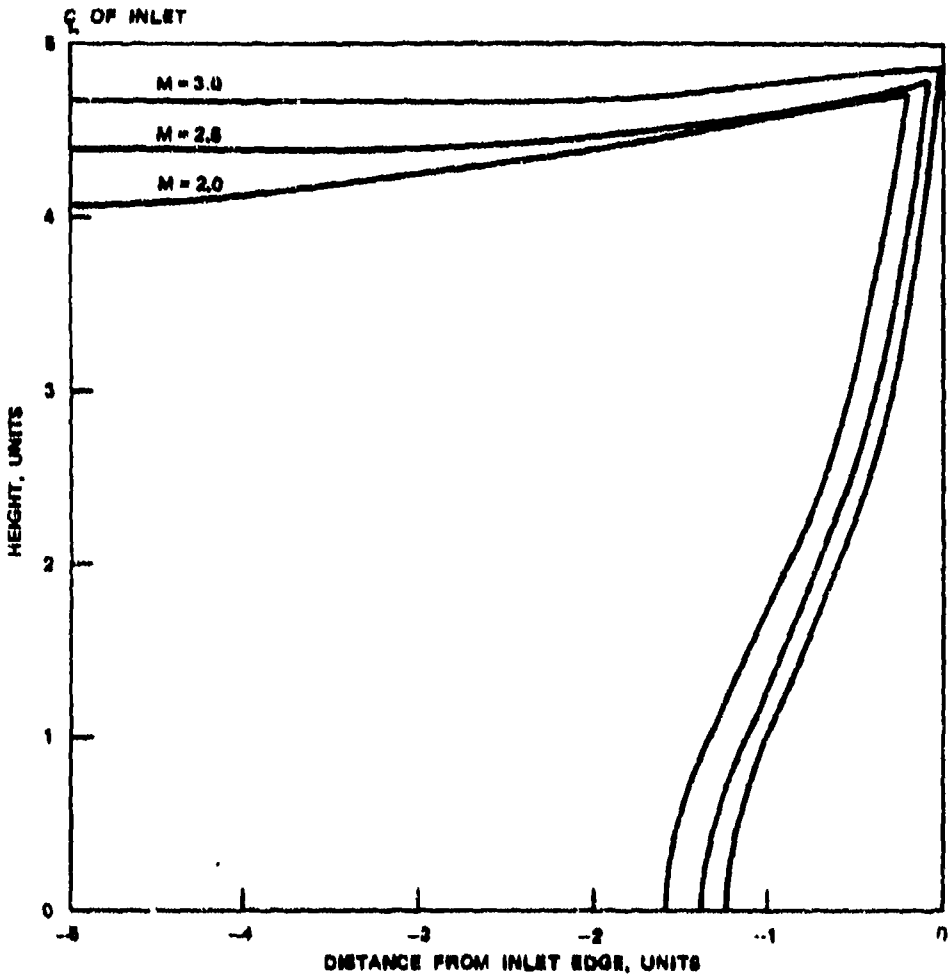

FIGURE 48. Shape of Captured Streamtubes at Various Mach Numbers, Ramp Angle = 10 Degrees.

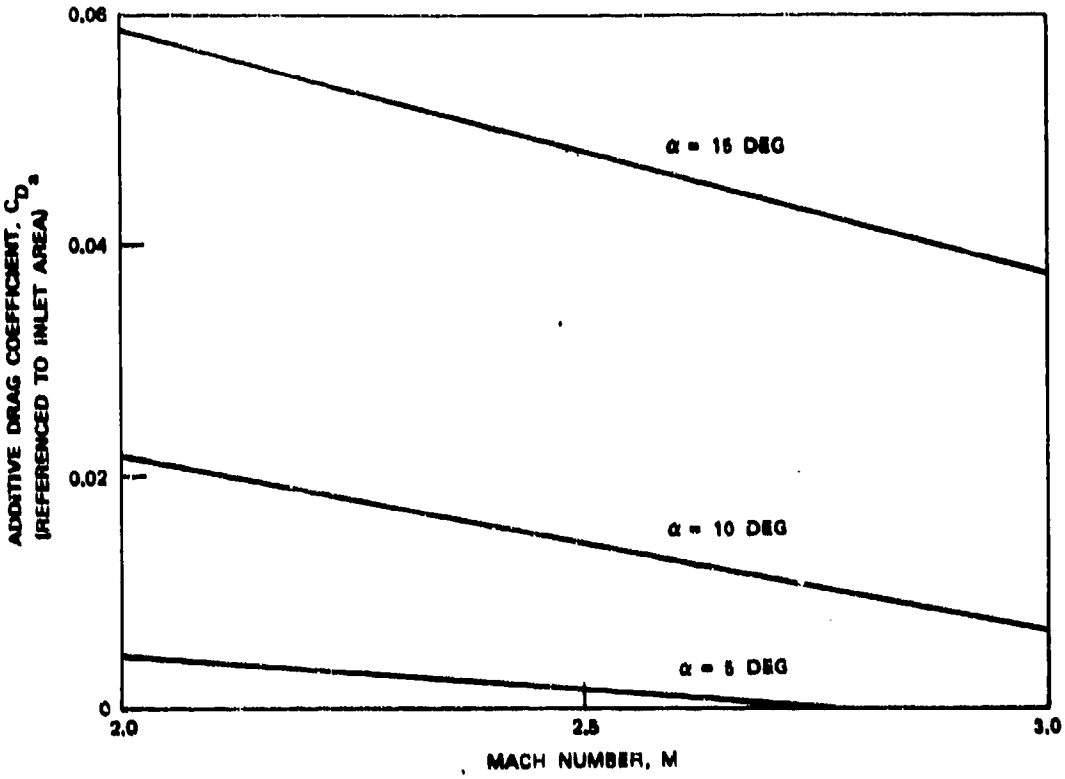

FIGURE 49. Effect of Mach Number on Inlet Additive Drag.

points are specified along the leading edge of the sideplate for tracing back to freestream. The number of points, spacing, and incremental change in the x direction are determined by the program such that new points are introduced at each data printing interval, and the planar relation of each printing is maintained. As in the case without sidewalls, two points are specified in the vicinity of the side edge of the ramp, one slightly above and one on the ramp surface. The determination of perturbation velocities and the streamline trace are calculated in the same manner as without sidewalls. The analytical model requires that the forward portion of the ramp is not bounded by the sidewall. A portion of the ramp is necessary to establish a conical flow regime originating from the corner of the ramp leading edge. The model does not consider the corner flow resulting from the intersection of the sideplate and the ramp. The complicated shock intersections and corner flow occur downstream of the cowl and sideplate leading edges and thus have no effect on a streamline trace upstream to determine mass capture area ratio and additive drag. A simple sidewall with straight cutback, as illustrated in Figure 50, was assumed. Other sidewall shapes could be accomodated with slight changes to the computer program. Various ratios of the sideplate length to inlet length were assumed. The effect of sideplate geometry on inlet capture area ratio is presented in Figure 51 for the case of a 10-degree ramp. As

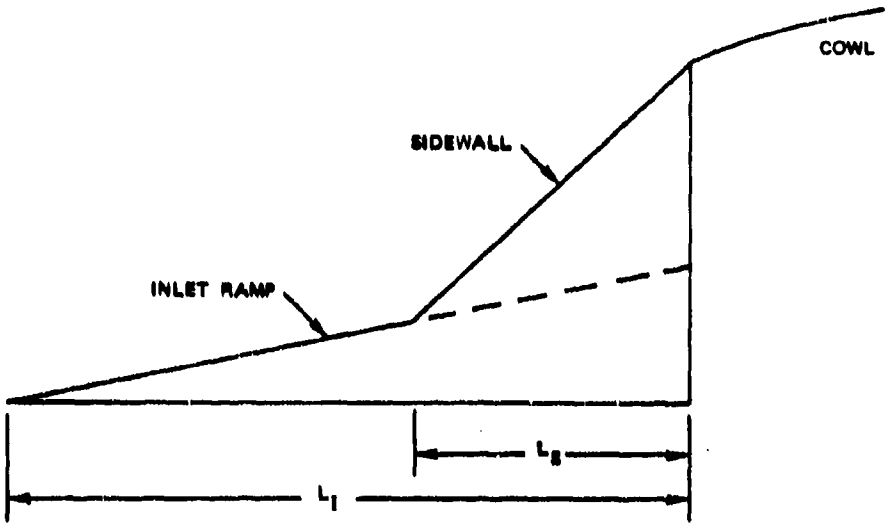

FIGURE 50. Inlet Showing Sidewall Configuration.

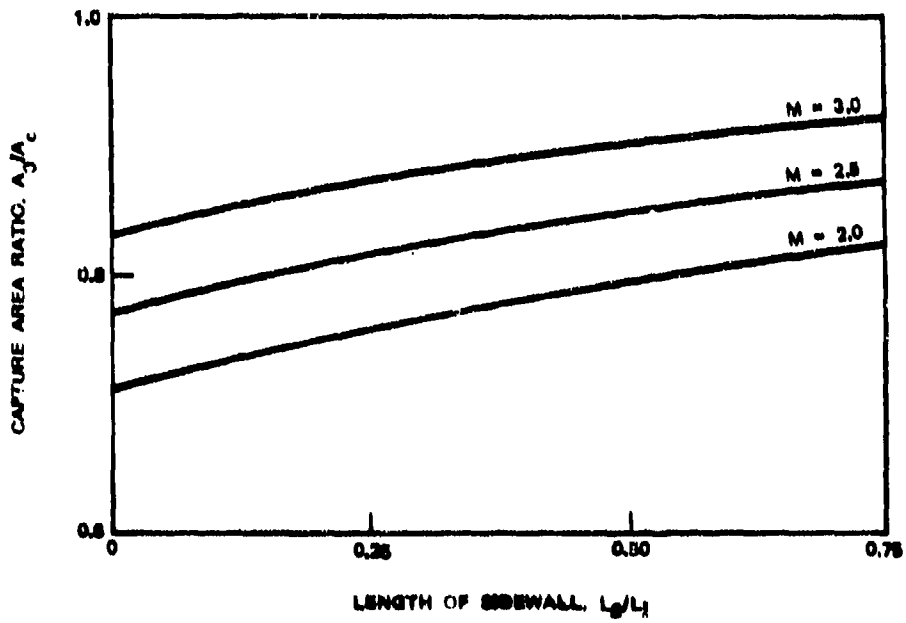

FIGURE 51. Effect of Sidewalls on Inlet Capture Area Ratio.

expected, increasing the sidewall area reduces the spillage, thus increasing the capture area ratio. The shapes of the captured streamtubes are illustrated in Figure 52 for Mach number of 2.5. All of the effect of sidewalls is shown by the distortion of the side of the streamtube. Since the cowl was not changed, the upper portion, which was traced from the cowl, remains undistorted. As the sidewall area is increased, the sidespillage is reduced, and the capture area increases.

The effect of sidewalls on additive drag is shown in Figure 53. The upper portion of the streamtube provides most of the drag. The forces on the side changes

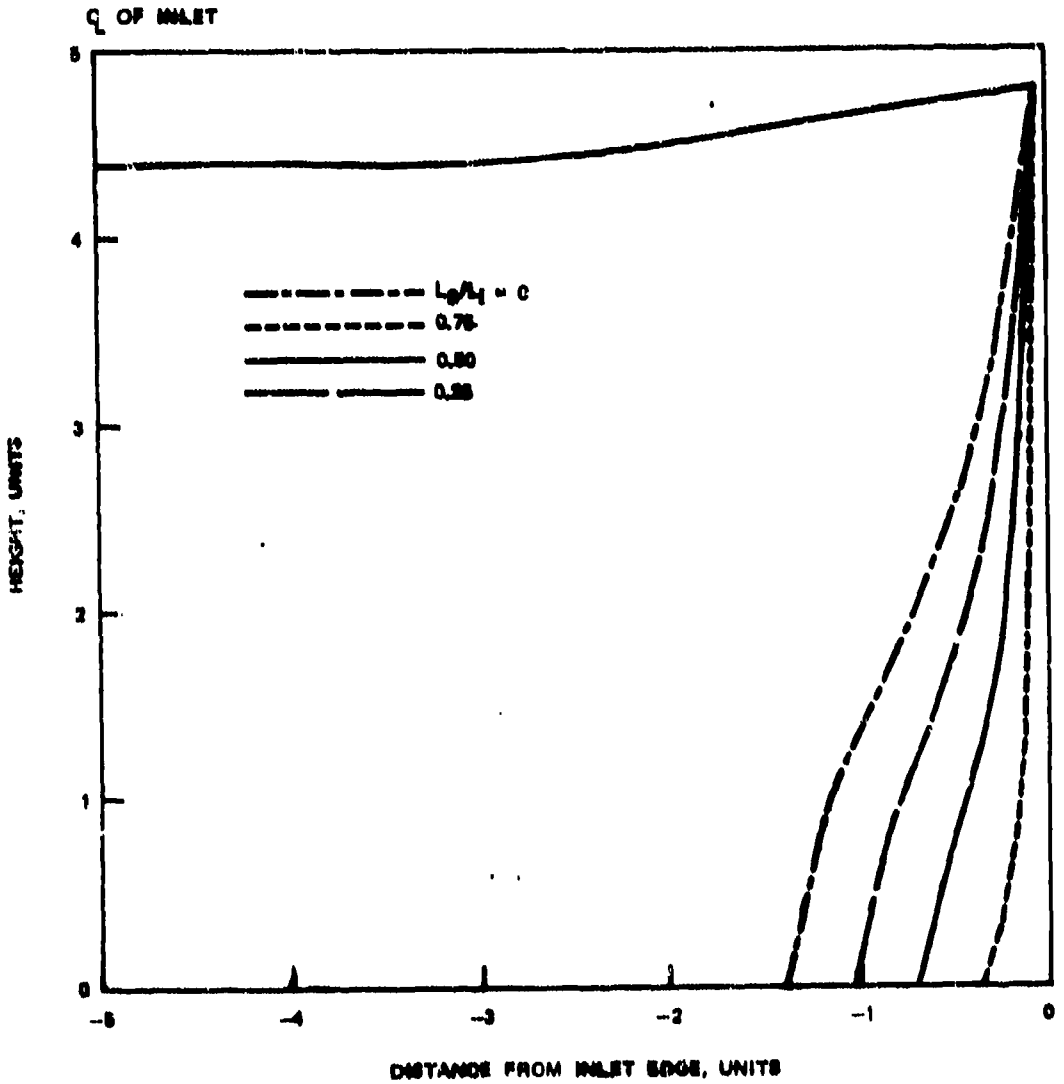

FIGURE 52. Effect of Sidewalls on Captured Streamtubes, M = 2.5.

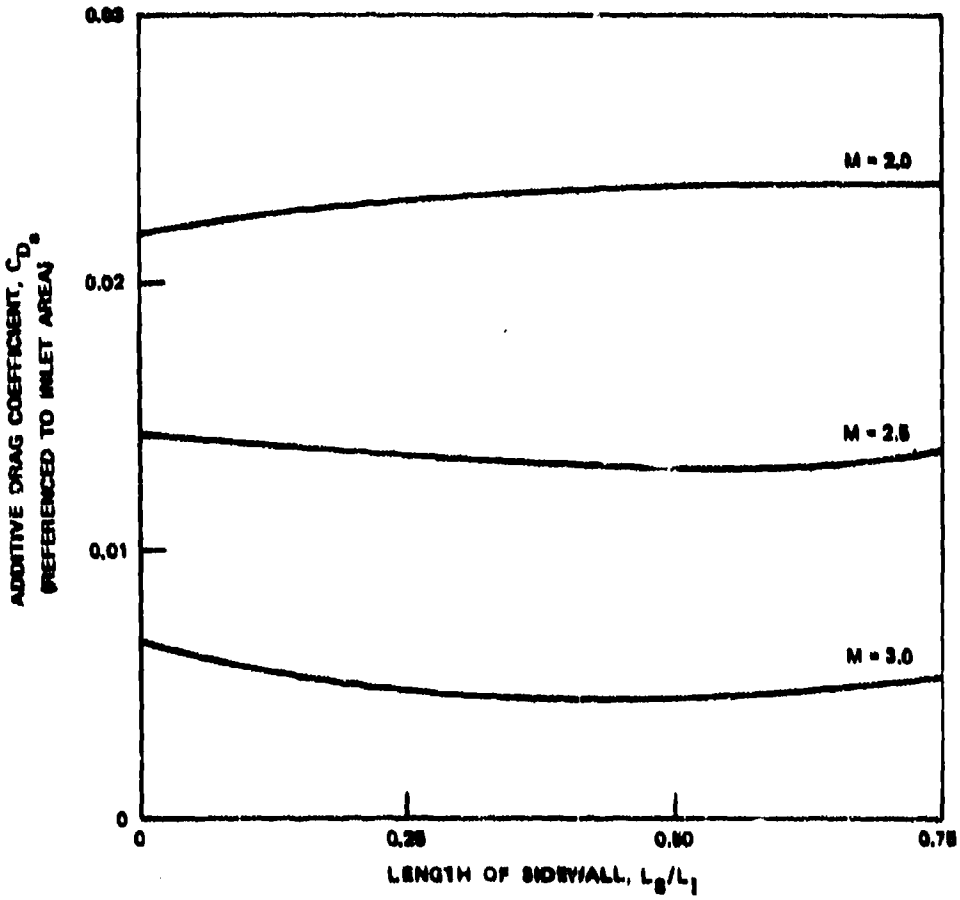

FIGURE 53. Effect of Sidewalls on Inlet Additive Drag.

this value only slightly. Both positive and negative pressure coefficients are found in the side of the streamtube. Near the edge of the ramp, the lateral perturbations increase, resulting in local pressures less than freestream. This tends to decrease the net drag of the streamtube. Depending on the amount of lateral spillage and the area of the streamtube, the contribution of sidewalls may be an increase or decrease in additive drag. This is indicated in Figure 53. At a Mach number of 2.0, the presence of sidewalls reduces the lateral spillage and increases additive drag. At the higher Mach numbers, a minimum drag occurs. In all cases, the effect of the side is small relative to the greater contribution of the upper surface of the streamtube.

Effect of Leading Edge Sweepback

In general, two-dimensional inlets are constructed with the leading edge perpendicular to the sides, i.e., with no sweepback. The computer program was

employed to examine the effects of leading edge sweepback. The derivation of the perturbation velocity components was general, not limited to the case of no sweepback. An inlet with sweepback is illustrated in Figure 54. The inlet cowl is also swept such that the cowl is parallel to the leading edge. To consider an inlet with sweepback, two sides must be considered separately with supplementary sweepback angles. The individual solutions must be combined to obtain the solution for the full inlet.

The effect of leading edge sweepback on the capture area ratio of the baseline 10-degree ramp inlet is illustrated in Figure 55. There is no change in the capture area ratio at any of the Mach numbers considered for sweepback angles of up to 20 degrees. This may be explained by examining the captured streamtube shown in Figure 56. This was determined for the case of 20-degree sweepback at a Mach number of

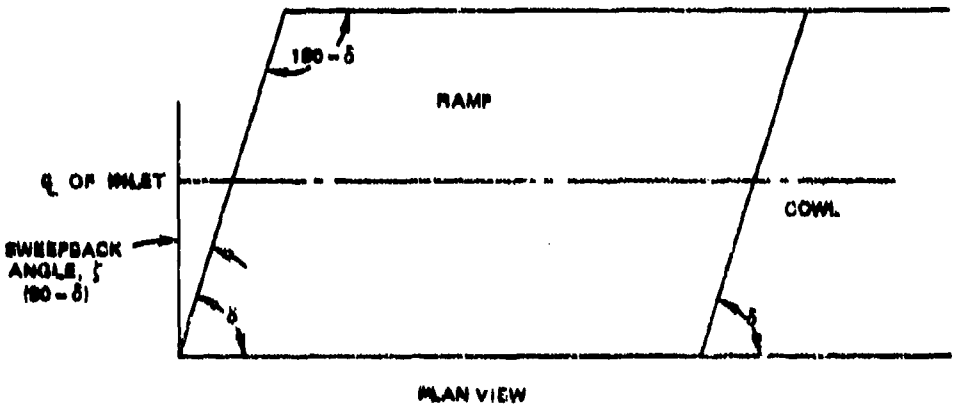

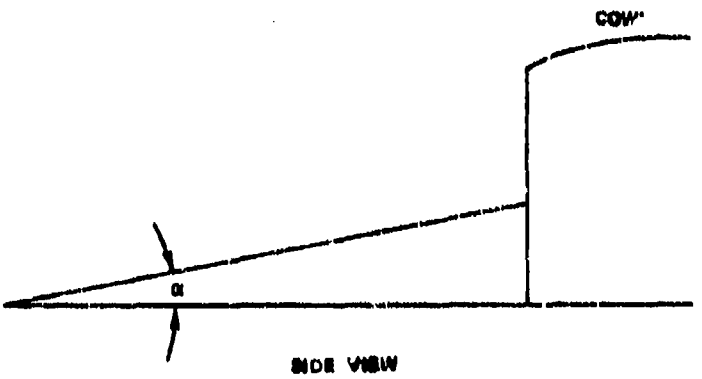

FIGURE 54. Inlet With Leading Edge Sweepback.

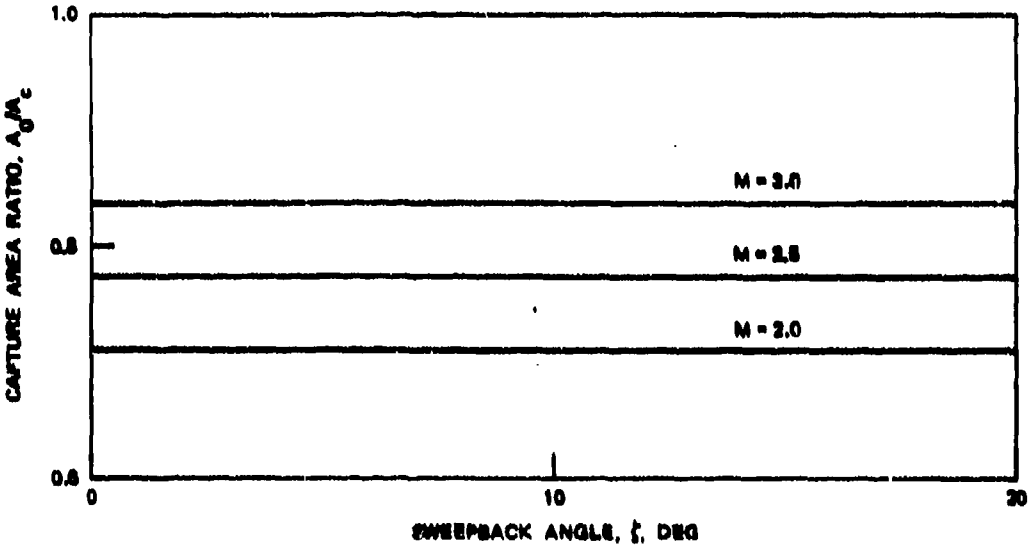

FIGURE 55. Effect of Sweepback Angle on Inlet Capture Area Ratio.

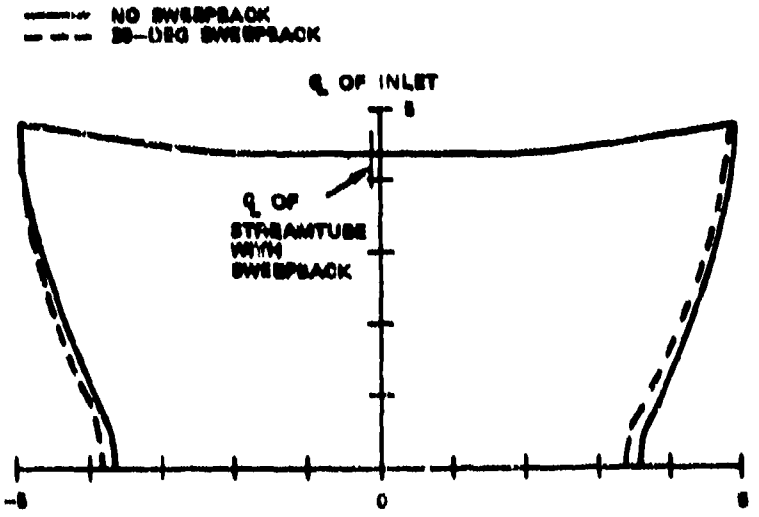

FIGURE 56. Effect of Sweepback on Captured Streamtube, M = 2.5, α = 10 Degrees.

2.5. The effect of sweepback is to shift the flow laterally. Thus, the centerline of the streamtube is displaced from the centerline of the inlet. Comparing the streamtube with sweepback to that without sweepback, it appears that lateral displacements on one side are approximately matched by similar displacements on the other side. Thus, little effect on capture area ratio is anticipated. Similarly, sweepback has no effect on additive drag as shown in Figure 57. Increases in drag on one side of the streamtube are counteracted by decreases on the other side.

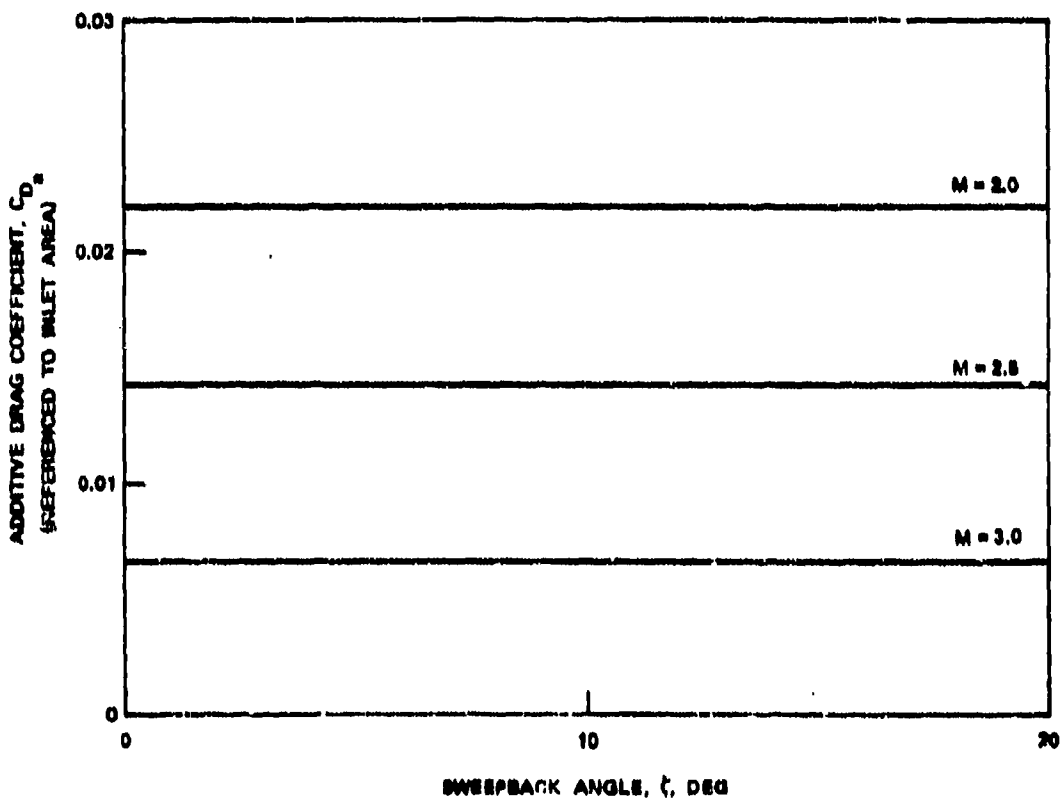

FIGURE 57. Effect of Sweepback Angle on Inlet Additive Drag.

Chapter 6. SUMMARY AND DISCUSSION OF APPLICABILITY

The problem of additive drag of two-dimensional inlets has been examined. The theory of homogeneous conical flows as described by Milne-Thomson was expanded to determine the three-dimensional perturbation velocity components within a region of conical flow as formed by the edge of an inlet. A computer program was written to trace streamlines upstream from an arbitrary inlet cowl to freestream conditions. This technique is used to determine the shape and area of the captured streamtube. The local static pressures, as computed from the velocity field, are numerically integrated to determine the inlet additive drag.

The computer program was applied to a baseline inlet configuration to evaluate the effects of various inlet design parameters: freestream Mach number, ramp angle, sidewalls, and leading edge sweepback. Further application of the program to other configurations such as both sidewalls and sweepback is simple.

Consideration must be given to the range of applicability of this technique. One limitation is the small perturbation assumption which is the basis of the method of homogeneous conical flows. It is assumed that the perturbation components are small relative to freestream velocity or $u_i/V \ll 1$. For two-dimensional flow,

$$\frac{u}{V} = -\alpha \tan \mu$$

and

$$\frac{w}{V} = \alpha \tag{6-1}$$

For Mach numbers greater than $\sqrt{2}$ or 1.41, the tangent of the Mach angle is less than unity and the vertical component w is the limiting condition.

If, for example, it is assumed that $w/V = 0.3$ is a reasonable limit of the assumption of a small perturbation velocity, the theory may be applied to ramp angles of up to 17.2 degrees, independent of Mach number. Other choices of the definition of a "small perturbation" will result in different limiting ramp angles.

An alternate approach is to compare the perturbation velocities obtained by oblique shock theory and by linearized theory for two-dimensional flow. These perturbation velocities in the vertical and axial directions are compared in Figures 58 and 59, respectively. As has been previously observed, the vertical perturbation velocity in two-dimensional linearized theory is independent of Mach number. Since the perturbation velocities by both theories are less than freestream velocity, the magnitude of the differences in perturbation velocity divided by freestream velocity was considered to be a valid criterion in determining the range of applicability of the additive drag analysis. The range is presented in Figure 60 for various differences. This

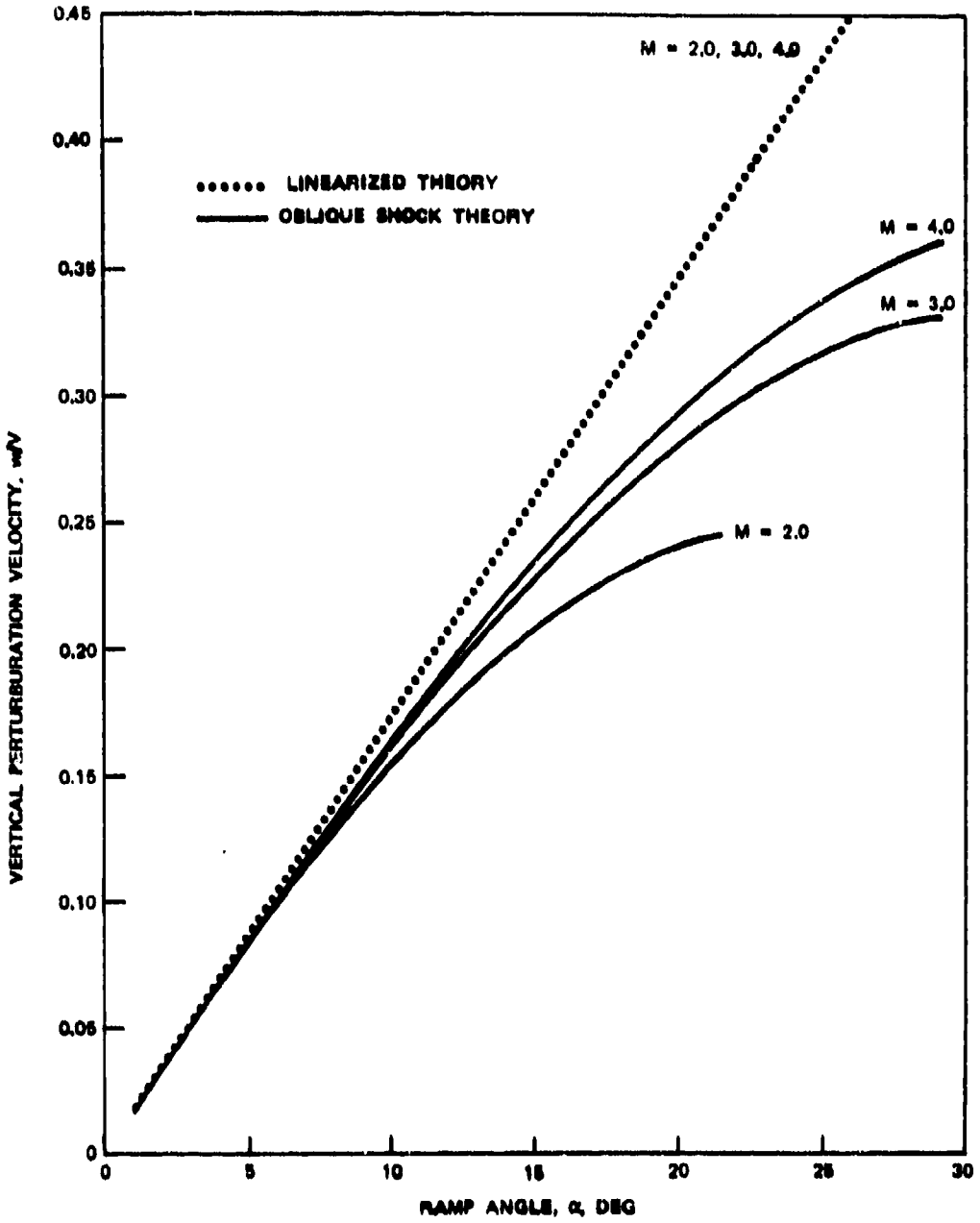

FIGURE 58. Comparison of Vertical Perturbation Velocities.

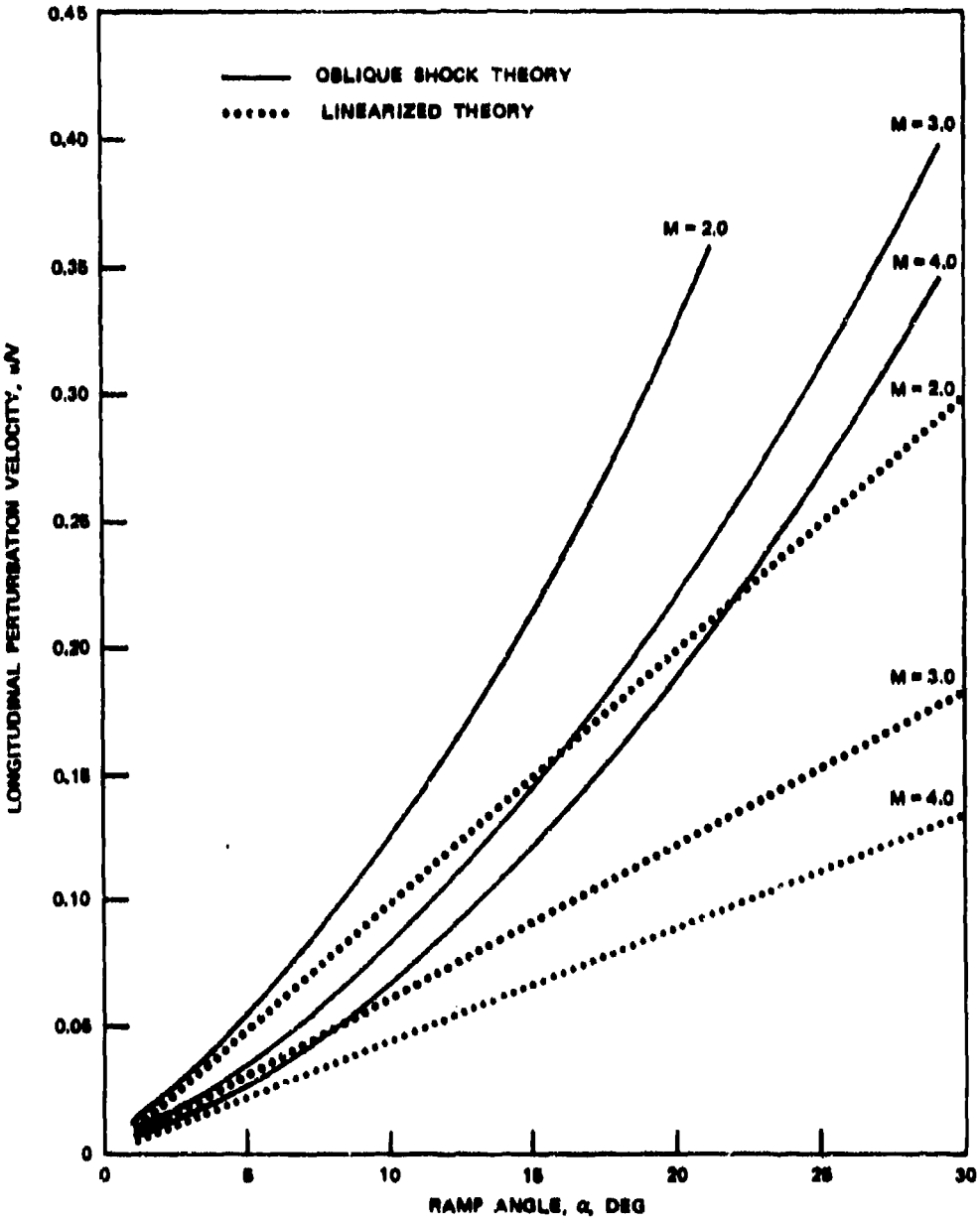

FIGURE 59. Comparison of Longitudinal Perturbation Velocities.

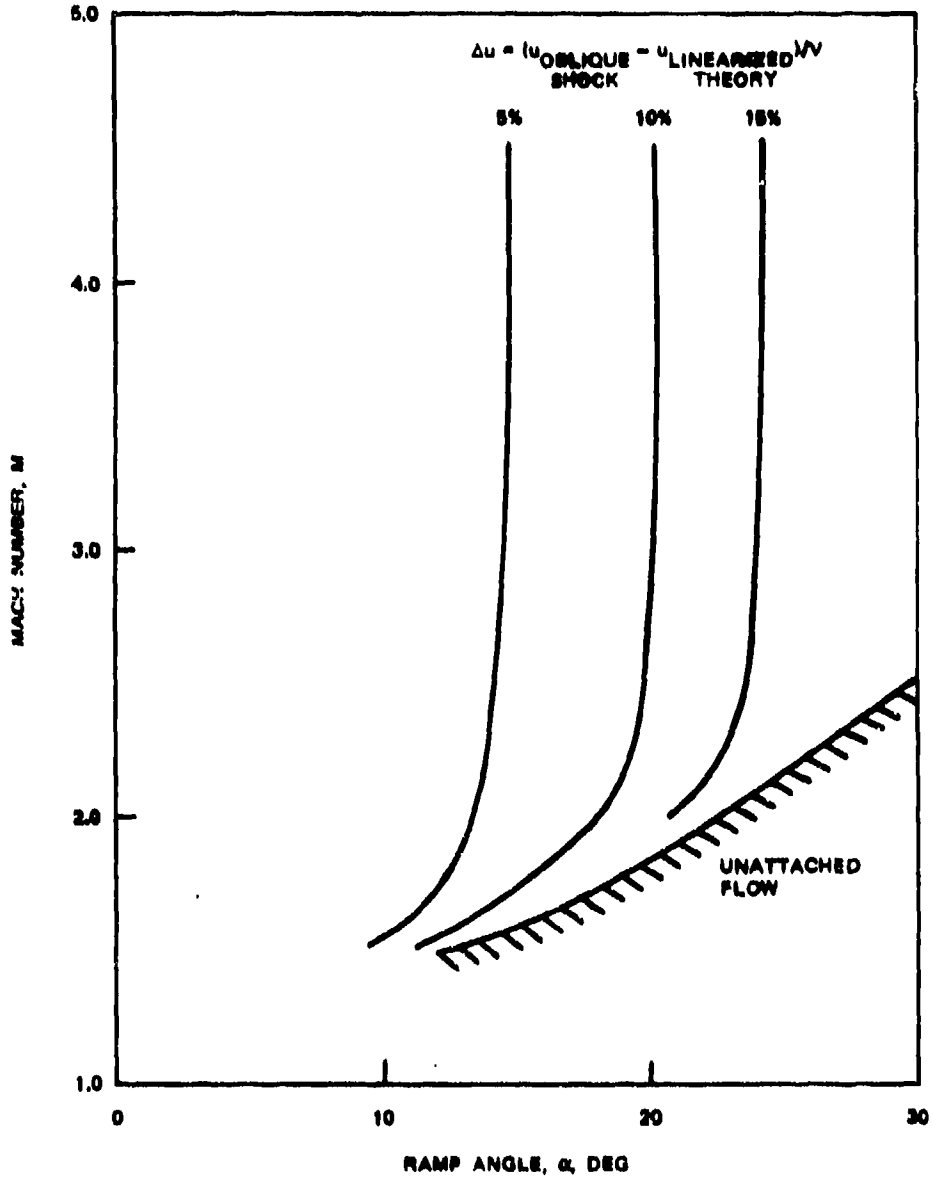

FIGURE 60. Range of Applicability.

figure was controlled by the longitudinal perturbation velocities. The vertical velocities demonstrated smaller differences for the same conditions. As can be seen from the figure, this method may be applied for reasonable ranges of Mach number and inlet ramp angle.

REFERENCES

1. NATO Advisory Group for Aerospace Research and Development. *Supersonic Inlets*, by I. D. V. Faro. May 1975. (AGARDograph 102.)

2. Johns Hopkins University Applied Physics Laboratory. *Handbook of Supersonic Aerodynamics – Section 17, Ducts, Nozzles, and Diffusers*, January 1964. (NAVWEPS Report 1488, Vol. 6.)

3. National Advisory Committee for Aeronautics. *Preliminary Investigation of a New Type of Supersonic Inlet*, by A. Ferri and L. M. Nucci. 1952. (NACA Report 1104.)

4. ———. *Theoretical and Experimental Investigation of Additive Drag*, by M. Sibulkin. 1954. (NACA Report 1187.)

5. J. S. Mount. "Effect of Inlet Additive Drag on Aircraft Performance," *Journal of Aircraft*, Vol. 2, No. 5 (September/October 1965), pp. 374-78.

6. R. V. Osmon. "Improved Methods of Spillage Drag Prediction for Two-Dimensional Inlets," *Journal of Aircraft*, Vol. 5, No. 4 (May/June 1968), pp. 254-60.

7. National Advisory Committee for Aeronautics. *Approximate Method for Predicting Form and Location of Detached Shock Waves Ahead of Plane or Axially Symmetric Bodies*, by W. R. Moeckel. July 1949. (NACA TN 1921.)

8. Naval Weapons Center. *Procedures for Estimating Inlet External and Internal Performance*, by B. M. Sharp and J. P. Howe. April 1974. (NWC TP 5555.)

9. P. Carriere and J. Leynaert. "Recherches sur les Prises D'Air Supersoniques," Jahrbuch 1959 der WGL, pp. 80-89.

10. T. P. Pawlikowski. "Additive Drag Resulting from Lateral Air Flow on Two-Dimensional Inlets," Master of Science Thesis, St. Louis University, August 1967.

11. L. M. Milne-Thomson. *Theoretical Aerodynamics*. MacMillan & Co., Ltd., London, 1952.

12. National Advisory Committee for Aeronautics. *Infinitesimal Conical Supersonic Flow*, by A. Busemann. March 1947. (NACA Technical Memorandum No. 1100.)

13. ———. *Linearized Supersonic Theory of Conical Wings*, by P. A. Lagerstrom. January 1950. (NACA TN 1685.)

14. Vought Corporation. *"As-Cast" Inlet Test Report*, by R. G. Kemper. March 1976. (Report No. 2-53390/6R-51310.)

Appendix A
DERIVATION OF COMPATIBILITY RELATIONSHIPS

The complex velocity components $U(\epsilon)$, $V(\epsilon)$, and $W(\epsilon)$ are not independent since their real parts, u, v, and w, are velocity components of an irrotational flow. Since u, v, and w are homogeneous functions of degree zero in coordinates x, y, and z, the velocity potential from which they are derived must be homogeneous of degree one. Let f(x,y,z) be a homogeneous function of degree n. Euler's theorem states that

$$xf_x + yf_y + zf_z = nf \tag{A-1}$$

where subscripts indicate partial differentiation. For the velocity potential Φ, n = 1

$$x\Phi_x + y\Phi_y + z\Phi_z = \Phi \tag{A-2}$$

Since

$$\frac{\partial \Phi}{\partial x_k} = - u_k$$

$$\Phi = - xu - yv - zw \tag{A-3}$$

Therefore

$$d\Phi = - udx - vdy - wdz - xdu - ydv - zdw \tag{A-4}$$

But by chain rule of differentiation,

$$d\Phi = \Phi_x dx + \Phi_y dy + \Phi_z dz = - udx - vdy - wdz \tag{A-5}$$

By subtracting from Equation A-4

$$xdu + ydv + wdz = 0 \tag{A-6}$$

Since the complex components u*, v*, and w* are also perturbation components of some conical flow, it follows that

$$xdu^* + ydv^* + wdz^* = 0 \tag{A-7}$$

By multiplying by i and adding to Equation A-6

$$x(du + idu^*) + y(dv + idv^*) + z(dw + idw^*) = 0 \tag{A-8}$$

Since

$$du + i du^* = dU = U' de$$

where ' indicates differentiation with respect to e, Equation A-8 becomes

$$xU' + yV' + zW' = 0 \tag{A-9}$$

Partial differentiation with respect to x yields

$$U' + (xU'' + yV'' + zW'')e_x = 0 \tag{A-10}$$

or

$$U'/e_x = -(xU'' + yV'' + zW'') \tag{A-11}$$

Differentiating Equation A-10 with respect to y and z yields

$$\frac{U'}{e_x} = \frac{V'}{e_y} = \frac{W'}{e_z} = -(xU'' + yV'' + zW'') \tag{A-12}$$

This is the compatibility equation for irrotational flow. It may be reduced further for application. From the definition of e,

$$\frac{y + iz}{x \tan \mu + R_2} \tag{A-13}$$

where

$$R_2 = (x^2 \tan^2 \mu - y^2 - z^2)^{1/2}$$

By logarithmic differential of Equation A-13

$$\frac{de}{e} = \frac{dy + i dz}{y + iz} - \frac{\tan \mu \, dx + dR_2}{x \tan \mu + R_2} \tag{A-14}$$

Differentiating $R_2^2 = x^2 \tan^2 \mu - y^2 - z^2$ yield

$$2R_2 dR_2 = 2x \tan^2 \mu \, dx - 2y dy - 2z dz \tag{A-15}$$

By substituting into Equation A-14

$$\frac{d\epsilon}{\epsilon} = \frac{dy + idz}{y + iz} - \frac{\tan\mu\, dx + 1/R_2(x\tan^2\mu\, dx - ydy - zdz)}{x\tan\mu + R_2} \tag{A-16}$$

$$\frac{d\epsilon}{\epsilon} = \frac{e_x}{\epsilon}dx + \frac{e_y}{\epsilon}dy + \frac{e_z}{\epsilon}dz \tag{A-17}$$

By collecting terms of dx

$$\frac{e_x}{\epsilon}dx = -\frac{\tan\mu\, dx + 1/R_2\,(x\tan^2\mu\, dx)}{x\tan\mu + R_2} \tag{A-18}$$

$$\frac{e_x}{\epsilon} = -\frac{R_2\tan\mu + x\tan^2\mu}{R_2(x\tan\mu + R_2)}$$

$$= -\frac{\tan\mu\,(R_2 + x\tan\mu)}{R_2(x\tan\mu + R_2)}$$

$$\frac{e_x}{\epsilon} = -\frac{\tan\mu}{R_2} \text{ or } -\frac{e_x}{\epsilon\tan\mu} = \frac{1}{R_2} \tag{A-19}$$

By collecting terms of dy in Equation A-16

$$\frac{e_y}{\epsilon}dy = \frac{dy}{y + iz} - \frac{1/R_2(-ydy)}{x\tan\mu\, R_2} \tag{A-20}$$

Since

$$\epsilon = \frac{y + iz}{x\tan\mu + R_2}$$

$$y + iz = \epsilon(x\tan\mu + R_2) \tag{A-21}$$

Thus,

$$\frac{e_y}{\epsilon} = \frac{1}{\epsilon(x\tan\mu + R_2)} + \frac{y}{R_2(x\tan\mu + R_2)}$$

$$\frac{e_y}{\epsilon} = \frac{R_2 + y^2}{\epsilon R_2(x\tan\mu + R_2)} \tag{A-22}$$

or

$$e_y = \frac{R_2 + ye}{R_2(x \tan \mu + R_2)}$$

or

$$\frac{\frac{e_y}{R_2 + ye}}{x \tan \mu + R_2} = \frac{1}{R_2} \tag{A-23}$$

By collecting terms of dz in Equation A-16

$$\frac{e_z}{e} dz = \frac{i dz}{y + iz} - \frac{1/R_2(-z dz)}{x \tan \mu + R_2} \tag{A-24}$$

Similar to the y components,

$$\frac{\frac{e_z}{iR_2 + ze}}{x \tan \mu + R_2} = \frac{1}{R_2} \tag{A-25}$$

Thus, from Equations A-19, A-23, and A-25

$$\frac{e_x}{-e \tan \mu} = \frac{\frac{e_y}{R_2 + y}}{x \tan \mu + R_2} = \frac{\frac{e_z}{iR_2 + z}}{x \tan \mu + R_2} \tag{A-26}$$

From Equation A-12

$$\frac{U'}{e_x} = \frac{V'}{e_y} = \frac{W'}{e_z}$$

$$\frac{V'}{U'} = \frac{e_y}{e_x} = \frac{R_2 + ye}{(x \tan \mu + R_2)(-e \tan \mu)} \tag{A-27}$$

Consider each term separately

$$\text{Term 1} = \frac{R_2}{(x \tan \mu + R_2)(-e \tan \mu)}$$

From Equation B-5 in Appendix B

$$R_2^2 = x^2 \tan^2 \mu (1 - r^2)$$

$$\text{Term 1} = \frac{-x \tan \mu (1 - r^2)^{1/2}}{(x \tan \mu + \tan \mu (1 - r^2)^{1/2})(e \tan \mu)}$$

$$\text{Term 1} = \frac{-(1 - r^2)^{1/2}}{[1 + (1 - r^2)^{1/2}] e \tan \mu}$$

From Equation B-9

$$1 - R^2 = \frac{2\sqrt{1 - r^2}}{1 + \sqrt{1 - r^2}}$$

Thus,

$$\text{Term 1} = \frac{-(1 - R^2)}{2e \tan \mu} \qquad \text{(A-28)}$$

The second term in Equation A-27 is

$$\text{Term 2} = \frac{ye}{(x \tan \mu + R_2)(-e \tan \mu)}$$

From Equation B-2

$$s = r \cos \theta = \frac{y}{x \tan \mu}$$

$$y = (r \cos \theta)(x \tan \mu)$$

By substituting for y and for R_2 from Equation B-5

$$\text{Term 2} = \frac{e(r \cos \theta)(x \tan \mu)}{[x \tan \mu + x \tan \mu (1 - r^2)^{1/2}][-e \tan \mu]}$$

$$\text{Term 2} = \frac{-er \cos \theta}{e \tan \mu (1 + (1 - r^2)^{1/2})} \qquad \text{(A-29)}$$

From Equation B-8

$$\sqrt{1 - r^2} = \frac{1 - R^2}{1 + R^2}$$

and from Equation B-10

$$r = \frac{2R}{1 + R^2}$$

Equation A-29 becomes

$$\text{Term 2} = \frac{- e \cos\theta \, \frac{2R}{1 + R^2}}{e \tan\mu \; 1 + \frac{1 - R^2}{1 + R^2}} = \frac{- e \cos\theta \; 2R}{e \tan\mu \, (1 + R^2 + 1 - R^2)}$$

$$\text{Term 2} = \frac{- 2eR \cos\theta}{2e \tan\mu} \qquad \text{(A-30)}$$

Combining the terms A-28 and A-30, Equation A-27 becomes

$$\frac{V'}{U'} = \frac{e_y}{e_x} = \frac{- (1 - R^2)}{2e \tan\mu} - \frac{2eR \cos\theta}{2e \tan\mu}$$

$$\frac{V'}{U'} = \frac{e_y}{e_x} = \frac{R^2 - 2eR \cos\theta - 1}{2e \tan\mu} \qquad \text{(A-31)}$$

Since

$$\begin{aligned} e &= Re^{i\theta} = R \cos\theta + Ri \sin\theta \\ e/R &= \cos\theta + i \sin\theta \\ R/e &= e^{-i\theta} = \cos\theta - i \sin\theta \\ e/R + R/e &= 2 \cos\theta \\ e^2 + R^2 &= 2Re \cos\theta \\ e^2 &= 2Re \cos\theta - R^2 \\ - (1 + e^2) &= - 1 - 2Re \cos\theta + R^2) \end{aligned} \qquad \text{(A-32)}$$

By substituting into Equation A-31

$$\frac{V'}{U'} = \frac{e_y}{e_x} = \frac{- (1 + e^2)}{2e \tan\mu}$$

or

$$\frac{U'}{2\epsilon \tan \mu} = \frac{V'}{-(1+\epsilon^2)} \tag{A-33}$$

In a manner similar to the above deviation for V', from Equations A-12 and A-26

$$\frac{U'}{e_x} = \frac{W'}{e_z}$$

$$\frac{W'}{U'} = \frac{e_z}{e_x} = \frac{iR_2 + z\epsilon}{(x \tan \mu + R_2)(-\epsilon \tan \mu)} \tag{A-34}$$

as before, in Equation A-28, the first term becomes

$$\text{Term 1} = \frac{-i(1-R^2)}{2\epsilon \tan \mu}$$

Since $s^* = r \sin \theta = z/x \tan \mu$, the second term of Equation A-34 becomes

$$\text{Term 2} = \frac{z\epsilon}{(x \tan \mu + R_2)(-\epsilon \tan \mu)}$$

$$\text{Term 2} = \frac{-2\epsilon r \sin \theta}{2\epsilon \tan \mu}$$

and Equation A-39 becomes

$$\frac{W'}{U'} = \frac{e_z}{e_x} = \frac{-i(1-R^2) - 2\epsilon r \sin \theta}{2\epsilon \tan \mu} \tag{A-35}$$

Again,

$$\epsilon/R = \cos \theta + i \sin \theta$$
$$R/\epsilon = e^{-i\theta} = \cos \theta - i \sin \theta$$
$$\epsilon/R - R/\epsilon = 2i \sin \theta$$
$$\epsilon^2 = 2R\epsilon i \sin \theta + R^2$$
$$1 - \epsilon^2 = 1 - 2R\epsilon i \sin \theta - R^2$$
$$-i(1-\epsilon^2) = -i(1-R^2) - 2R\epsilon \sin \theta$$

From Equation A-34

$$\frac{W'}{U'} = \frac{e_z}{e_x} = -\frac{i(1 - e^2)}{2e \tan \mu}$$

Combining with Equation A-33

$$\frac{U'}{2e \tan \mu} = \frac{V'}{-(1 + e^2)} = \frac{W'}{-i(1 - e^2)} \qquad \text{(A-36)}$$

which are the compatibility relationships for irrotational flow.

Appendix B
DERIVATION OF SIMPLIFYING RELATIONSHIPS FOR THE BUSEMANN TRANSFORMATION

The following relationships are useful in deriving the compatibility relationships described in Appendix A. Consider Busemann's complex variable

$$\epsilon \equiv \frac{y + iz}{x \tan \mu + R_2} \tag{B-1}$$

where $R_2 = (x^2 \tan^2 \mu - y^2 - z^2)^{1/2}$

The x, y, and z symbols are Cartesian coordinates and μ is the Mach angle $\sin^{-1} 1/M$. The dimensionless variables r, s, and s* may be employed in mapping from the physical plane to the ϵ plane, where

$$s = r \cos \theta = \frac{y}{x \tan \mu} \tag{B-2}$$

$$s^* = r \sin \theta = \frac{z}{x \tan \mu}$$

$$\epsilon = \frac{s + is^*}{1 + (1 - s^2 - s^{*2})^{1/2}}$$

$$\epsilon = \frac{r(\cos \theta + i \sin \theta)}{1 + (1 - r^2)^{1/2}} = Re^{i\theta} \tag{B-3}$$

where

$$R = \frac{r}{1 + (1 - r^2)^{1/2}} = \frac{1 - (1 - r^2)^{1/2}}{r} \tag{B-4}$$

Proof 1: $R_2^2 = x^2 \tan^2 \mu (1 - r^2)$

$$R_2^2 = x^2 \tan^2 \mu - y^2 - z^2 = x^2 \tan^2 \mu - s^2 \tan^2 \mu - s^{*2} \tan^2 \mu$$

$$= x^2 \tan^2 \mu (1 - s^2 - s^{*2}) = x^2 \tan^2 \mu (1 - r^2 \cos^2 \theta - r^2 \sin^2 \theta)$$

$$R_2^2 = x^2 \tan^2 \mu (1 - r^2) \tag{B-5}$$

Proof 2: $\sqrt{(1 - r^2)} = \frac{1 - R^2}{1 + R^2}$

from Equation B-4

$$R = \frac{1 - (1 - r^2)^{1/2}}{r}$$

$$R^2 = \frac{1 - 2(1 - r^2)^{1/2} + 1 - r^2}{r^2}$$

$$R^2 = \frac{2 - 2(1 - r^2)^{1/2} - r^2}{r^2}$$

$$1 - R^2 = 1 - \frac{2 - 2(1 - r^2)^{1/2} - r^2}{r^2}$$

$$1 - R^2 = \frac{r^2 - 2 + 2(1 - r^2)^{1/2} + r^2}{r^2} = \frac{2r^2 - 2 + 2(1 - r^2)^{1/2}}{r^2} \qquad \text{(B-6)}$$

$$1 + R^2 = \frac{r^2 + 2 - 2(1 - r^2)^{1/2} - r^2}{r^2}$$

$$1 + R^2 = \frac{2 - 2(1 - r^2)^{1/2}}{r^2} \qquad \text{(B-7)}$$

$$\frac{1 - R^2}{1 + R^2} = \frac{2r^2 - 2 + 2(1 - r^2)^{1/2}/r^2}{2 - 2(1 - r^2)^{1/2}/r^2} = \frac{r^2 - 1 + (1 - r^2)^{1/2}}{1 - (1 - r^2)^{1/2}}$$

$$= \frac{[r^2 - 1 + (1 - r^2)^{1/2}][1 + (1 - r^2)^{1/2}]}{1 - (1 - r^2)}$$

$$= \frac{r^2 - 1 + (1 - r^2)^{1/2} - (1 - r^2)^{1/2} - (1 - r^2)^{1/2} + (1 - r^2)}{r^2}$$

$$= \frac{r^2(1 - r^2)^{1/2}}{r^2}$$

$$\frac{1 - R^2}{1 + R^2} = \sqrt{(1 - r^2)} \qquad \text{(B-8)}$$

Proof 3: $\frac{2\sqrt{1-r^2}}{1+\sqrt{1-r^2}} = 1 - R^2$

From Equation B-6

$$1 - R^2 = \frac{2r^2 - 2 + 2(1-r^2)^{1/2}}{r^2} = \frac{[2r^2 - 2 + 2(1-r^2)^{1/2}][1 + (1-r^2)^{1/2}]}{r^2[1 + (1-r^2)^{1/2}]}$$

$$= \frac{2r^2 - 2 + 2(1-r^2)^{1/2} + 2r^2(1-r^2)^{1/2} - 2(1-r^2)^{1/2} + 2(1-r^2)}{r^2[1 + (1-r^2)^{1/2}]}$$

$$= \frac{2r^2(1-r^2)^{1/2}}{r^2[1 + (1-r^2)^{1/2}]}$$

$$1 - R^2 = \frac{2\sqrt{1-r^2}}{1+\sqrt{1-r^2}} \qquad \text{(B-9)}$$

Proof 4: $r = \frac{2R}{1+R^2}$

From Equation B-4

$$R = \frac{1 - (1-r^2)^{1/2}}{r}$$

From Equation B-7

$$1 + R^2 = \frac{2 - 2(1-r^2)^{1/2}}{r^2} = \frac{2(1 - (1-r^2)^{1/2})}{r^2}$$

By substitution for R

$$1 + R^2 = \frac{2R}{r}$$

Thus,

$$r = \frac{2R}{1+R^2} \qquad \text{(B-10)}$$

Appendix C
LISTING AND SAMPLE PRINTOUT OF COMPUTER PROGRAM

Program Listing

```
C       THIS PROGRAM TRACES THE STREAMLINES FROM THE COWL
C      OF AN INLET USING THE METHOD OF HOMOGENEOUS CONICAL
C      FLOWS - MILNE-THOMSON
       COMPLEX EPS,ANU,A1,B1,CU,CV,CW1,CW2,CFNU
       COMPLEX CVEL1,CVEL2,CVEL3
       COMPLEX T1,T2,T3,T4,T5,T6
       DIMENSION X(300,30),Y(300,30),Z(300,30),P(300,30)
       WRITE(6,138)
  138 FORMAT(1H1)
C      INITIALIZE PROBLEM
       CRAD = 3.14159265/180.
   95 READ(5,110) AMACH
  110 FORMAT(8F10.3)
       IF(AMACH.LT.0.0) GO TO 96
       WRITE(6,111) AMACH
  111 FORMAT(/,26H FREESTREAM MACH NUMBER = ,F10.3)
       VASTAR=SQRT(1.2*AMACH*AMACH/(1.+.2*AMACH*AMACH))
       PZERO=1./((1.+.2*AMACH*AMACH)**3.5)
       QZERO=.7*AMACH*AMACH*PZERO
       AMU=ASIN(1./AMACH)
       TANMU=TAN(AMU)
       UINF=1.0
       VINF=0.0
C      DESCRIBE INLET AND INITIALIZE GRID
       READ(5,110)ALPHA,XCOWL,ZCOWL,XSIDE,WIDTH,DELTA
       WIDTH=WIDTH/2.0
       ZSIDE=XSIDE*TAN(ALPHA*CRAD)
       AREF=WIDTH*ZCOWL
       NSIDE=5+10.0*(XCOWL-XSIDE)/XCOWL
       NLINE=11+NSIDE
       DZ=(ZCOWL-ZSIDE)/NSIDE
  120 FORMAT(2I10,F10.4)
       WRITE(6,112)ALPHA,XCOWL,ZCOWL,XSIDE,ZSIDE
  112 FORMAT(' INLET RAMP ANGLE = ',F10.3,/,
      1' COWL COORDS = ',2F10.3,/,' SIDE COORDS = ',2F10.3)
       WRITE(6,113)WIDTH,DELTA
  113 FORMAT(15H INLET WIDTH = ,F10.3,/,
      121H INLET SWEEP ANGLE = ,F10.3)
       WRITE(6,116)
       WINF=-ALPHA*CRAD
       IF(DELTA.EQ.90.0) GO TO 90
       C3=1.0/(TAN(DELTA*CRAD))
       COSLAM=-TANMU/(TAN(DELTA*CRAD))
       ALMBDA=ACOS(COSLAM)
       THETA=.5*ALMBDA
       GO TO 91
   90 THETA=45.0*CRAD
       ALMBDA=90.0*CRAD
       C3=0.0
   91 D1=COS(THETA)
```

```
      DZ=SIN(THETA)
      A1=CMPLX(D1,DZ)
      B1=CONJG(A1)
      UZERO=-ALPHA*CRAD*TANMU/SIN(ALMBDA)
      DY=WIDTH/10.
      I=1
      WRITE(6,135)
  135 FORMAT(4X,1HI,4X,1HJ,8X,8HX(I,J),4X,8HY(I,J),4X,
     18HZ(I,J))
      DO 20 J=1,11
      X(I,J)=XCOWL
      Y(I,J)=(J-11)*DY
      Z(I,J)=ZCOWL
   20 WRITE(6,114)I,J,X(I,J),Y(I,J),Z(I,J)
  114 FORMAT (2I5,5X,3F10.3)
      IF(XCOWL.NE.XSIDE)GO TO 21
C     NO SIDEPLATE
      WRITE(6,121)
  121 FORMAT(/,14H NO SIDEPLATE  )
      KSIDE=0
      NXX=201
      JX=0
      DX=XCOWL/200.
      ND=NLINE-1
      DO 22 J=12,ND
      X(I,J)=XCOWL
      Y(I,J)=0.0
      Z(I,J)=ZCOWL-(J-11)*DZ
   22 WRITE(6,114)I,J,X(I,J),Y(I,J),Z(I,J)
      IX=1
      GO TO 24
C     INLET WITH SIDEPLATE
   21 DX=(XCOWL-XSIDE)/NSIDE
      WRITE(6,122)
  122 FORMAT(/,14H    SIDEPLATE  )
      KSIDE=1
      JX=1
      NXX=10*XCOWL/DX + 1
      ND=NLINE-1
      DO 23 J=12,ND
      I=10*(J-11)+1
      X(I,J)=XCOWL-(J-11)*DX
      Y(I,J)=0.0
      Z(I,J)=ZCOWL-(J-11)*DZ
   23 WRITE(6,114)I,J,X(I,J),Y(I,J),Z(I,J)
      IX=I+10
      ND=11
      DX=DX/10.
   24 J=NLINE
      I=IX
      X(I,J)=XSIDE
      Y(I,J)=0.0
      Z(I,J)=ZSIDE+.20*DZ
      WRITE(6,114)I,J,X(I,J),Y(I,J),Z(I,J)
      J=NLINE+1
      X(I,J)=XSIDE
      Y(I,J)=-.20*DZ
```

```
      Z(I,J)=ZSIDE
      WRITE(6,114)I,J,X(I,J),Y(I,J),Z(I,J)
      WRITE(6,116)
      WRITE(6,116)
C     EVALUATION OF CONSTANTS
      C1=COS(ALPHA*CRAD)
      C2=SIN(ALPHA*CRAD)
      CU=-UZERO*CMPLX(0.0,1.0)/3.141592654
      CV=-CU/(2*TANMU)
      CW1=-UZERO*CMPLX(1.0,0.0)/(2.0*3.141592654*TANMU)
      CW2=-2.0*UZERO*D1*D2/TANMU
C     STREAMLINE TRACE
      ND=NLINE+1-JX*(NSIDE+1)
      KX=ND*10
      DO 31 I=1,NXX
      DO 30 J=1,ND
C     ROTATE COORDINATES
      XR=C1*X(I,J)+C2*Z(I,J)
      ZR=-C2*X(I,J)+C1*Z(I,J)
      YR=Y(I,J)
      IF(J.EQ.NLINE+1)ZR=0.0
      IF(XR.LE.0.0) GO TO 34
      CHECK=(XR*XR*TANMU*TANMU-YR*YR-ZR*ZR)
      IF (CHECK.LT.0.0)GO TO 32
C     POINT IS WITHIN MACH CONE, USE CONICAL FLOW
      R2=SQRT(CHECK)
      DENOM =XR*TANMU+R2
      EPS=CMPLX(YR/DENOM,ZR/DENOM)
      ANU=CSQRT(EPS)
C     CONICAL PERTURBATION COMPONENTS
      KTYPE=1
      CFNU=((A1+ANU)*(B1+ANU))/((A1-ANU)*(B1-ANU))
      CVEL1=CU*CLOG(CFNU)
      UX=REAL(CVEL1)
      T1=2./(A1*ANU)+2./(B1*ANU)
      T2=2.*A1*ANU+2.*B1*ANU
      T3=(1./(A1*A1))*CLOG((A1+ANU)/ANU)+(1./(B1*B1))
     1*CLOG((B1+ANU)/ANU)
      T4=(1./(A1*A1))*CLOG((A1-ANU)/ANU)+(1./(B1*B1))
     1*CLOG((B1-ANU)/ANU)
      T5=A1*A1*CLOG(A1+ANU)+B1*B1*CLOG(B1+ANU)
      T6=A1*A1*CLOG(A1-ANU)+B1*B1*CLOG(B1-ANU)
      CVEL2=CV*(-T1-T2+T3-T4+T5-T6)
      UY=REAL(CVEL2)
      CVEL3=CW1*(-T1+T2+T3-T4-T5+T6)+CW2
      UZ=REAL(CVEL3)
      GO TO 36
C     TWO DIMENSIONAL FLOW
   32 TANA = ZR/XR
      IF(TANA.GE.TANMU)GO TO 34
C     TWO DIMENSIONAL (PLANAR) FLOW
      KTYPE=2
      UX=UZERO
      UY=UZERO*C2
      UZ=ALPHA*CRAD
      GO TO 36
C     UNDISTURBED FLOW
```

```
   34 KTYPE= 3
      UX=0.0
      UY=0.0
      UZ=0.0
C     STREAMLINE TRACE TO UPSTREAM POSITION
   36 VELX=UINF+UX
      VELY=VINF+UY
      VELZ=WINF+UZ
      DY=DX+VELY/VELX
      DZ=DX+VELZ/VELX
      VV=SQRT(VELX+VELX+VELY+VELY+VELZ+VELZ)
      VP=VV+VASTAR
      PP=(1.-VP+VP/6.)++3.5
      P(I,J)=PP-PZERO
   38 XT=XR-DX
      YT=YR-DY
      ZT=ZR-DZ
      XR=XT
      YR=YT
   40 ZR=ZT
  150 FORMAT(2I5,4F10.5)
      X(I+1,J)=C1+XT-C2+ZT
      Z(I+1,J)=C2+XT+C1+ZT
      Y(I+1,J)=YT
   30 CONTINUE
  115 FORMAT(3I5,7F10.4)
      KX=KX+JX
      ND=KX/10
      IF(ND.NE.NLINE)GO TO 31
      ND=ND+JX
      KX=KX+10
      JX=0
   31 CONTINUE
  151 FORMAT(5I5)
      JX=KSIDE
      ND=NLINE+1-JX+(NSIDE+1)
      DO 71 I=1,NXX,10
      WRITE(6,139)
  139 FORMAT(4X,1HI,4X,1HJ,4X,6HX(I,J),4X,6HY(I,J),4X,
     16HZ(I,J),4X,6HP(I,J))
      DO 72 J=1,ND
   72 WRITE(6,150)I,J,X(I,J),Y(I,J),Z(I,J),P(I,J)
      ND=ND+JX
      IF(ND.NE.NLINE)GO TO 71
      ND=ND+JX
      JX=0
   71 WRITE(6,116)
  116 FORMAT(1H0)
C     STREAMTUBE AREA CALCULATION
      AREA = 0.0
      DO 45 J=1,NLINE
      DAREA=.5+(Y(NXX,J+1)-Y(NXX,J))+(Z(NXX,J+1)+Z(NXX,J))
   45 AREA = AREA+DAREA
      AOAC=AREA/AREF
      WRITE(6,132) AREA,AOAC
  132 FORMAT(/,19H STREAMTUBE AREA = ,F10.3,/,6H AO/AC =
     1,F10.5)
```

```
C       ADDITIVE DRAG CALCULATION
        DRAG=0.0
        ATOT=0.0
        DTOT=0.0
        ND=NXX-1
        JXX=11
        DO 81 I=1,ND
        DO 80 J=1,10
        PBAR=(P(I,J)+P(I+1,J)+P(I,J+1)+P(I+1,J+1))/4.
        AD1=.5*(Y(I,J+1)-Y(I,J))*(Z(I,J+1)+Z(I,J))
        AD2=.5*(Y(I+1,J+1)-Y(I,J+1))*(Z(I+1,J+1)+Z(I,J+1))
        AD3=.5*(Y(I+1,J)-Y(I+1,J+1))*(Z(I+1,J)+Z(I+1,J+1))
        AD4=.5*(Y(I,J)-Y(I+1,J))*(Z(I,J)+Z(I+1,J))
        ADRAG=AD1+AD2+AD3+AD4
        DTOT=DTOT+ADRAG
        ATOT=ATOT+ADRAG
        DDRAG=PBAR*ADRAG
     80 DRAG=DRAG+DDRAG
     81 DTOT=0.0
        WRITE(6,137)
    137 FORMAT(/,14H UPPER SURFACE)
        CDRAG=DRAG/(AREF*QZERO)
        WRITE(6,131)DRAG,CDRAG,ATOT
        DO 87 I=1,ND,10
        DO 86 J=11,NLINE
        IF(KSIDE.EQ.0)GO TO 85
        IF(I.GE.NLINE-10)GO TO 85
        IF(J.LT.JXX) GO TO 85
        IF(J.GT.JXX) GO TO 87
        PBAR=(P(I,J)+P(I+10,J)+P(I,J+1)+P(I+10,J+1))/3.0
        AD1=.5*(Y(I+10,J+1)-Y(I,J))*(Z(I+10,J+1)+Z(I,J))
        AD2=.5*(Y(I+10,J)-Y(I+10,J+1))*(Z(I+10,J)+Z(I+10,J+1))
        AD3=.5*(Y(I,J)-Y(I+10,J))*(Z(I,J)+Z(I+10,J))
        ADRAG=AD1+AD2+AD3
        GO TO 86
     85 PBAR=(P(I,J)+P(I+10,J)+P(I,J+1)+P(I+10,J+1))/4.0
        AD1=.5*(Y(I,J+1)-Y(I,J))*(Z(I,J+1)+Z(I,J))
        AD2=.5*(Y(I+10,J+1)-Y(I,J+1))*(Z(I+10,J+1)+Z(I,J+1))
        AD3=.5*(Y(I+10,J)-Y(I+10,J+1))*(Z(I+10,J)+Z(I+10,J+1))
        AD4=.5*(Y(I,J)-Y(I+10,J))*(Z(I,J)+Z(I+10,J))
        ADRAG=AD1+AD2+AD3+AD4
     86 DTOT=DTOT+ADRAG
        ATOT=ATOT+ADRAG
        DDRAG=PBAR*ADRAG
     80 DRAG=DRAG+DDRAG
     87 CONTINUE
        JXX=JXX+1
     81 DTOT=0.0
        WRITE(6,138)
    138 FORMAT(/,17H TOTAL STREAMTUBE)
        CDRAG=DRAG/(AREF*QZERO)
        WRITE(6,131)DRAG,CDRAG,ATOT
    131 FORMAT(8H DRAG = ,F10.5,/,8H CDRAG = ,F10.5,/,
       121H TUBE SURFACE AREA = ,F10.5)
        WRITE(6,116)
        GO TO 88
     88 WRITE(6,126)
        STOP
        END
```

Sample Printout

```
FREESTREAM MACH NUMBER =       2.500
INLET RAMP ANGLE =        10.000
COWL COORDS =       10.000       5.000
SIDE COORDS =       10.000       1.783
INLET WIDTH =        5.000
INLET SWEEP ANGLE =       90.000

   I     J          X(I,J)       Y(I,J)       Z(I,J)
   1     1          10.000       -5.000        5.000
   1     2          10.000       -4.500        5.000
   1     3          10.000       -4.000        5.000
   1     4          10.000       -3.500        5.000
   1     5          10.000       -3.000        5.000
   1     6          10.000       -2.500        5.000
   1     7          10.000       -2.000        5.000
   1     8          10.000       -1.500        5.000
   1     9          10.000       -1.000        5.000
   1    10          10.000        -.500        5.000
   1    11          10.000         .000        5.000

NO SIDEPLATE
   1    12          10.000         .000        4.383
   1    13          10.000         .000        3.705
   1    14          10.000         .000        3.059
   1    15          10.000         .000        2.411
   1    16          10.000         .000        1.893
   1    17          10.000        -.129        1.783


   I     J          X(I,J)       Y(I,J)       Z(I,J)       P(I,J)
   1     1        10.00000     -5.00000      5.00000      .04692
   1     2        10.00000     -4.50000      5.00000      .04692
   1     3        10.00000     -4.00000      5.00000      .04692
   1     4        10.00000     -3.50000      5.00000      .04692
   1     5        10.00000     -3.00000      5.00000      .03521
   1     6        10.00000     -2.50000      5.00000      .02925
   1     7        10.00000     -2.00000      5.00000      .02493
   1     8        10.00000     -1.50000      5.00000      .02040
   1     9        10.00000     -1.00000      5.00000      .01685
   1    10        10.00000      -.50000      5.00000      .01382
   1    11        10.00000       .00000      5.00000      .01011
   1    12        10.00000       .00000      4.35285      .00780
   1    13        10.00000       .00000      3.70531      .00350
   1    14        10.00000       .00000      3.05786     -.00213
   1    15        10.00000       .00000      2.41052     -.01428
   1    16        10.00000       .00000      1.89274     -.03414
   1    17        10.00000      -.12847      1.78327     -.03308


   I     J          X(I,J)       Y(I,J)       Z(I,J)       P(I,J)
  11     1         9.90760     -5.00000      4.91318      .04692
  11     2         9.90760     -4.50000      4.91318      .04692
```

11	3	9.50760	-4.00000	4.91318	.04692
11	4	9.50760	-3.50000	4.91318	.04692
11	5	9.50562	-3.01125	4.92438	.04125
11	6	9.50400	-2.51875	4.93388	.03257
11	7	9.50252	-2.02344	4.94139	.02704
11	8	9.50127	-1.52646	4.94902	.02243
11	9	9.49993	-1.02794	4.95663	.01834
11	10	9.49852	-.52788	4.96407	.01483
11	11	9.49740	-.02637	4.97098	.01124
11	12	9.49651	-.03514	4.32888	.00838
11	13	9.49531	-.04610	3.68815	.00493
11	14	9.49340	-.08233	3.05185	-.00003
11	15	9.48945	-.09813	2.42667	-.00930
11	16	9.48218	-.20037	1.84987	-.02969
11	17	9.80788	-.38824	1.87648	-.02201

I	J	X(I,J)	Y(I,J)	Z(I,J)	P(I,J)
21	1	9.01519	-5.00000	4.82635	.04692
21	2	9.01519	-4.50000	4.82635	.04692
21	3	9.01519	-4.00000	4.82635	.04692
21	4	9.01519	-3.50000	4.82635	.04692
21	5	9.01293	-3.01283	4.83918	.04692
21	6	9.00993	-2.53232	4.86241	.03778
21	7	9.00585	-2.04278	4.87934	.03037
21	8	9.00305	-1.54928	4.89519	.02498
21	9	9.00031	-1.05252	4.91076	.02038
21	10	8.99784	-.55263	4.92587	.01625
21	11	8.99516	-.04982	4.93995	.01248
21	12	8.99343	-.06748	4.30238	.00963
21	13	8.99117	-.08925	3.66787	.00636
21	14	8.98772	-.12109	3.04008	.00188
21	15	8.98138	-.18400	2.42871	-.00829
21	16	8.97628	-.35449	1.83978	-.01762
21	17	9.01519	-.52985	1.88662	-.01073

I	J	X(I,J)	Y(I,J)	Z(I,J)	P(I,J)
31	1	8.52279	-5.00000	4.73953	.04692
31	2	8.52279	-4.50000	4.73953	.04692
31	3	8.52279	-4.00000	4.73953	.04692
31	4	8.52279	-3.50000	4.73953	.04692
31	5	8.52092	-3.01283	4.75237	.04692
31	6	8.51845	-2.53880	4.78113	.04692
31	7	8.50987	-2.05707	4.81220	.03863
31	8	8.50950	-1.56792	4.83784	.02853
31	9	8.50123	-1.07335	4.86178	.02304
31	10	8.49712	-.57390	4.88507	.01828
31	11	8.49329	-.07002	4.90879	.01388
31	12	8.49076	-.09887	4.27381	.01094
31	13	8.48755	-.12031	3.64464	.00780
31	14	8.48287	-.17819	3.02388	.00384
31	15	8.47512	-.28630	2.42047	-.00191
31	16	8.47388	-.48338	1.80268	-.00853
31	17	8.52278	-.66388	1.80260	-.00409

I	J	X(I,J)	Y(I,J)	Z(I,J)	P(I,J)
41	1	8.03038	-5.00000	4.65270	.04692
41	2	8.03038	-4.50000	4.65270	.04692
41	3	8.03038	-4.00000	4.65270	.04692
41	4	8.03038	-3.50000	4.65270	.04692
41	5	8.02812	-3.01283	4.66554	.04692
41	6	8.02306	-2.53688	4.69430	.04692
41	7	8.01607	-2.08277	4.73385	.04692
41	8	8.00801	-1.68128	4.77391	.03473
41	9	8.00293	-1.08971	4.80837	.02718
41	10	7.99720	-.59112	4.84091	.02111
41	11	7.99185	-.08642	4.87122	.01581
41	12	7.98850	-.12303	4.24288	.01238
41	13	7.98443	-.18612	3.81859	.00928
41	14	7.97874	-.22738	3.00352	.00569
41	15	7.97028	-.34240	2.40431	.00105
41	16	7.97331	-.59525	1.88910	-.00190
41	17	8.03038	-.77939	1.41597	.00068

I	J	X(I,J)	Y(I,J)	Z(I,J)	P(I,J)
81	1	7.93798	-5.00000	4.58588	.04692
81	2	7.93798	-4.50000	4.58588	.04692
81	3	7.93798	-4.00000	4.58588	.04692
81	4	7.93798	-3.50000	4.58588	.04692
81	5	7.93571	-3.01283	4.57872	.04692
81	6	7.93084	-2.53688	4.60748	.04692
81	7	7.92387	-2.08277	4.64703	.04692
81	8	7.91618	-1.68543	4.68810	.04692
81	9	7.90813	-1.10001	4.74847	.03771
81	10	7.49828	-.60319	4.79114	.02724
81	11	7.49097	-.09783	4.83447	.01847
81	12	7.48667	-.14582	4.20548	.01378
81	13	7.48180	-.19950	3.58877	.01044
81	14	7.47929	-.27487	2.97936	.00752
81	15	7.48691	-.41229	2.38180	.00374
81	16	7.47390	-.68413	1.82200	.00248
81	17	7.93797	-.88117	1.32815	.00452

I	J	X(I,J)	Y(I,J)	Z(I,J)	P(I,J)
81	1	7.84587	-5.00000	4.47805	.04692
81	2	7.84587	-4.50000	4.47805	.04692
81	3	7.84587	-4.00000	4.47805	.04692
81	4	7.84587	-3.50000	4.47805	.04692
81	5	7.84331	-3.01283	4.49189	.04692
81	6	7.83824	-2.53688	4.52065	.04692
81	7	7.83128	-2.08277	4.56020	.04692
81	8	7.82378	-1.68543	4.60228	.04692
81	9	7.81330	-1.10005	4.66206	-.00744
81	10	7.80059	-.60615	4.73417	-.00744
81	11	6.99720	-.10083	4.81010	-.00744
81	12	6.99534	-.16408	4.17330	.01602
81	13	6.97868	-.22918	3.55816	.01255
81	14	6.97848	-.31788	2.95167	.00939
81	15	6.96370	-.47623	2.35401	.00627
81	16	6.97832	-.78233	1.77023	.00550

61	17	7.04557	-.97178	1.24232	.00784

I	J	X(I,J)	Y(I,J)	Z(I,J)	P(I,J)
71	1	6.55165	-5.00000	4.40082	-.00744
71	2	6.55165	-4.50000	4.40082	-.00744
71	3	6.55165	-4.00000	4.40082	-.00744
71	4	6.55165	-3.50000	4.40082	-.00744
71	5	6.54787	-3.01283	4.42226	-.00744
71	6	6.54129	-2.53688	4.45851	-.00744
71	7	6.53128	-2.08277	4.51635	-.00744
71	8	6.51878	-1.68543	4.58161	-.00744
71	9	6.50575	-1.10085	4.66119	-.00744
71	10	6.49303	-.80815	4.73329	-.00744
71	11	6.47984	-.10083	4.80822	-.00744
71	12	6.46467	-.17732	4.13336	.01948
71	13	6.47804	-.25477	3.82382	.01481
71	14	6.47022	-.35884	2.92060	.01139
71	15	6.46109	-.53435	2.32167	.00872
71	16	6.47737	-.95126	1.71487	.00900
71	17	6.55317	-1.05271	1.16550	.01089

I	J	X(I,J)	Y(I,J)	Z(I,J)	P(I,J)
81	1	6.04410	-5.00000	4.39894	-.00744
81	2	6.04410	-4.50000	4.39894	-.00744
81	3	6.04410	-4.00000	4.39894	-.00744
81	4	6.04410	-3.50000	4.39894	-.00744
81	5	6.04032	-3.01283	4.42137	-.00744
81	6	6.03373	-2.53688	4.45872	-.00744
81	7	6.02372	-2.08277	4.51646	-.00744
81	8	6.01222	-1.68543	4.58073	-.00744
81	9	5.99819	-1.10085	4.66029	-.00744
81	10	5.98547	-.80815	4.73241	-.00744
81	11	5.97208	-.10083	4.80833	-.00744
81	12	5.98381	-.18144	4.09822	-.00744
81	13	5.97700	-.27570	3.48574	.01704
81	14	5.96898	-.39128	2.88817	.01381
81	15	5.95039	-.58689	2.28526	.01120
81	16	5.97894	-.93178	1.65654	.01106
81	17	6.06076	-1.12498	1.08668	.01383

I	J	X(I,J)	Y(I,J)	Z(I,J)	P(I,J)
91	1	5.53654	-5.00000	4.39905	-.00744
91	2	5.53654	-4.50000	4.39905	-.00744
91	3	5.53654	-4.00000	4.39905	-.00744
91	4	5.53654	-3.50000	4.39905	-.00744
91	5	5.53276	-3.01283	4.42049	-.00744
91	6	5.52617	-2.53688	4.45704	-.00744
91	7	5.51617	-2.08277	4.51488	-.00744
91	8	5.50466	-1.68543	4.57904	-.00744
91	9	5.49063	-1.10085	4.65841	-.00744
91	10	5.47791	-.80815	4.73152	-.00744
91	11	5.46453	-.10083	4.80745	-.00744
91	12	5.47625	-.18144	4.09733	-.00744
91	13	5.47070	-.29080	3.44322	.02148

91	14	5.46756	-.42075	2.84821	.01603
91	15	5.46977	-.63318	2.24905	.01380
91	16	5.46296	-.99444	1.59565	.01491
91	17	5.56836	-1.18815	.99185	.01678

I	J	X(I,J)	Y(I,J)	Z(I,J)	P(I,J)
101	1	5.02898	-5.00000	4.39817	-.00744
101	2	5.02898	-4.50000	4.39817	-.00744
101	3	5.02898	-4.00000	4.39817	-.00744
101	4	5.02898	-3.50000	4.39817	-.00744
101	5	5.02920	-3.01283	4.41961	-.00744
101	6	5.01861	-2.53888	4.45898	-.00744
101	7	5.00861	-2.08277	4.51370	-.00744
101	8	4.99710	-1.58543	4.57898	-.00744
101	9	4.98307	-1.10085	4.65883	-.00744
101	10	4.97036	-.60615	4.73084	-.00744
101	11	4.96887	-.10083	4.80857	-.00744
101	12	4.96839	-.18144	4.88445	-.00744
101	13	4.97881	-.29591	3.40903	-.00744
101	14	4.96727	-.44483	2.80612	.01838
101	15	4.95881	-.67382	2.20109	.01889
101	16	4.96640	-1.04845	1.53237	.01801
101	17	5.07505	-1.24847	.99503	.01898

I	J	X(I,J)	Y(I,J)	Z(I,J)	P(I,J)
111	1	4.92142	-5.00000	4.39729	-.00744
111	2	4.92142	-4.50000	4.39729	-.00744
111	3	4.92142	-4.00000	4.39729	-.00744
111	4	4.92142	-3.50000	4.39729	-.00744
111	5	4.91784	-3.01283	4.41972	-.00744
111	6	4.91106	-2.53888	4.45807	-.00744
111	7	4.90105	-2.08277	4.51281	-.00744
111	8	4.48954	-1.58543	4.57800	-.00744
111	9	4.47651	-1.10085	4.65784	-.00744
111	10	4.46280	-.60615	4.72975	-.00744
111	11	4.44941	-.10083	4.80568	-.00744
111	12	4.46083	-.18144	4.88356	-.00744
111	13	4.46825	-.29591	3.40414	-.00744
111	14	4.46805	-.44183	2.79782	.02878
111	15	4.46056	-.70784	2.19305	.02880
111	16	4.48027	-1.09878	1.46671	.02145
111	17	4.58356	-1.29306	.99820	.02336

I	J	X(I,J)	Y(I,J)	Z(I,J)	P(I,J)
121	1	4.81386	-5.00000	4.39840	-.00744
121	2	4.81386	-4.50000	4.39840	-.00744
121	3	4.81386	-4.00000	4.39840	-.00744
121	4	4.81386	-3.50000	4.39840	-.00744
121	5	4.81008	-3.01283	4.41784	-.00744
121	6	4.80350	-2.53888	4.45819	-.00744
121	7	3.99349	-2.08277	4.51183	-.00744
121	8	3.98199	-1.58543	4.57719	-.00744
121	9	3.96796	-1.10085	4.65876	-.00744
121	10	3.95524	-.60615	4.72887	-.00744

121	11	3.94185	-.10083	4.80480	-.00744
121	12	3.95327	-.18144	4.09268	-.00744
121	13	3.96069	-.29591	3.40325	-.00744
121	14	3.96890	-.46849	2.70370	-.00744
121	15	3.98221	-.73408	2.09997	.02517
121	16	3.98480	-1.13599	1.39841	.02869
121	17	4.09114	-1.33388	.72138	.02748

I	J	X(I,J)	Y(I,J)	Z(I,J)	P(I,J)
131	1	3.50631	-5.00000	4.39552	-.00744
131	2	3.50631	-4.50000	4.39552	-.00744
131	3	3.50631	-4.00000	4.39552	-.00744
131	4	3.50631	-3.50000	4.39552	-.00744
131	5	3.50253	-3.01283	4.41695	-.00744
131	6	3.49594	-2.53688	4.45430	-.00744
131	7	3.48594	-2.08277	4.51104	-.00744
131	8	3.47443	-1.58543	4.57831	-.00744
131	9	3.46040	-1.10085	4.65587	-.00744
131	10	3.44768	-.80615	4.72798	-.00744
131	11	3.43430	-.10083	4.80391	-.00744
131	12	3.44672	-.18144	4.09180	-.00744
131	13	3.45314	-.29591	3.40237	-.00744
131	14	3.46234	-.46849	2.70281	-.00744
131	15	3.46538	-.75095	2.03825	.03621
131	16	3.48882	-1.16597	1.32678	.03126
131	17	3.59874	-1.36431	.63455	.03308

I	J	X(I,J)	Y(I,J)	Z(I,J)	P(I,J)
141	1	2.99875	-5.00000	4.39463	-.00744
141	2	2.99875	-4.50000	4.39463	-.00744
141	3	2.99875	-4.00000	4.39463	-.00744
141	4	2.99875	-3.50000	4.39463	-.00744
141	5	2.99497	-3.01283	4.41607	-.00744
141	6	2.98838	-2.53688	4.45342	-.00744
141	7	2.97838	-2.08277	4.51016	-.00744
141	8	2.96687	-1.58543	4.57742	-.00744
141	9	2.95284	-1.10085	4.65499	-.00744
141	10	2.94013	-.80615	4.72710	-.00744
141	11	2.92674	-.10083	4.80303	-.00744
141	12	2.93916	-.18144	4.09091	-.00744
141	13	2.94558	-.29591	3.40148	-.00744
141	14	2.95478	-.46849	2.70193	-.00744
141	15	2.97242	-.75276	1.95459	.04692
141	16	3.00543	-1.16328	1.24948	.04408
141	17	3.10834	-1.36120	.64773	.04682

I	J	X(I,J)	Y(I,J)	Z(I,J)	P(I,J)
151	1	2.49119	-5.00000	4.39375	-.00744
151	2	2.49119	-4.50000	4.39375	-.00744
151	3	2.49119	-4.00000	4.39375	-.00744
151	4	2.49119	-3.50000	4.39375	-.00744
151	5	2.48741	-3.01283	4.41519	-.00744
151	6	2.48083	-2.53688	4.45254	-.00744
151	7	2.47082	-2.08277	4.50927	-.00744

161	8	2.45931	-1.58543	4.57484	-.00744
161	9	2.44528	-1.10085	4.65411	-.00744
161	10	2.43257	-.60615	4.72522	-.00744
161	11	2.41918	-.10083	4.80214	-.00744
161	12	2.43080	-.18144	4.09003	-.00744
161	13	2.43002	-.29581	3.40081	-.00744
161	14	2.44723	-.48649	2.70104	-.00744
161	15	2.46837	-.75276	1.94511	-.00744
161	16	2.51298	-1.10370	1.16290	.04692
161	17	2.61303	-1.38120	.46091	.04692

I	J	X(I,J)	Y(I,J)	Z(I,J)	P(I,J)
161	1	1.98383	-5.00000	4.39287	-.00744
161	2	1.98383	-4.50000	4.39287	-.00744
161	3	1.98383	-4.00000	4.39287	-.00744
161	4	1.98383	-3.50000	4.39287	-.00744
161	5	1.97985	-3.01283	4.41430	-.00744
161	6	1.97327	-2.53588	4.45185	-.00744
161	7	1.96328	-2.06277	4.50039	-.00744
161	8	1.95178	-1.58543	4.57365	-.00744
161	9	1.93773	-1.10085	4.65322	-.00744
161	10	1.92501	-.60615	4.72533	-.00744
161	11	1.91162	-.10083	4.80126	-.00744
161	12	1.92304	-.18144	4.08914	-.00744
161	13	1.93048	-.29581	3.39872	-.00744
161	14	1.93967	-.48649	2.70016	-.00744
161	15	1.95882	-.75276	1.94423	-.00744
161	16	2.02058	-1.10370	1.07608	.04692
161	17	2.12153	-1.38120	.37409	.04692

I	J	X(I,J)	Y(I,J)	Z(I,J)	P(I,J)
171	1	1.47608	-5.00000	4.39198	-.00744
171	2	1.47608	-4.50000	4.39198	-.00744
171	3	1.47608	-4.00000	4.39198	-.00744
171	4	1.47608	-3.50000	4.39198	-.00744
171	5	1.47230	-3.01283	4.41342	-.00744
171	6	1.46571	-2.53588	4.45077	-.00744
171	7	1.45571	-2.06277	4.50781	-.00744
171	8	1.44420	-1.58543	4.57277	-.00744
171	9	1.43017	-1.10085	4.65234	-.00744
171	10	1.41745	-.60615	4.72445	-.00744
171	11	1.40407	-.10083	4.80037	-.00744
171	12	1.41549	-.18144	4.08826	-.00744
171	13	1.42291	-.29581	3.39884	-.00744
171	14	1.43211	-.48649	2.69928	-.00744
171	15	1.45126	-.75276	1.94334	-.00744
171	16	1.51318	-1.10370	.99925	.04692
171	17	1.61312	-1.38120	.29726	.04692

I	J	X(I,J)	Y(I,J)	Z(I,J)	P(I,J)
181	1	.98052	-5.00000	4.39110	-.00744
181	2	.98052	-4.50000	4.39110	-.00744
181	3	.98052	-4.00000	4.39110	-.00744
181	4	.98052	-3.50000	4.39110	-.00744

101	5	.05474	-3.01283	4.41253	-.00744
101	6	.05015	-2.53588	4.44988	-.00744
101	7	.04915	-2.06277	4.50652	-.00744
101	8	.03884	-1.58543	4.57189	-.00744
101	9	.02261	-1.10088	4.63145	-.00744
101	10	.00990	-.60615	4.72388	-.00744
101	11	.00651	-.10083	4.78949	-.00744
101	12	.00793	-.18144	4.08737	-.00744
101	13	.01535	-.28691	3.39795	-.00744
101	14	.02455	-.48549	2.69836	-.00744
101	15	.04370	-.75276	1.94248	-.00744
101	16	1.02365	-1.18370	.97118	-.00744
101	17	1.13672	-1.38120	.20043	.04692

I	J	X(I,J)	Y(I,J)	Z(I,J)	P(I,J)
101	1	.48096	-5.00000	4.39021	-.00744
101	2	.48096	-4.50000	4.39021	-.00744
101	3	.48096	-4.00000	4.39021	-.00744
101	4	.48096	-3.50000	4.39021	-.00744
101	5	.45718	-3.01283	4.41165	-.00744
101	6	.45060	-2.53588	4.44800	-.00744
101	7	.44059	-2.06277	4.50574	-.00744
101	8	.42908	-1.58543	4.57100	-.00744
101	9	.41505	-1.10088	4.63057	-.00744
101	10	.40234	-.60615	4.72288	-.00744
101	11	.39895	-.10083	4.78860	-.00744
101	12	.40037	-.18144	4.08649	-.00744
101	13	.40778	-.28691	3.39707	-.00744
101	14	.41700	-.48549	2.69751	-.00744
101	15	.43614	-.75276	1.94158	-.00744
101	16	.51509	-1.18370	.97030	-.00744
101	17	.64431	-1.38120	.11361	.04692

I	J	X(I,J)	Y(I,J)	Z(I,J)	P(I,J)
201	1	-.04860	-5.00000	4.38933	-.00744
201	2	-.04860	-4.50000	4.38933	-.00744
201	3	-.04860	-4.00000	4.38933	-.00744
201	4	-.04860	-3.50000	4.38933	-.00744
201	5	-.05038	-3.01283	4.41076	-.00744
201	6	-.05696	-2.53588	4.44811	-.00744
201	7	-.06697	-2.06277	4.50485	-.00744
201	8	-.07847	-1.58543	4.57012	-.00744
201	9	-.09250	-1.10088	4.64969	-.00744
201	10	-.10522	-.60615	4.72179	-.00744
201	11	-.11861	-.10083	4.78772	-.00744
201	12	-.10718	-.18144	4.08561	-.00744
201	13	-.09977	-.28691	3.39619	-.00744
201	14	-.09056	-.48549	2.69662	-.00744
201	15	-.07141	-.75276	1.94069	-.00744
201	16	.00883	-1.18370	.96941	-.00744
201	17	.13191	-1.38120	.02879	.04692

```
STREAMTUBE AREA =      10.386
AO/AC =      .77844

UPPER SURFACE
DRAG =      .09808
CDRAG =      .01485
TUBE SURFACE AREA =    8.42167

TOTAL STREAMTUBE
DRAG =      .09080
CDRAG =      .01414
TUBE SURFACE AREA =    8.07837
```

Appendix D
DERIVATIONS OF TWO-DIMENSIONAL PERTURBATION VELOCITIES

This appendix presents the derivation of the two-dimensional perturbation velocities to be used as boundary conditions for conical flow analysis. First, the perturbation velocities are derived for an airfoil without sweepback. These results are employed to determine the perturbation velocity components for an airfoil with sweepback.

AIRFOIL WITHOUT SWEEPBACK

The small perturbation equation of velocity potential Φ for supersonic flow in two dimensions is:

$$\frac{\partial^2 \Phi}{\partial x^2} = \tan^2 \mu_0 \frac{\partial^2 \Phi}{\partial z^2} \tag{D-1}$$

This has the general solution

$$\Phi = f_1(z - x \tan \mu_0) + f_2(z + x \tan \mu_0)$$

where f_1 and f_2 are arbitrary functions.

Now consider a velocity potential

$$\Phi = Vx + V\alpha(z + x \tan \mu_0) \tag{D-2}$$

For $\alpha = 0$, $u = -\partial\Phi/\partial x = -V$ which is a uniform velocity V in the negative x direction. Note that in Milne-Thomson's terminology, $u_i = -\partial\Phi/\partial x_i$ which is opposite in sign to most terminologies.

For a small but non-zero α, the velocity components are $-V(1 + \alpha \tan \mu)$, $-V\alpha$. Physically, this is equivalent to flow turned through an angle α. The uniform velocity V is separated from the perturbed flow by a characteristic line inclined at the Mach angle μ_0. Thus, the perturbation components may be written as

$$u_\infty = \alpha \tan \mu_0$$

$$w_\infty = \alpha V \tag{D-3}$$

AIRFOIL WITH SWEEPBACK

Now, consider a flat plate of infinite span with sweepback as shown in Figure D-1. The leading edge is swept back with an angle δ between the leading edge and an axis parallel to the freestream velocity vector V. The airfoil is at an angle of attack, α.

At point O on the leading edge, define two planes, OAB in the plane of the airfoil and OCD the freestream velocity vector V and the leading edge. From this, draw three more planes; plane OAD through V and perpendicular to the airfoil, plane OCB perpendicular to the leading edge, and plane ABCD perpendicular to plane OCD and parallel to the leading edge.

Angle AOD is the angle of attack α. Let angle BOC be called α_1.

$$\tan \alpha = \frac{AD}{OD}$$

$$\tan \alpha_1 = \frac{BC}{OC}$$

Since AD = BC

$$\tan \alpha / \tan \alpha_1 = OC/OD = \sin \delta$$

as is apparent from the projection in Figure D-2

$$OC/OD = \cos (\delta - \pi/2) = \sin \delta$$

Since α is small and $\tan \alpha \approx \alpha$,

$$\alpha = \alpha_1 \sin \delta \tag{D-4}$$

The freestream velocity V may be resolved into components $-V \cos \delta$ parallel to the leading edge and $V \sin \delta$ perpendicular to the leading edge along OC. The component parallel to the leading edge remains unchanged. The perturbation velocity $u_{l\infty}$ based on the component $V \sin \delta$ is found by the treatment of the unswept edge

$$u_{l\infty} = \alpha_1 V \sin \delta \tan \mu_1 \tag{D-5}$$

where

$$\sin \mu_1 = a_0/(V \sin \delta) \tag{D-6}$$

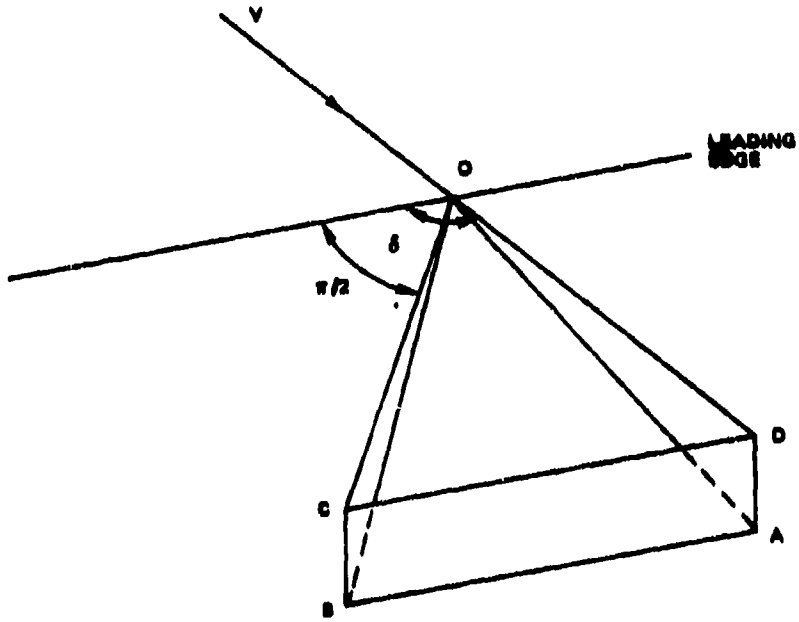

FIGURE D-1. Construction for Derivation of Perturbation Velocities.

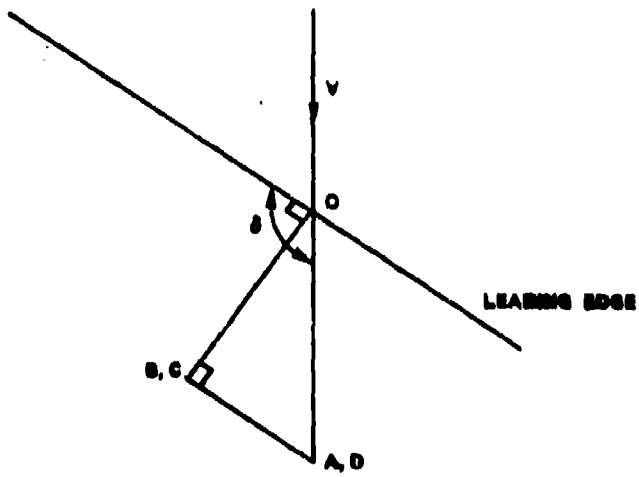

FIGURE D-2. Vertical Projection of Airfoil.

The perturbation velocity u_{1_∞} is in the direction of OC. This velocity may be resolved into components.

$$u_0 = u_{1_\infty} \sin \delta$$

$$v_0 = u_{1_\infty} \cos \delta \tag{D-7}$$

From Equations D-6 and D-7,

$$\sin \mu_1 = \sin \mu_0 / \sin \delta$$

Since $\tan \mu_1 = \sin \mu_1 / \cos \mu_1$,

$$\tan \mu_1 = \frac{1}{\sin \delta} \frac{\sin \mu_0}{\cos \mu_1} = \operatorname{cosec} \delta \frac{\sin \mu_0}{\cos \mu_1} \tag{D-8}$$

In addition, since $\cos \mu_1 = (1 - \sin^2 \mu_1)^{1/2} = \left(1 - \frac{\sin^2 \mu_0}{\sin^2 \delta}\right)^{1/2}$, Equation D-8 becomes:

$$\tan \mu_1 = \operatorname{cosec} \delta \frac{\sin \mu_0}{\left(1 - \frac{\sin \mu_0}{\sin^2 \delta}\right)^{1/2}} = \operatorname{cosec} \delta \, (\operatorname{cosec}^2 \mu_0 - \operatorname{cosec}^2 \delta)^{-1/2} \tag{D-9}$$

The term $(\operatorname{cosec}^2 \mu_0 - \operatorname{cosec}^2 \delta)$ may be rewritten:

$$(\operatorname{cosec}^2 \mu_0 - \operatorname{cosec}^2 \delta) = [(\cot^2 \mu_0 + 1) - (\cot^2 \delta + 1)] = (\cot^2 \mu_0 - \cot^2 \delta)$$

Thus, Equation D-9 becomes

$$\tan \mu_1 = \operatorname{cosec} \delta \, (\cot^2 \mu_0 - \cot^2 \delta)^{-1/2} \tag{D-10}$$

Combining Equations D-4, D-5, and D-10 yields:

$$u_{1_\infty} = \alpha V \operatorname{cosec} \delta \, (\cot^2 \mu_0 - \cot^2 \delta)^{-1/2} \tag{D-11}$$

Introduce the angle λ which is defined:

$$\cos \lambda = \tan \mu_0 \cot \delta = \cot \delta / \cot \mu_0 \tag{D-12}$$

Note that this is identical with Equation 3-46 in the text. Thus, the nomenclature is consistent between the two-dimensional analysis and the analysis of the complex perturbation velocities in conical flow. This places a physical meaning to the geometry in the complex ϵ plane.

Using Equation D-12, Equation D-11 becomes:

$$u_{1_\infty} = \alpha V \tan \mu_0 \operatorname{cosec} \delta \operatorname{cosec} \lambda \tag{D-13}$$

Thus, the perturbation components of Equation D-7 may be written

$$u_0 = \alpha V \tan \mu \operatorname{cosec} \lambda$$

$$v_0 = \alpha V \tan \mu \cot \delta \operatorname{cosec} \lambda \tag{D-14}$$

From the two-dimensional analysis, the vertical component may be written as:

$$w_0 = \alpha V \tag{D-15}$$

NOMENCLATURE

A	Area
A_o/A_c	Inlet mass capture area ratio
a	Speed of sound
a	Real part of ν_1
b	Imaginary part of ν_1
C	Constant
C_{D_a}	Coefficient of additive drag
D	Drag force
E'	Complete elliptic integral of the second kind of modulus k'
F	Force
F	Stream thrust = $\dot{m}V + A(p - p_0)$
g	Acceleration of gravity
h	Height
K'	Complete elliptic integral of the first kind of modulus k'
k	$\beta \tan \xi$
k'	$\sqrt{1 - k^2}$
L	Length dimension
ℓ	Length dimension
L_1	Length of inlet ramp from leading edge to cowl (Figure 50)
L_S	Length of inlet sidewall from cowl (Figure 50)
L_oA	Identification of airfoil shape: one leading edge outside the Mach cone, one axial edge
L_oL_o	Identification of airfoil shape: two leading edges, both outside the Mach cone
L_oT_i	Identification of airfoil shape: one leading edge outside the Mach cone, one trailing edge inside the Mach cone
M	Mach number
$\dot{m}$	Mass flow rate
p	Pressure
p_{t_2}/p_{t_∞}	Inlet total pressure recovery

q	Dynamic pressure
R	Tschaplygin transformation = $\frac{1 - \sqrt{1 - r^2}}{r}$
R	Gas constant
R_1	Radius
R_2	$\sqrt{x^2 \tan^2 \mu - y^2 - z^2}$
r	Radius
S	Dependent variable of small perturbation equation
s	Transformed coordinate in physical plane
T	Temperature
U_0	Freestream velocity
U	Complex perturbation velocity
u	Normalized perturbation velocity
V	Velocity
V	Complex perturbation velocity
v	Normalized perturbation velocity
W	Width of inlet
W	Complex perturbation velocity
w	Normalized perturbation velocity
$\dot{w}$	Weight flow rate
X	Substitution variable = $ix \tan \mu$
x	Linear dimension
y	Linear dimension
z	Linear dimension
α	Deflection angle
β	$\cot \mu = \sqrt{M^2 - 1}$
γ	Ratio of specific heats
δ	Leading edge angle

e	Busemann's complex variable = $\frac{y + iz}{x \tan \mu + R_2}$
ζ	Sweepback angle = $\lvert\pi - \delta\rvert$
θ	Angle
λ	Angle ($\cos \lambda = \tan \mu \cot \delta$)
μ	Mach angle = $\sin^{-1}(1/M)$
ν	Transformed complex coordinate = $\sqrt{e}$
ξ	Sideplate angle (Figure 12)
π	Constant = 3.1416
ρ	Density
Φ	Velocity potential
ϕ_1, ϕ_2	Angles (Figure 36)
χ	Substitution variable = log tan $1/2\omega$
ψ	Inlet ramp angle (Figure 12)
ω	Coordinate angle

Subscripts

0	Freestream
1	Cowl
a	Additive
c	Cowl
d	Drag
e	Exit
i	Internal
ℓ	Local
n	Net
OSS	Sidespill
p	Propulsive
ref	Reference
s	Surface
t	Total
w	Wave

∞ Freestream

$*$ Sonic

Superscripts

∞ Two-dimensional analysis

$*$ Imaginary component